MITOCHONDRIAL PYRUVATE METABOLISM IN CANCER AND STEM CELLS OF THE COLON EPITHELIUM

by

Kristofor Aksamit Olson

A dissertation submitted to the faculty of
The University of Utah
in partial fulfillment of the requirements for the degree of

Doctor of Philosophy

Department of Biochemistry

The University of Utah

May 2016

The University of Utah Graduate School

STATEMENT OF DISSERTATION APPROVAL

The dissertation of **Kristofor Aksamit Olson**

has been approved by the following supervisory committee members:

Jared P. Rutter	, Chair	**03/16/2016** Date Approved
Janet E. Lindsley	, Member	**03/16/2016** Date Approved
Janet M. Shaw	, Member	**03/16/2016** Date Approved
Donald E. Ayer	, Member	**03/16/2016** Date Approved
Adam Lucas Hughes	, Member	**03/16/2016** Date Approved

and by **Wesley I. Sundquist** ,Chair/Dean of the

Department/College/School of **Biochemistry**

and by David B. Kieda, Dean of The Graduate School.

ABSTRACT

The study of metabolism is fundamental to understanding the basis of disease. Subtle differences in metabolites, and shunting of molecules from one pathway to another can have profound effects on cellular physiology. In the case of cancer cells this metabolic balance is often severely disrupted. Many cancer cells rapidly consume glucose to produce pyruvate, but rather than entering the mitochondria for oxidation, it is reduced to lactate and excreted from the cell. This phenomenon is known as the "Warburg effect" and provides the cell ample biosynthetic precursors for proliferation, many of which are side-reactions of glycolysis.

Similar to cancer cells, stem cells also place a heavy metabolic emphasis on glycolysis. During the process of differentiation, however, stem cells shift their metabolic profile towards oxidative phosphorylation and mitochondrial respiration. Unlike stem cells, many cancer cells are limited in their ability to adapt to a different, more oxidative metabolic regime.

In both cancer cells and stem cells, the fate of pyruvate is tightly controlled. The mitochondrial pyruvate carrier (MPC), a heterodimeric protein complex, is required for pyruvate import into the mitochondria. The recent discovery of the genes encoding the MPC have provided a new lens to

evaluate pyruvate metabolism in normal and disease physiology. Herein, the role of the MPC and its connection to the Warburg effect are described in the context of normal physiology, colon cancer, and resident colon stem cells.

To my parents, for sowing the seeds of curiosity.
To my brother, for always challenging me.
To my wife, for endless love and support.

The cure of human cancer will be the resultant of biochemistry of cancer and of biochemistry of man.

Dr. Otto Warburg
Meeting of the Nobel Laureates, Lindau, Germany
June 30, 1966

TABLE OF CONTENTS

LIST OF FIGURES

ACKNOWLEDGEMENTS

I would like to thank Christel Nordhausen for teaching the framework of scientific thought to an inquiring young mind. Unequivocally, the exposure to the Montessori method that I received at her school has been the single greatest influence on my education.

I would like to thank Dr. Henry A. Charlier, for the early exposure to research in his laboratory after I graduated high school. I would like to thank Dr. C. Dale Poulter for his years of mentorship while I was an undergraduate researcher in his laboratory. The encouragement, independence, and scientific training I received in his laboratory was essential to my success in graduate school.

Finally, I thank my graduate mentor Dr. Jared P. Rutter for the freedom to explore interesting scientific topics, wherever they may lead; and John C. Schell, a fellow lab mate, MD/PhD student, and frequent companion on these scientific odysseys.

The work presented herein has been supported by the Norah Eccles Treadwell Foundation, NIH Hematology Training grant T32 DK007115, and the Howard Hughes Medical Institute.

CHAPTER 1

INTRODUCTION

1.1 An Historic Perspective

Any thesis on cancer metabolism would be remiss if not to discuss the pioneering work of Dr. Otto Warburg. In the 1920s, Dr. Warburg observed that tissue homogenized from a rat liver tumors respired differently than that of a normal rat liver. The studies were simple and elegant in their construction and quantified the consumption of glucose in a buffered solution, and its conversion to carbon dioxide versus its excretion from the cell as lactate. Dr. Warburg attributed this difference in cellular metabolism to be due to defective respiratory enzymes within the cancer cells. He received the Nobel Prize in Physiology for this discovery in 1931.[1]

However, Dr. Warburg's theory was dismissed when mitochondria isolated from cancer cells were shown to still contain machinery which would actively respire, and the 'Warburg effect' fell out of vogue for many years. Still, Dr. Warburg continued his research on cancer metabolism and cellular respiration.

Four years before his death, at the 1966 meeting of Nobel Laureates in

Lindau, Germany, Dr. Warburg presented another discovery, where he showed that hypoxia was sufficient to irreversibly drive a change from "normal" embryonic metabolism to cancer metabolism:

> If one puts embryonic mouse cells into a suitable culture medium saturated with physiological oxygen pressures, they will grow outside the mouse body, in vitro, and indeed as pure aerobes, with a pure oxygen respiration, without a trace of fermentation. However, if during the growth one provides an oxygen pressure so reduced that the oxygen respiration is partially inhibited, the purely aerobic metabolism of the mouse embryonic cells is quantitatively altered within 48 h, in the course of two cell divisions, into the metabolism characteristic of fermenting cancer cells.
>
> If one then brings such cells, in which during their growth under reduced oxygen pressure a cancer cell metabolism has been produced, back under the original high oxygen pressure, and allows the cell to grow further, the cancer metabolism remains. The transformation of embryonic cell metabolism into cancer cell metabolism can thus be irreversible, an important result, since the origin of cancer cells from normal body cells is an irreversible process.[2]

In effect, Dr. Warburg's lecture was the first mention of the concept of "metabolic inflexibility" of cancer cells, a hypothesis that is central to both the research presented herein and the development of metabolic cancer therapies.

1.2 References

(1) *Nobel Lectures, Physiology or Medicine 1922-1941*; Elsevier Publishing Company: Amsterdam, 1965.

(2) Warburg, O.; The Prime Cause and Prevention of Cancer. Presented at the Lindau Meeting of the Nobel Laureates, Lindau, Germany, 1966.

CHAPTER 2

PYRUVATE AND METABOLIC FLEXIBILITY: ILLUMINATING A PATH TOWARD SELECTIVE CANCER THERAPIES

Kristofor A. Olson, John C. Shell, Jared Rutter

Reprinted from Trends in Biochemical Sciences, 41(3), doi: 10.1016/j.tibs.2016.01.002,

Trends in Biochemical Sciences

CellPress

Special Issue: Mitochondria and Metabolism

Review

Pyruvate and Metabolic Flexibility: Illuminating a Path Toward Selective Cancer Therapies

Kristofor A. Olson,[1] John C. Schell,[1] and Jared Rutter[1,2,*]

Dysregulated metabolism is an emerging hallmark of cancer, and there is abundant interest in developing therapies to selectively target these aberrant metabolic phenotypes. Sitting at the decision-point between mitochondrial carbohydrate oxidation and aerobic glycolysis (i.e., the 'Warburg effect'), the synthesis and consumption of pyruvate is tightly controlled and is often differentially regulated in cancer cells. This review examines recent efforts toward understanding and targeting mitochondrial pyruvate metabolism, and addresses some of the successes, pitfalls, and significant challenges of metabolic therapy to date.

The Dynamic and Flexible Metabolic Network

Many of us can relate to the experience of a metabolic enzyme popping up in a dataset, and then having to scramble to find a lab that has the metabolic map taped to the wall. Dr Donald Nicholson, the originator of most of these maps, passed away in 2012 at the age of 96 [1]. For decades Dr Nicholson's maps have provided the framework for our conception of metabolism, and this was generally to our great benefit. In one respect, however, this depiction of metabolism has perhaps contributed to a common misconception regarding the true nature of cellular metabolism. Those printed words and arrows of fixed dimension and orientation belie the dynamism and complexity that characterizes the metabolic network of a living cell.

To a greater or lesser extent, every cell on Earth carries out metabolism differently from every other cell. Even a single given cell does not behave in the same manner from one minute to the next. Most cells constantly monitor their available nutrients, their own needs, and other aspects of their environment, and make (sometimes dramatic) alterations to the wiring and flux of their metabolic network. When the combination of internal, neuronal, environmental, and hormonal signals cause a cell to change its fate or behavior (e.g., to grow, differentiate, divide, change its gene expression program), this usually involves an adjustment to optimize the metabolism of the cell to this new behavior.

This dynamic character of the cellular metabolic network is commonly known as 'metabolic flexibility', and we posit that this metabolic flexibility is a crucially important, but often unappreciated, feature of cellular physiology. In the case of cancer, however, adaptations that optimize the oncogenic process may ultimately limit the metabolic flexibility of some cancer cells and thereby increase susceptibility to metabolism-targeted therapies. While this hypothesis is still being

Trends

The ability of cells to respond to different nutrient conditions and energetic demands is known as 'metabolic flexibility' and is an essential feature of normal cellular physiology.

Adaptations that occur during the process of cancer formation may limit the metabolic flexibility of some cancers.

Metabolic therapies designed to target cancers are predicated on the hypothesis that some cancers are less metabolically flexible than normal tissues, and this may be a means to selectively target cancer while sparing other tissues.

Pyruvate metabolism is a central, differentially regulated, nexus of carbon metabolism that both provides and limits flexibility in normal and cancer tissues.

[1]Department of Biochemistry, University of Utah School of Medicine, Salt Lake City, UT 84112-5650, USA
[2]Howard Hughes Medical Institute, University of Utah School of Medicine, Salt Lake City, UT 84112-5650, USA

*Correspondence: rutter@biochem.utah.edu (J. Rutter).

tested, the promise of the metabolic approach to cancer therapy is predicated on this hypothesis being true, at least in a subset of cancers under a subset of conditions. Great challenges to this approach remain, however, including the flexibility that tumors retain, both in a cell-autonomous manner and as a result of metabolic heterogeneity across the population of tumor cells. This review discusses metabolic flexibility, with a focus on mitochondrial pyruvate metabolism and the successes, failures, opportunities, and pitfalls of modulating pyruvate metabolism in cancer.

Metabolic Flexibility in Normal and Disease Physiology

All living organisms rely on metabolic flexibility for survival in an evolving environment. Persistent adaptations are common during development as stem cells give rise to the differentiated cells and tissues present in the adult body, and continue to adapt during remodeling, regeneration, and aging [2]. In general, stem cell differentiation is associated with a change in the carbohydrate metabolic program, with pyruvate being the site of bifurcation. Most differentiation paradigms are characterized by a transition from glycolytic metabolism to mitochondrial oxidative metabolism [3,4] (Figure 1; discussed in more detail below).

Acute adaptations are also common and crucial. During vigorous exercise, when the ATP demand outstrips the availability of oxygen, skeletal muscle tissue shifts from mitochondrial oxidative phosphorylation to glycolytic ATP generation. Instead of entering the mitochondria, pyruvate is converted to lactate and excreted from the cell. This acute adaptation is necessary to enable the continued contractile function of muscle during extended exercise, and is familiar to all with sore muscles or a 'Charlie horse'. Christian Metallo and colleagues recently elegantly demonstrated this adaptability at the level of isolated individual cells. Using C2C12 myoblasts, they studied the impact of blocking the mitochondrial oxidation of three of the principal oxidative fuels of these cells: pyruvate (from carbohydrates), glutamine, and fatty acids [5] (Figure 1). Blocking any two of these pathways had negligible effects on oxygen consumption associated with ATP production. It was only when all three were simultaneously inhibited that a significant decrease in oxygen consumption was observed, and that was only a 30% decrement. Shuttling pyruvate-derived alanine into the mitochondria, which was recently shown in the liver [6,7], might bypass the **mitochondrial pyruvate carrier** (MPC, see Glossary) and thereby contribute to the observed resiliency of oxygen consumption.

While metabolic flexibility is a nearly universal property of normal healthy cells, it appears to be compromised in several disease settings. One example is the failing adult heart [8]. The fetal heart primarily produces ATP through glycolytic metabolism of carbohydrate substrates [9]. Over the course of development, the heart transitions such that fatty acid **β-oxidation** largely fuels the adult heart, but the heart retains the flexibility to temporarily switch to a glycolytic phenotype depending on nutrient availability and energetic demand [10]. It is becoming clear that the development of heart failure is accompanied by reversion back to the fetal glycolytic program and loss of metabolic flexibility [11–14], which may be potentiated by decreased expression of the MPC [15,16]. This metabolic regime was first described over 100 years ago when patients with various heart maladies temporarily improved after administration of cane sugar [17].

Metabolic Inflexibility in Cancer

During the process of oncogenesis, cells destined to populate a tumor acquire a series of adaptive phenotypes that are beneficial or even necessary for survival and/or proliferation, as evidenced by their strong positive selection [18]. Some of these phenotypes, such as the establishment of a specific transcriptional program, are readily reversible and probably evolve or revert over time as the demands and environment of the cell change. Other adaptations are irreversible, including genomic mutation, deletion, or amplification of tumor-suppressor genes or

Glossary

Acetyl-CoA synthetase isoform 2 (ACSS2): a nucleocytosolic enzyme that converts acetate to acetyl-CoA.
Alanine transaminase (ALT): an enzyme that transaminates pyruvate and glutamate to form alanine and α-ketoglutarate. Isoform 1 is in the cytosol, and isoform 2 localizes to mitochondria.
β-Oxidation: a four-step process within the mitochondria where fatty acids are oxidized to form acetyl-CoA.
Dichloroacetate (DCA): an inhibitor of PDK.
Glucose transporter (GLUT): a family of proteins that transport glucose across the plasma membrane.
Glutamate dehydrogenase (GDH): an enzyme that converts glutamate to α-ketoglutarate.
Glutaminase (GLS): a metabolic enzyme that deamidates glutamine to form glutamate.
Hypoxia-inducible factors (HIFs): a family of transcription factors responsible for the metabolic and cellular adaptation to hypoxia (Box 1).
Lactate dehydrogenase (LDH): a metabolic enzyme that converts lactate to pyruvate. Isoform A favors the forward reaction, whereas isoform B favors the reverse reaction.
Malic enzyme (ME): a metabolic enzyme that converts malate to pyruvate.
Monocarboxylate transporter (MCT): isoforms 4 and 1 of this enzyme are responsible for lactate excretion and lactate uptake, respectively.
Mitochondrial pyruvate carrier (MPC): a heterodimeric complex required for mitochondrial pyruvate import, composed of proteins MPC1 and MPC2.
Pyruvate carboxylase (PC): a mitochondrial enzyme that catalyzes the carboxylation of pyruvate to form oxaloacetic acid.
Pyruvate dehydrogenase (PDH): the mitochondrial enzyme complex that converts pyruvate to acetyl-CoA.
Pyruvate dehydrogenase kinase (PDK): isoforms 1–4 of this enzyme phosphorylate and inactivate PDH.
Pyruvate dehydrogenase phosphatase (PDP): isoforms 1 and 2 reverse the inhibitory phosphorylation of PDH by PDK.
Pyruvate kinase (PK): isoforms M1 or M2 of this enzyme perform the

terminal step in glycolysis to yield pyruvate.
Sirtuin 3 (SIRT3): a mitochondrial deacetylase that activates MPC1.
UK-5099: 2-cyano-3-(1-phenyl-1*H*-indol-3-yl)-2-propenoic acid, an inhibitor of the MPC complex.

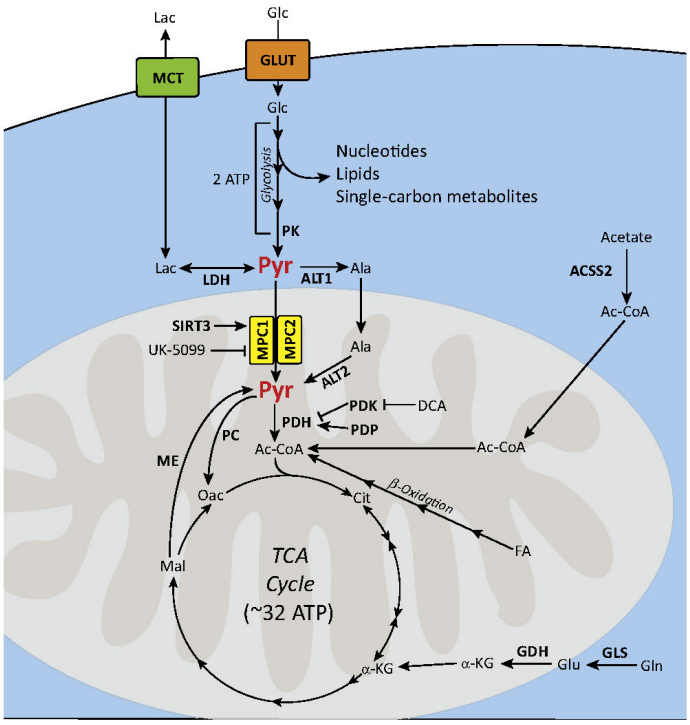

Trends in Biochemical Sciences

Figure 1. The Centrality of Pyruvate Metabolism. Glucose (Glc) enters the cell via the **glucose transporter** (GLUT) family of transporters. It is then catabolized by several enzymes during the process of glycolysis, yielding two molecules of ATP. Intermediates of glycolysis contribute to nucleotide and lipid biosynthesis, as well as to the synthesis of single-carbon donors. The final enzyme of glycolysis, **pyruvate kinase** (PK), yields two molecules of pyruvate (Pyr). Pyruvate can either be utilized in other biosynthetic reactions (such as an amine receptor for **alanine transaminase**, ALT), reduced to lactate (Lac) by **lactate dehydrogenase** (LDH) and excreted from the cell via the **monocarboxylate transporters** (MCT), or transported into the mitochondrial matrix via the **mitochondrial pyruvate carrier** (MPC). The MPC can be activated by deacetylation of K45 and K46 by **sirtuin 3** (SIRT3), and inhibited by the small molecule UK-5099. Once in the mitochondria, pyruvate can be oxidized via **pyruvate dehydrogenase** (PDH) to form acetyl-CoA (Ac-CoA). The **PDH kinases** (PDK) phosphorylate PDH to make it inactive. This phosphorylation can be reversed by the PDH phosphatases (PDP), or prevented by the PDK inhibitor dichloroacetate (DCA). Acetyl-CoA is then condensed with oxaloacetate (Oac) to form citrate (Cit) and begin the first turn of the tricarboxylic acid (TCA) cycle to yield an additional ~30–34 molecules of ATP. In some conditions, acetyl-CoA can be generated from scavenged acetate via **acetyl-CoA synthetase 2** (ACSS2), or via β-oxidation of fatty acids (FA). Some cancers cells *in vitro* heavily rely on glutamine (Gln) to replenish TCA cycle intermediates by converting it to glutamate (Glu) via **glutaminase** (GLS), and then to α-ketoglutarate (α-KG) via **glutamate dehydrogenase** (GDH). In other situations, pyruvate may additionally be consumed by **pyruvate carboxylase** (PC) to form oxaloacetate and bypass the TCA cycle. Similarly, pyruvate can be replenished in the mitochondria from malate (Mal) by **malic enzyme** (ME). Transporters are illustrated in rounded boxes, proteins and relevant enzymes are shown in **bold**, major biochemical pathways are shown in *italic*, metabolites and small molecules are shown in regular type, with the exception of pyruvate.

proto-oncogenes. For example, every progeny of a cell with a homozygous mutation destroying succinate dehydrogenase will forever be succinate dehydrogenase-deficient [19–21], even if that status becomes detrimental to the cell in some future scenario. While there are some cases wherein metabolic adaptations in cancer have been irreversibly established by genetic mutation, deletion, or amplification of metabolic enzymes, the majority of cancer metabolic adaptations seem to belong to a third class of adaptive phenotypes. They are theoretically reversible, but that reversion comes at a significant cost in oncogenic potential. The efficacy of the majority of cancer therapies relies on the exploitation of these latter two classes of adaptations (irreversible or costly reversible), and we will discuss below the promise and challenges of targeting the latter metabolic phenotypes.

The prototypical metabolic profile of cancer was first described by Otto Warburg in 1927 [22] and involves cancer cells oxidizing a lower fraction of their glucose completely to CO_2 than normal tissue, despite adequate oxygenation. The consequence of this so-called 'Warburg effect' is a compensatory increase in glucose consumption and lactate production. Under this paradigm the majority of glucose taken up by the cancer cell undergoes glycolysis to form two molecules of pyruvate (Figure 1). At this step, however, pyruvate is diverted from the mitochondrial oxidative pathway, converted to lactate through **lactate dehydrogenase** (LDH-A), and the lactate produced is exported from the cell, typically via the **monocarboxylate transporter** MCT-4 [23,24].

As described, this energetically inefficient metabolic profile seems counterintuitive. In fact, much of the glucose-derived carbon is diverted into biosynthetic pathways, which is likely a major reason that cancer cells bias against complete pyruvate oxidation because it results in losing carbon as CO_2. It appears that ATP production is simply not rate-limiting for cancer cell proliferation, and the cell places a greater emphasis on the synthesis and acquisition of the building blocks that are necessary to construct a new cell. To this end, the Warburg effect is accompanied by several additional adaptations that optimize for biosynthesis. While the frequency and extent of these individual effects is less well established than for aerobic glycolysis, this principle of enhancing biosynthetic metabolism through limiting pyruvate oxidation is likely to apply to most cancers [25,26].

The Centrality and Multi-Layered Regulation of Pyruvate Metabolism

One could make a compelling argument that pyruvate is the nexus of the entire cellular metabolic network (Figure 1). It occupies the junction between cytosolic and mitochondrial metabolism and, of specific relevance to this review, the pattern of pyruvate generation and disposition is the cardinal distinction between normal metabolism and 'cancer metabolism'. Essentially every protein that manages pyruvate synthesis and consumption has been described as somehow differentially regulated in cancer cells relative to normal cells. These adaptations, hypothesized to be costly to reverse for cancer cells, are the subject of intense exploration for therapeutic exploitation.

Pyruvate is synthesized as the last step of glycolysis by **pyruvate kinase** (PK), which exists as either the M1 or M2 isoform in most cell types. The regulation of expression of these isoforms is complex [27]; however, it appears that in many cancers the M2 isoform is 4–6-fold more prevalent than M1 [28], whereas normal tissues with high ATP demand tend to predominantly express the M1 isoform. The M2 isoform is sensitive to inhibition by phosphotyrosine motifs [29,30] and by other inputs that are stimulated by growth factor signaling [31]. As a result, cells with an elevated PK-M2/PK-M1 ratio have the potential to slow the production of pyruvate in response to proliferation signals. This phenomenon presumably enables preferential utilization of glycolytic intermediates for the biosynthesis of building blocks, including nucleotides, amino acids, and one-carbon donors [31–33].

The cytosolic pyruvate synthesized by PK lies at a site of bifurcation. It can either be transported into mitochondria (see below) or, in cells expressing the non-oxidative glycolytic (Warburg effect) program, it remains in the cytosol to be converted to lactate and exported from the cell, or for use in other biosynthetic reactions such as aspartate synthesis [34,35]. Pyruvate is converted to lactate by lactate dehydrogenase (typically the LDH-A isoform), which is frequently overexpressed and serves as a prognostic marker for poor survival in many cancers [36]. Inhibition of LDH-A increases oxygen consumption, presumably owing to an increase in mitochondrial pyruvate oxidation [5,37]. As would be expected if the Warburg metabolic profile is positively selected in cancer cells, numerous studies [38] have shown that colony formation [39], proliferation [39–41], metastasis [40], and survival [37] are dependent upon LDH-A activity.

Lactate can then be exported from the cell by the monocarboxylate transporter (MCT) family of integral membrane proteins. MCT-1 and MCT-4 have both been implicated in lactate export, although recent data suggest that MCT-4 plays the predominant role in many cancers. Much like LDH-A, several studies have demonstrated that MCT-4 expression, which is elevated in many cancers, is required for the full expression of the cancer phenotype and is associated with poor clinical outcomes [42–46].

In oxidative cells, pyruvate is transported into mitochondria by the MPC, which is composed of the MPC1 and MPC2 subunits. The activity of this transporter was described decades ago but was only recently molecularly identified [47,48]. The discovery of the encoding genes enabled the observation that most cancers exhibit decreased expression of *MPC1* and *MPC2*, with *MPC1* being the most strongly and consistently affected. This decreased expression and activity of the MPC seems to be an essential feature of the metabolic program, at least in colon cancer cells, because forced re-expression of *MPC1* and *MPC2* impaired colony formation *in vitro* and tumor xenograft growth in mice [49]. Recently, MPC activity was shown to be modulated by the mitochondrial deacetylase **sirtuin-3** (SIRT3), with MPC1 acetylation at K45 and K46 reducing mitochondrial pyruvate oxidation [50].

The next step in the carbohydrate oxidation pathway is the conversion of pyruvate to acetyl-CoA in the mitochondrial matrix by the **pyruvate dehydrogenase** (PDH) enzyme complex. Unlike the other proteins and complexes described in this section, there is little evidence of cancer-associated changes in the expression of the genes encoding PDH. There is also little evidence of the expression of distinct isoforms or splice variants of PDH complex genes in cancer cells. There is abundant evidence, however, of profound post-translational regulation of PDH in cancer by inhibitory phosphorylation. **Pyruvate dehydrogenase kinase isoform 1** (PDK1), which is frequently overexpressed in cancer cells, phosphorylates and inactivates PDH, and PDK1 expression has been strongly implicated in oncogenesis [51–53]. This phosphorylation can be reversed, and PDH activity restored, by **pyruvate dehydrogenase phosphatase isoform 2** (PDP2) and other PDPs [51].

Acetyl-CoA (produced by PDH) is then condensed with oxaloacetate to form citrate by the enzyme citrate synthase, which initiates the first turn of the TCA cycle. In some situations, cancer cells produce acetyl-CoA from scavenged acetate via **acetyl-CoA synthetase isoform 2** (ACSS2) to maintain proliferation during metabolic stress [54–56].

The extent and diversity of regulatory modalities employed to limit pyruvate oxidation in cancer cells suggests its importance. As briefly described for each protein, the data suggest that, although these metabolic adaptations that divert pyruvate metabolism are enacted and reversed in a facile manner in normal cells, such as in skeletal muscle during exercise, they have become difficult to reverse in cancer cells. One might hope that a cancer trapped in this 'costly reversible'

metabolic state might be selectively killed with the appropriate combination of metabolism-modulating agents.

Catching Cancer in the Metabolic Crab Pot: Attempts, Failures, and Hope for the Future

The mainstay of cancer therapy has been, and will probably continue to be, the exploitation of the irreversible or costly reversible adaptations made during the oncogenic process, which act like a 'crab pot' from which the cancer cannot easily escape. The cancer cell, in pursuit of energetic, biosynthetic, or survival advantage, may have trapped itself in a 'metabolic crab pot'. If that is true, then the remaining question is whether we can capitalize on that entrapment to selectively kill cancer cells while allowing the escape of normal cells that have retained their metabolic flexibility.

Perhaps the best-studied example of a candidate cancer therapy that acts by directly modulating metabolism is the drug **dichloroacetate** (DCA). An abundant byproduct of industrial organic halogenation reactions, its pharmacologic utility was investigated as early as the mid-20th century. By the 1970s, DCA was shown to be highly effective as an antidiabetic and lipid-lowering agent [57]. Shortly thereafter, one mechanism of DCA (although it likely has other effects) was discovered because it was shown to stimulate PDH activity by inhibiting the PDH kinases, thereby preventing inhibitory PDH phosphorylation [58]. It was not until 2007, with renewed interest in cancer metabolism, that Bonnet *et al.* hypothesized that DCA could potentially act to reverse the Warburg effect, promote mitochondrial pyruvate oxidation, and decrease tumor proliferation [59]. Since then, for a curious (and unfortunately erroneous) range of reasons, DCA has developed something of a cult following, with several reports of patients self-administering the drug in hopes that it may reduce tumor burden [60].

Over 150 manuscripts have been published on DCA in recent years, and 19 clinical trials have been conducted to evaluate its effectiveness in treating various cancers and metabolic diseases. In some cases DCA has shown positive signs of efficacy and great promise as an adjunct chemotherapy. For example, in combination with particular platinum-based chemotherapies, DCA has been shown to enhance cytotoxicity in several solid tumor-derived cell lines [61,62] and to reverse cisplatin resistance [63]. It is possible that DCA exacerbates the effects of these DNA crosslinking agents by reducing the biosynthesis of nucleotides necessary for DNA repair [64] or through other as-yet-undetermined metabolic effects.

While some studies have shown promise for DCA as a cancer treatment, several others suggest that its therapeutic potential may be limited. In the colorectal cancer cell line HCT116, DCA has been shown to affect cell proliferation without affecting survival or inducing apoptosis [65]. In other cancer cell lines the effects were more varied [66]. In fact, one study showed that DCA reduced apoptosis in hypoxic tumors, while enhancing proliferation and xenograft formation [67]. Similar results were found in neuroblastoma xenografts, where DCA promoted their progression [68]. Why has DCA shown anticancer efficacy in some situations and not in others? One clear possibility is that pyruvate metabolism is regulated at other points in the pathway, as described above. For example, in a situation where *MPC1* is deleted from the genome, a common occurrence in cancer [49,69], and pyruvate entry into the mitochondria is limited, the activation state of the PDH complex might be of less consequence, and thus DCA has little effect. Overexpression of LDHA/MCT-4 to siphon off cytosolic pyruvate for lactate export or the inhibition of PK might similarly mitigate the effects of PDH activation.

It is important to appreciate the complexity and redundancy of the regulation of mitochondrial pyruvate oxidation as we try to exploit the potential inflexibility of the cancer metabolic phenotype. Many new drug candidates are in development to target these metabolic 'crab pots', and

one hopes that they will be useful therapies alone and/or in combination. For example, many colon cancers reduce or eliminate mitochondrial pyruvate oxidation via downregulation or genomic deletion of the *MPC1* gene. A recent study [70] demonstrated that, by reducing pyruvate flux into the mitochondria, the cell becomes more reliant on the mitochondrial catabolism of glutamate. By inhibiting **glutaminase** or **glutamate dehydrogenase** (GDH), in concert with the MPC, the mitochondria became depleted of available carbon sources, which decreased cell growth and increased cell death [70]. This finding directly lends itself to therapeutic application, provided that MPC status can be determined in a tumor biopsy. In tumors with low or absent MPC expression, one might expect increased susceptibility to glutaminase inhibition. By contrast, normal or differentiated cells, which retain their metabolic flexibility, would be better able to compensate for the loss of this source of glutamate and α-ketoglutarate through pyruvate fueling of the TCA cycle.

As we continue to build on the previous decades of metabolic biochemistry, the development of small molecules that target additional metabolic nodes will supply new tools to target the metabolic inflexibilities of tumors. However, it is essential that we understand the integration of these biosynthetic pathways, the nature of these irreversible (or costly reversible) adaptations, and the points of inflexibility that they cause. When we are capable of ascertaining this for a given tumor in a given patient, then a combination of agents that target different facets of the tumor's metabolism might be used to precisely apply pressure to these specific liabilities. If this 'pressure' is supplied sufficiently precisely, it may spare non-neoplastic tissues owing to their retained metabolic flexibility. While this field is rapidly expanding, and there is great hope that it will change the course of cancer treatment, many significant hurdles remain.

Why Has Metabolic Therapy Not Cured Cancer?

It is well established that the cells within tumors are genetically, epigenetically, and metabolically heterogeneous, as has been extensively reviewed elsewhere [71,72]. In the same way that tumor heterogeneity poses challenges to conventional chemotherapies, tumor heterogeneity is likely to be a major hurdle for metabolic therapies. In the context of conventional chemotherapy, some cells rapidly proliferate and therefore their replication machinery can be effectively targeted; however, other tumor cells quiesce and remain resistant to conventional chemotherapy. This cell population has been shown in some cases to provide the cells responsible for proliferation after remission [73]. A similar challenge might be expected for metabolic therapies, in that some cells within a tumor might not exhibit the same dependence and sensitivity that are being exploited to target the bulk of the tumor.

One source of tumor heterogeneity is the varying physical proximity of different parts of the tumor to the vasculature (Figure 2A). Proximity to vasculature provides pro-growth signaling to the tumor, as well as providing oxygen to fuel oxidative metabolism. Conversely, those regions of the tumor distant from vessels where oxygen is severely limited would be forced to adapt to a different metabolic regime within the hypoxic environment (Figure 2A). Transcriptional control of metabolic adaptations to hypoxia are regulated by **hypoxia-inducible factors** (HIFs), which are discussed further in Box 1.

In addition to spatially organized heterogeneity, it has recently been shown in the case of several solid tumors types that even adjacent cells adopt distinct metabolic programs (Figure 2B) [74]. One cell can perform aerobic glycolysis, which will generate lactate that is exported by one of the MCT transporters; an adjacent cell can then take up that lactate and, by the action of lactate dehydrogenase, convert the lactate to pyruvate for use in mitochondrial oxidation (Figure 2C) [75,76]. This phenomenon has been coined the 'reverse Warburg effect' and has also been described to occur between the tumor and tumor stroma [77,78].

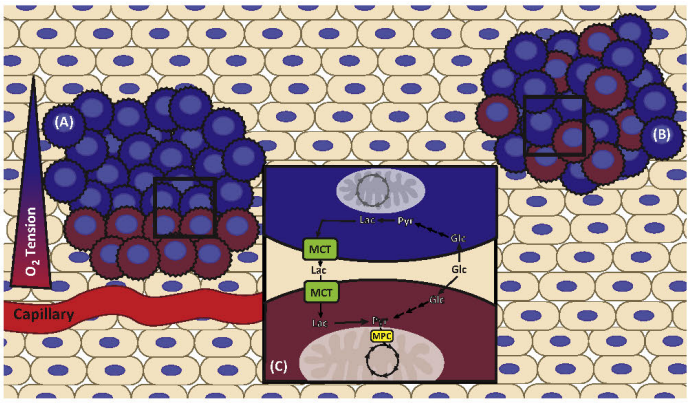

Trends in Biochemical Sciences

Figure 2. Metabolic Tumor Heterogeneity. Within a given tumor, adjacent cancer cells may operate under different metabolic regimes, lending to whole-tumor flexibility even if individual cancer cells (jagged edges) have limited metabolic flexibility. In the figure, two metabolic regimes are represented: one predominantly performing mitochondrial oxidation (red), the other predominantly performing aerobic glycolysis (blue). The architecture of metabolically heterogeneous tumors may be stratified by proximity of cancer cells to the vasculature, depending on nutrient and oxygen availability (A). Tumor heterogeneity may also be more interspersed, where stochastic mutations during the oncogenic process select for individual cells that may complement the metabolic needs of an adjacent cell or cancer cell (B). In this example (C), the blue cells perform glycolysis to convert glucose (Glc) to pyruvate (Pyr) and then to lactate (Lac) which is exported from the cell via the monocarboxylate transporter (MCT). The adjacent red cells can take up that lactate (via another MCT) and convert it to pyruvate for use in mitochondrial oxidation. It is likely that tumors comprise many more metabolic phenotypes than the simplistic two-part system illustrated here, based on the numerous mutations and aberrations to their metabolic machinery that are mutually selected for during oncogenesis.

Box 1. The Role of Hypoxia and HIF

Transcriptional regulation of the metabolic adaptation to hypoxia is largely driven by heterodimeric transcription factors, collectively known as the hypoxia-inducible factors (HIFs). Under conditions of normoxia, HIF activity is very low because the α subunits are rapidly degraded by the process of oxygen-dependent prolyl hydroxylation, binding of von Hippel–Lindau factor (VHL), E3 ubiquitin ligation, and proteasomal degradation [88,89]. In hypoxic conditions, however, HIF is stabilized and modulates the expression of several metabolic genes.

Some of the early discovered metabolic adaptations tied HIF to increased glucose uptake via the GLUT transporters [90,91] and an increased rate of glycolysis by upregulating expression of many glycolytic enzymes [92–94], increased lactate production via LDH-A [94], and lactate excretion by MCT4 [95,96]. In sum, these studies show that HIF may be a master regulator of glycolysis under hypoxic conditions. However, in 2006 two studies showed that not only does HIF promote glycolysis but it represses mitochondrial oxidation by increasing the expression of PDK1 [97,98], thus inhibiting PDH and preventing pyruvate from entering the TCA cycle. Many cancer-associated mutations have been shown to increase HIF expression and/or stability [88], irrespective of cellular oxygen tension. These important discoveries revived study of the Warburg effect, and provided rationale for the development of HIF inhibitors that could theoretically reverse the Warburg effect in one fell swoop. The study, development, and clinical application of HIF regulation and inhibition is complex and ever-evolving, and we refer the reader to recent reviews for more in-depth discussion of this topic [99–103].

The combination of both glycolytic and oxidative cells within a tumor poses significant therapeutic challenges, even if the cells themselves are metabolically inflexible. For example, treatment with an LDH or MCT inhibitor may successfully target the glycolytic population of cells within a tumor by depleting NAD^+ and/or decreasing the intracellular pH. However, those cells with an oxidative metabolic regime would be largely unaffected by such a treatment strategy because they may not employ the same isoforms of LDH or MCT. This would pose a particularly

unfortunate therapeutic problem because it has been shown that oxidative phosphorylation and mitochondrial carbon oxidation are essential for metastasis [79] and the epithelial–mesenchymal transition [80] in several solid tumor types. The outcome of the therapy, while potentially debulking the primary lesion, could result in an increasingly malignant and nefarious population of cancer cells. In effect, the metabolic heterogeneity within a tumor could provide whole-tumor 'metabolic flexibility'.

Another challenge inherent to targeting cancer cell metabolism is that normal stem cells frequently have a very similar metabolic phenotype [81]. Stem cells, perhaps because of their need to avoid oxidative damage or to thrive in a hypoxic niche [82,83], often adopt a glycolytic metabolic phenotype. In this situation, the cytotoxic effects of forcing a glycolytic tumor to engage mitochondrial oxidative metabolism could also damage the stem cell compartment [84], and this would result in similar toxicities to conventional chemotherapeutics. To truly achieve stem cell-sparing metabolic therapies, we must further understand the differences between the metabolic phenotypes of cancer cells and stem cells, while realizing that each tumor and each stem cell niche contains a heterogeneous cell population.

Beyond merely having similar physiology, the transcriptional and signaling drivers of the metabolic profiles of cancer and stem cells also seem to be similar. The pre-eminent example of this role duality is the oncogenic transcription factor Myc. On the one hand, Myc amplification and activation is found in numerous solid and lymphoid tumors, and its constitutive activation results in a dramatic and deranged metabolic program favoring a glycolytic phenotype by both activating and repressing numerous metabolic genes involved in glycolysis and glutaminolysis [85]. On the other hand, it has been shown that Myc is essential for maintaining stem cell self-renewal and pluripotency [86,87]. In both cases, key outputs for Myc include those that promote a glycolytic phenotype.

With such regulatory mechanisms common to both stem cells and cancer, we clearly need a new and improved level of understanding of both systems to enable us to kill one cell while sparing the other. One specific reason for hope is that the adaptations of cancer cells might have come at the cost of losing metabolic flexibility that is otherwise retained within the stem cell population. Another reason for optimism is that our growing understanding will teach us how to design combination therapies that will increase the metabolic therapeutic window enough that cancer cells are specifically targeted.

Concluding Remarks

There is much excitement and renewed fervor in the study of metabolism, and particularly in its application to cancer. A new appreciation of its complexity and dynamism provides a spatial and temporal elaboration on the rigid maps of Dr Nicholson. The key to moving forward (see Outstanding Questions) is determining where the flexibility exists, where it is lost, and how to best exploit the inflexibilities that characterize some cancer cells. There are many substantial difficulties in targeting these metabolic inflexibilities in cancer, in particularly those surrounding pyruvate metabolism. That cancer and stem cells share metabolic phenotype and machinery is a particularly troublesome hurdle, as is the metabolic heterogeneity of tumors.

Despite these challenges, there are great possibilities. To be successful we must understand and evaluate each tumor on an individual basis, and balance targeting its inflexibilities with sparing sensitive normal cells. Recent discoveries are providing insight with which to understand why particular metabolic modulators are effective and others are not, and why some cancers respond and others do not. We are already seeing early successes of metabolic therapy in combination with conventional chemotherapy, such as with DCA and cisplatin. As the metabolic adaptations of cancers come more sharply into focus, so too will our ability to target them,

Outstanding Questions

Through the lens of newly discovered metabolic enzymes and regulators, such as the MPC, can we determine why previous therapeutic metabolic modulators have been inefficient, and can we make them more effective?

How can we identify scenarios where tumor metabolic flexibility is sufficiently limited to favor responsiveness to metabolic modulators, either alone or in combination with conventional chemotherapeutics?

Is it possible to better define tumor metabolic heterogeneity to target it in a way that eradicates metabolically symbiotic cancer cells?

Is the metabolic regime of stem cells sufficiently more flexible than cancer cells such that we can create stem cell-sparing metabolic therapies that retain potent anticancer efficacy?

increasing our therapeutic precision and creating the potential for stem cell-sparing therapies. We have just begun a great odyssey, one that will inevitably be filled with great difficulty, but there is great promise that this path will lead us to the goal of more safe and effective therapies for cancer.

Acknowledgments

The authors would like to thank Drs Matt Vander Heiden and Ralph DeBerardinis for their critical appraisal of this review. Related work in the laboratory of J.R. is supported by the Howard Hughes Medical Institute, the Nora Eccles Treadwell Foundation, the National Institutes of Health (NIH; grant R01 GM094232 to J.R.), and NIH Hematology Training grant T32 DK007115 (to K.A.O.).

References

1. Azzi, A. (2012) In memory of Donald Nicholson. *IUBMB Life* 648, 659–660
2. Petersen, K.F. *et al.* (2015) Effect of aging on muscle mitochondrial substrate utilization in humans. *Proc. Natl. Acad. Sci. U.S.A.* 112, 11330–11334
3. Takubo, K. *et al.* (2013) Regulation of glycolysis by Pdk functions as a metabolic checkpoint for cell cycle quiescence in hematopoietic stem cells. *Cell Stem Cell* 12, 49–61
4. Yu, W-M. *et al.* (2013) Metabolic regulation by the mitochondrial phosphatase PTPMT1 is required for hematopoietic stem cell differentiation. *Cell Stem Cell* 12, 62–74
5. Vacanti, N.M. *et al.* (2014) Regulation of substrate utilization by the mitochondrial pyruvate carrier. *Mol. Cell* 56, 425–435
6. Gray, L.R. *et al.* (2015) Hepatic mitochondrial pyruvate carrier 1 is required for efficient regulation of gluconeogenesis and whole-body glucose homeostasis. *Cell Metab.* 22, 669–681
7. McCommis, K.S. *et al.* (2015) Loss of mitochondrial pyruvate carrier 2 in the liver leads to defects in gluconeogenesis and compensation via pyruvate-alanine cycling. *Cell Metab.* 22, 682–694
8. Bishop, S.P. and Altschuld, R.A. (1970) Increased glycolytic metabolism in cardiac hypertrophy and congestive failure. *Am. J. Physiol.* 218, 153–159
9. Breckenridge, R.A. *et al.* (2013) Hypoxic regulation of hand1 controls the fetal-neonatal switch in cardiac metabolism. *PLoS Biol.* 11, e1001666
10. Goodwin, G.W. *et al.* (2000) Improved energy homeostasis of the heart in the metabolic state of exercise. *Am. J. Physiol. Heart Circ. Physiol.* 279, H1490–H1501
11. Masoud, W.G.T. *et al.* (2014) Failing mouse hearts utilize energy inefficiently and benefit from improved coupling of glycolysis and glucose oxidation. *Cardiovasc. Res.* 101, 30–38
12. Melenovsky, V. *et al.* (2012) Availability of energetic substrates and exercise performance in heart failure with or without diabetes. *Eur. J. Heart Fail.* 14, 754–763
13. Ussher, J.R. *et al.* (2012) Stimulation of glucose oxidation protects against acute myocardial infarction and reperfusion injury. *Cardiovasc. Res.* 94, 359–369
14. Doenst, T. *et al.* (2013) Cardiac metabolism in heart failure: implications beyond ATP production. *Circ. Res.* 113, 709–724
15. Martínez-Zamora, A. *et al.* (2015) Defective expression of the mitochondrial-tRNA modifying enzyme GTPBP3 triggers AMPK-mediated adaptive responses involving complex I assembly factors, uncoupling protein 2, and the mitochondrial pyruvate carrier. *PLoS ONE* 10, e0144273
16. Fernández-Caggiano, M. *et al.* (2016) Analysis of mitochondrial proteins in the surviving myocardium after ischemia identifies mitochondrial pyruvate carrier expression as possible mediator of tissue viability. *Mol. Cell Proteomics* 15, 246–255
17. Goulston, A. (1911) A note on the beneficial effect of the ingestion of cane sugar in certain forms of heart disease. *BMJ* 1, 615
18. Hanahan, D. and Weinberg, R.A. (2011) Hallmarks of cancer: the next generation. *Cell* 144, 646–674
19. Bardella, C. *et al.* (2011) SDH mutations in cancer. *Biochim. Biophys. Acta* 1807, 1432–1443
20. King, A. *et al.* (2006) Succinate dehydrogenase and fumarate hydratase: linking mitochondrial dysfunction and cancer. *Oncogene* 25, 4675–4682
21. Rutter, J. *et al.* (2010) Succinate dehydrogenase – assembly, regulation and role in human disease. *Mitochondrion* 10, 393–401
22. Warburg, O. *et al.* (1927) The metabolism of tumors in the body. *J. Gen. Physiol.* 8, 519–530
23. Halestrap, A.P. and Wilson, M.C. (2012) The monocarboxylate transporter family – role and regulation. *IUBMB Life* 64, 109–119
24. Halestrap, A.P. (2012) The monocarboxylate transporter family – structure and functional characterization. *IUBMB Life* 64, 1–9
25. Boroughs, L.K. and DeBerardinis, R.J. (2015) Metabolic pathways promoting cancer cell survival and growth. *Nat. Cell Biol.* 17, 351–359
26. DeNicola, G.M. and Cantley, L.C. (2015) Cancer's fuel choice: new flavors for a picky eater. *Mol. Cell* 60, 514–523
27. Li, Z. *et al.* (2014) The multifaceted regulation and functions of PKM2 in tumor progression. *Biochim. Biophys. Acta* 1846, 285–296
28. Desai, S. *et al.* (2013) Tissue-specific isoform switch and DNA hypomethylation of the pyruvate kinase PKM gene in human cancers. *Oncotarget* 5, 8202–8210
29. Christofk, H.R. *et al.* (2008) Pyruvate kinase M2 is a phosphotyrosine-binding protein. *Nature* 452, 181–186
30. Christofk, H.R. *et al.* (2008) The M2 splice isoform of pyruvate kinase is important for cancer metabolism and tumour growth. *Nature* 452, 230–233
31. Bettaieb, A. *et al.* (2013) Protein tyrosine phosphatase 1B regulates pyruvate kinase M2 tyrosine phosphorylation. *J. Biol. Chem.* 288, 17360–17371
32. Anastasiou, D. *et al.* (2012) Pyruvate kinase M2 activators promote tetramer formation and suppress tumorigenesis. *Nat. Chem. Biol.* 8, 839–847
33. Lunt, S.Y. *et al.* (2015) Pyruvate kinase isoform expression alters nucleotide synthesis to impact cell proliferation. *Mol. Cell* 57, 95–107
34. Birsoy, K. *et al.* (2015) An essential role of the mitochondrial electron transport chain in cell proliferation is to enable aspartate synthesis. *Cell* 162, 540–551
35. Sullivan, L.B. *et al.* (2015) Supporting aspartate biosynthesis is an essential function of respiration in proliferating cells. *Cell* 162, 552–563
36. Miao, P. *et al.* (2013) Lactate dehydrogenase a in cancer: a promising target for diagnosis and therapy. *IUBMB Life* 65, 904–910
37. Le, A. *et al.* (2010) Inhibition of lactate dehydrogenase A induces oxidative stress and inhibits tumor progression. *Proc. Natl. Acad. Sci. U.S.A.* 107, 2037–2042
38. Fantin, V.R. *et al.* (2006) Attenuation of LDH-A expression uncovers a link between glycolysis, mitochondrial physiology, and tumor maintenance. *Cancer Cell* 9, 425–434
39. Xie, H. *et al.* (2014) Targeting lactate dehydrogenase-A inhibits tumorigenesis and tumor progression in mouse models of lung cancer and impacts tumor-initiating cells. *Cell Metab.* 19, 795–809

40. Sheng, S.L. *et al.* (2012) Knockdown of lactate dehydrogenase A suppresses tumor growth and metastasis of human hepatocellular carcinoma. *FEBS J.* 279, 3898–3910
41. Wang, J. *et al.* (2015) Lactate dehydrogenase A negatively regulated by miRNAs promotes aerobic glycolysis and is increased in colorectal cancer. *Oncotarget* 6, 19456–19468
42. Zhu, J. *et al.* (2014) Monocarboxylate transporter 4 facilitates cell proliferation and migration and is associated with poor prognosis in oral squamous cell carcinoma patients. *PLoS ONE* 9, e87904
43. Witkiewicz, A.K. *et al.* (2012) Using the 'reverse Warburg effect' to identify high-risk breast cancer patients: stromal MCT4 predicts poor clinical outcome in triple-negative breast cancers. *Cell Cycle* 11, 1108–1117
44. Nakayama, Y. (2012) Prognostic significance of monocarboxylate transporter 4 expression in patients with colorectal cancer. *Exp. Ther. Med.* 3, 25–30
45. Baek, G. *et al.* (2014) MCT4 defines a glycolytic subtype of pancreatic cancer with poor prognosis and unique metabolic dependencies. *Cell Rep.* 9, 2233–2249
46. Hao, J. *et al.* (2010) Co-expression of CD147 (EMMPRIN), CD44v3-10, MDR1 and monocarboxylate transporters is associated with prostate cancer drug resistance and progression. *Br. J. Cancer* 103, 1008–1018
47. Herzig, S. *et al.* (2012) Identification and functional expression of the mitochondrial pyruvate carrier. *Science* 337, 93–96
48. Bricker, D.K. *et al.* (2012) A mitochondrial pyruvate carrier required for pyruvate uptake in yeast, Drosophila, and humans. *Science* 337, 96–100
49. Schell, J.C. *et al.* (2014) A role for the mitochondrial pyruvate carrier as a repressor of the Warburg effect and colon cancer cell growth. *Mol. Cell* 56, 400–413
50. Liang, L. *et al.* (2015) Sirt3 binds to and deacetylates mitochondrial pyruvate carrier 1 to enhance its activity. *Biochem. Biophys. Res. Commun.* 468, 807–812
51. Kaplon, J. *et al.* (2013) A key role for mitochondrial gatekeeper pyruvate dehydrogenase in oncogene-induced senescence. *Nature* 498, 109–112
52. Fujiwara, S. *et al.* (2013) PDK1 inhibition is a novel therapeutic target in multiple myeloma. *Br. J. Cancer* 108, 170–178
53. Hitosugi, T. *et al.* (2011) Tyrosine phosphorylation of mitochondrial pyruvate dehydrogenase kinase 1 is important for cancer metabolism. *Mol. Cell* 44, 864–877
54. Comerford, S.A. *et al.* (2014) Acetate dependence of tumors. *Cell* 159, 1591–1602
55. Schug, Z.T. *et al.* (2015) Acetyl-CoA synthetase 2 promotes acetate utilization and maintains cancer cell growth under metabolic stress. *Cancer Cell* 27, 57–71
56. Mashimo, T. *et al.* (2014) Acetate is a bioenergetic substrate for human glioblastoma and brain metastases. *Cell* 159, 1603–1614
57. Stacpoole, P.W. and Felts, J.M. (1970) Diisopropylammonium dichloroacetate (DIPA) and sodium dichloracetate (DCA): effect on glucose and fat metabolism in normal and diabetic tissue. *Metab. Clin. Exp.* 19, 71–78
58. Whitehouse, S. *et al.* (1974) Mechanism of activation of pyruvate dehydrogenase by dichloroacetate and other halogenated carboxylic acids. *Biochem. J.* 141, 761–774
59. Bonnet, S. *et al.* (2007) A mitochondria-K$^+$ channel axis is suppressed in cancer and its normalization promotes apoptosis and inhibits cancer growth. *Cancer Cell* 11, 37–51
60. Strum, S.B. *et al.* (2012) Case report: sodium dichloroacetate (DCA) inhibition of the 'Warburg effect' in a human cancer patient: complete response in non-Hodgkin's lymphoma after disease progression with rituximab-CHOP. *J. Bioenerg. Biomembr.* 45, 307–315
61. Olszewski, U. *et al.* (2010) In vitro cytotoxicity of combinations of dichloroacetate with anticancer platinum compounds. *Clin. Pharmacol.* 2, 177–183
62. Garon, E.B. *et al.* (2014) Dichloroacetate should be considered with platinum-based chemotherapy in hypoxic tumors rather than as a single agent in advanced non-small cell lung cancer. *J. Cancer Res. Clin. Oncol.* 140, 443–452
63. Roh, J-L. *et al.* (2015) Activation of mitochondrial oxidation by PDK2 inhibition reverses cisplatin resistance in head and neck cancer. *Cancer Lett.*
64. De Preter, G. *et al.* (2015) Inhibition of the pentose phosphate pathway by dichloroacetate unravels a missing link between aerobic glycolysis and cancer cell proliferation. *Oncotarget* 5, Published online November 2, 2015. http://dx.doi.org/10.18632/oncotarget.6272
65. Delaney, L.M. *et al.* (2015) Dichloroacetate affects proliferation but not survival of human colorectal cancer cells. *Apoptosis* 20, 63–74
66. Ho, N. and Coomber, B.L. (2015) Pyruvate dehydrogenase kinase expression and metabolic changes following dichloroacetate exposure in anoxic human colorectal cancer cells. *Exp. Cell Res.* 331, 73–81
67. Shahrzad, S. *et al.* (2010) Sodium dichloroacetate (DCA) reduces apoptosis in colorectal tumor hypoxia. *Cancer Lett.* 297, 75–83
68. Feuerecker, B. *et al.* (2015) DCA promotes progression of neuroblastoma tumors in nude mice. *Am. J. Cancer Res.* 5, 812–820
69. Tibiletti, M.G. *et al.* (1998) Physical map of the D6S149-D6S193 region on chromosome 6Q27 and its involvement in benign surface epithelial ovarian tumours. *Oncogene* 16, 1639–1642
70. Yang, C. *et al.* (2014) Glutamine oxidation maintains the TCA cycle and cell survival during impaired mitochondrial pyruvate transport. *Mol. Cell* 56, 414–424
71. Marusyk, A. and Polyak, K. (2010) Tumor heterogeneity: causes and consequences. *Biochim. Biophys. Acta* 1805, 105–117
72. Pribluda, A. *et al.* (2015) Intratumoral heterogeneity: from diversity comes resistance. *Clin. Cancer Res.* 21, 2916–2923
73. Abelson, S. *et al.* (2012) Intratumoral heterogeneity in the self-renewal and tumorigenic differentiation of ovarian cancer. *Stem Cells* 30, 415–424
74. Son, S.H. *et al.* (2014) Prognostic implication of intratumoral metabolic heterogeneity in invasive ductal carcinoma of the breast. *BMC Cancer* 14, 585
75. Sonveaux, P. *et al.* (2008) Targeting lactate-fueled respiration selectively kills hypoxic tumor cells in mice. *J. Clin. Invest.* 118, 3930–3942
76. McGillen, J.B. *et al.* (2014) Glucose–lactate metabolic cooperation in cancer: insights from a spatial mathematical model and implications for targeted therapy. *J. Theor. Biol.* 361, 190–203
77. Martinez-Outschoorn, U.E. *et al.* (2014) Catabolic cancer-associated fibroblasts transfer energy and biomass to anabolic cancer cells, fueling tumor growth. *Semin. Cancer Biol.* 25, 47–60
78. Fiaschi, T. *et al.* (2012) Reciprocal metabolic reprogramming through lactate shuttle coordinately influences tumor-stroma interplay. *Cancer Res.* 72, 5130–5140
79. LeBleu, V.S. *et al.* (2014) PGC-1α mediates mitochondrial biogenesis and oxidative phosphorylation in cancer cells to promote metastasis. *Nat. Cell Biol.* 16, 992–1003
80. Hamabe, A. *et al.* (2014) Role of pyruvate kinase M2 in transcriptional regulation leading to epithelial-mesenchymal transition. *Proc. Natl. Acad. Sci. U.S.A.* 111, 15526–15531
81. Ito, K. and Suda, T. (2014) Metabolic requirements for the maintenance of self-renewing stem cells. *Nat. Rev. Mol. Cell Biol.* 15, 243–256
82. Suda, T. *et al.* (2011) Metabolic regulation of hematopoietic stem cells in the hypoxic niche. *Cell Stem Cell* 9, 298–310
83. Ushio-Fukai, M. and Rehman, J. (2014) Redox and metabolic regulation of stem/progenitor cells and their niche. *Antioxid. Redox Signal.* 21, 1587–1590
84. Rodrigues, A.S. *et al.* (2015) Differentiate or die: 3-bromopyruvate and pluripotency in mouse embryonic stem cells. *PLoS ONE* 10, e0135617
85. Dang, C.V. (2013) MYC, metabolism, cell growth, and tumorigenesis. *Cold Spring Harb. Perspect. Med.* 3, 1–15
86. Wilson, A. *et al.* (2004) c-Myc controls the balance between hematopoietic stem cell self-renewal and differentiation. *Genes Dev.* 18, 2747–2763
87. Varlakhanova, N.V. *et al.* (2010) Myc maintains embryonic stem cell pluripotency and self-renewal. *Differentiation* 80, 9–19

88. Maxwell, P.H. *et al.* (1999) The tumour suppressor protein VHL targets hypoxia-inducible factors for oxygen-dependent proteolysis. *Nature* 399, 271–275
89. Bruick, R.K. and McKnight, S.L. (2001) A conserved family of prolyl-4-hydroxylases that modify HIF. *Science* 294, 1337–1340
90. Chen, C. *et al.* (2001) Regulation of glut1 mRNA by hypoxia-inducible factor-1. Interaction between H-ras and hypoxia. *J. Biol. Chem.* 276, 9519–9525
91. Gleadle, J.M. and Ratcliffe, P.J. (1997) Induction of hypoxia-inducible factor-1, erythropoietin, vascular endothelial growth factor, and glucose transporter-1 by hypoxia: evidence against a regulatory role for Src kinase. *Blood* 89, 503–509
92. Mathupala, S.P. *et al.* (2001) Glucose catabolism in cancer cells: identification and characterization of a marked activation response of the type II hexokinase gene to hypoxic conditions. *J. Biol. Chem.* 276, 43407–43412
93. Iyer, N.V. *et al.* (1998) Cellular and developmental control of O_2 homeostasis by hypoxia-inducible factor 1 alpha. *Genes Dev.* 12, 149–162
94. Semenza, G.L. *et al.* (1996) Hypoxia response elements in the aldolase A, enolase 1, and lactate dehydrogenase A gene promoters contain essential binding sites for hypoxia-inducible factor 1. *J. Biol. Chem.* 271, 32529–32537
95. Ullah, M.S. *et al.* (2006) The plasma membrane lactate transporter MCT4, but not MCT1, is up-regulated by hypoxia through a HIF-1alpha-dependent mechanism. *J. Biol. Chem.* 281, 9030–9037
96. Rosafio, K. and Pellerin, L. (2014) Oxygen tension controls the expression of the monocarboxylate transporter MCT4 in cultured mouse cortical astrocytes via a hypoxia-inducible factor-1α-mediated transcriptional regulation. *Glia* 62, 477–490
97. Kim, J-W. *et al.* (2006) HIF-1-mediated expression of pyruvate dehydrogenase kinase: a metabolic switch required for cellular adaptation to hypoxia. *Cell Metab.* 3, 177–185
98. Papandreou, I. *et al.* (2006) HIF-1 mediates adaptation to hypoxia by actively downregulating mitochondrial oxygen consumption. *Cell Metab.* 3, 187–197
99. Denko, N.C. (2008) Hypoxia, HIF1 and glucose metabolism in the solid tumour. *Nat. Rev. Cancer* 8, 705–713
100. Keith, B. *et al.* (2012) HIF1α and HIF2α: sibling rivalry in hypoxic tumour growth and progression. *Nat. Rev. Cancer* 12, 9–22
101. Semenza, G.L. (2013) HIF-1 mediates metabolic responses to intratumoral hypoxia and oncogenic mutations. *J. Clin. Invest.* 123, 3664–3671
102. Denko, N.C. (2014) Hypoxic regulation of metabolism offers new opportunities for anticancer therapy. *Expert Rev. Anticancer Ther.* 14, 979–981
103. Masoud, G.N. and Li, W. (2015) HIF-1α pathway: role, regulation and intervention for cancer therapy. *Acta Pharm. Sin. B* 5, 378–389

CHAPTER 3

A ROLE FOR THE MITOCHONDRIAL PYRUVATE CARRIER AS A REPRESSOR OF THE WARBURG EFFECT AND COLON CANCER CELL GROWTH

John C. Schell*, Kristofor A. Olson*, Lei Jiang, Amy J. Hawkins, Jonathan G. Van Vranken, Jianxin Xie, Robert A. Egnatchik, Espen G. Earl, Ralph J. DeBerardinis and Jared Rutter

*Co-first authors

Reprinted from Molecular Cell, 56(3), doi: 10.1016/j.molcel.2014.09.026,

Molecular Cell
Article

A Role for the Mitochondrial Pyruvate Carrier as a Repressor of the Warburg Effect and Colon Cancer Cell Growth

John C. Schell,[1,4] Kristofor A. Olson,[1,4] Lei Jiang,[2] Amy J. Hawkins,[1] Jonathan G. Van Vranken,[1] Jianxin Xie,[3] Robert A. Egnatchik,[2] Espen G. Earl,[1] Ralph J. DeBerardinis,[2] and Jared Rutter[1,*]
[1]Department of Biochemistry, University of Utah School of Medicine, Salt Lake City, UT 84112-5650, USA
[2]Children's Medical Center Research Institute, UT Southwestern Medical Center, Dallas, TX 75390-8502, USA
[3]Cell Signaling Technology, Inc., Danvers, MA 01923, USA
[4]Co-first Authors
*Correspondence: rutter@biochem.utah.edu
http://dx.doi.org/10.1016/j.molcel.2014.09.026

SUMMARY

Cancer cells are typically subject to profound metabolic alterations, including the Warburg effect wherein cancer cells oxidize a decreased fraction of the pyruvate generated from glycolysis. We show herein that the mitochondrial pyruvate carrier (MPC), composed of the products of the *MPC1* and *MPC2* genes, modulates fractional pyruvate oxidation. *MPC1* is deleted or underexpressed in multiple cancers and correlates with poor prognosis. Cancer cells re-expressing *MPC1* and *MPC2* display increased mitochondrial pyruvate oxidation, with no changes in cell growth in adherent culture. MPC re-expression exerted profound effects in anchorage-independent growth conditions, however, including impaired colony formation in soft agar, spheroid formation, and xenograft growth. We also observed a decrease in markers of stemness and traced the growth effects of MPC expression to the stem cell compartment. We propose that reduced MPC activity is an important aspect of cancer metabolism, perhaps through altering the maintenance and fate of stem cells.

INTRODUCTION

The fate of pyruvate is one of the most important metabolic decisions made by eukaryotic cells. Most differentiated mammalian cells direct pyruvate into mitochondria where it is oxidized for efficient ATP production. Cancer cells, however, divert pyruvate and its precursors to fuel other anabolic processes or convert it to lactate for excretion from the cell (Vander Heiden et al., 2009). This metabolic adaptation was first described by the eminent biochemist Otto Warburg in the 1920s and is known as the Warburg effect (Warburg et al., 1927). Multiple mechanisms contribute to this metabolic derangement in cancer, but the synthesis and metabolism of pyruvate play a central role (Bayley and Devilee, 2012).

First, the synthesis of pyruvate in glycolysis is catalyzed by pyruvate kinase. Cancer cells tend to express a partially inhibited splice variant of pyruvate kinase (PK-M2), leading to decreased pyruvate production (Christofk et al., 2008a; Christofk et al., 2008b; Luo and Semenza, 2011; Yang et al., 2011; Yeh et al., 2008). Second, the two proteins that mediate pyruvate conversion to lactate and its export, lactate dehydrogenase A (LDHA) and the monocarboxylate transporter MCT-4, are commonly upregulated in cancer cells leading to decreased pyruvate oxidation (Azuma et al., 2007; Le Floch et al., 2011; Gotanda et al., 2013; Koukourakis et al., 2003; Pinheiro et al., 2008). Third, the enzymatic step following mitochondrial entry is the conversion of pyruvate to acetyl-CoA by the pyruvate dehydrogenase (PDH) complex. Cancer cells frequently exhibit increased expression of the PDH kinase PDK1, which phosphorylates and inactivates PDH (Kim et al., 2006; McFate et al., 2008). This PDH regulatory mechanism is required for oncogene-induced transformation and reversed in oncogene-induced senescence (Kaplon et al., 2013). Further, the PDK inhibitor dichloroacetate has shown some clinical efficacy, which correlates with increased pyruvate oxidation (Michelakis et al., 2010). Altered pyruvate metabolism appears to be critical in enabling and promoting the transformed phenotype in many cancers.

One of the simplest mechanisms to explain decreased mitochondrial pyruvate oxidation in cancer cells, a loss of mitochondrial pyruvate import, has been observed repeatedly over the past 40 years (Eboli et al., 1977; Paradies et al., 1983). This process has been impossible to study at a molecular level until recently, however, as the identities of the protein(s) that mediate mitochondrial pyruvate uptake were unknown (Halestrap, 1975; Papa and Paradies, 1974). We and others recently described the mitochondrial pyruvate carrier (MPC) as a multimeric complex that is necessary for efficient mitochondrial pyruvate uptake (Bricker et al., 2012; Herzig et al., 2012). The MPC contains two distinct proteins, MPC1 and MPC2; the absence of either leads to a loss of mitochondrial pyruvate uptake and utilization in yeast, flies, and mammalian cells (Bricker et al., 2012; Herzig et al., 2012). Several groups subsequently confirmed this discovery in multiple contexts (Colca et al., 2013; Divakaruni et al., 2013; Li et al., 2014; Patterson et al., 2014; Rohatgi et al., 2013; Timón-Gómez et al., 2013).

Identification of the MPC genes and proteins finally permits the use of molecular genetics to interrogate the contribution of mitochondrial pyruvate uptake to cancer metabolism. Given the decades-old observation that the MPC might be inactivated in cancer cell lines and tumors (Eboli et al., 1977; Paradies et al., 1983) and the decrease in pyruvate oxidation associated with the Warburg effect, we first asked whether MPC expression or activity is lost in cancer. Indeed both genes, but particularly *MPC1*, are underexpressed or deleted in most cancers, and low expression correlates with poor survival. To determine whether MPC underexpression is an important feature of cancer, we re-expressed *MPC1* and *MPC2* in colon cancer cells and assessed their metabolic and proliferative phenotypes. MPC-expressing cells exhibited enhanced pyruvate oxidation and decreased glycolysis, consistent with reversal of the Warburg effect. While growth in standard adherent cell culture was unaffected, MPC re-expression impaired anchorage-independent growth, including in mouse xenograft assays. This was accompanied by decreased expression of stem cell markers. These data lead us to conclude that decreased MPC expression promotes the Warburg effect and the maintenance of stemness in colon cancer cells.

RESULTS

The discovery of the genes that encode the MPC enabled the assessment of the genomic status, expression, and impact of these genes in cancer. We first examined whether either *MPC1* or *MPC2* is deleted in cancer. While the genomic locus of *MPC2* does not appear to be frequently lost, *MPC1* is found within the most frequently deleted region across all cancer sample sets surveyed: 6q27 (Figure 1A) (Cai et al., 2014). The data are particularly striking for ovarian cancer, wherein 6q27 is deleted in 60%–80% of epithelial ovarian carcinoma (Figure S1A available online) (Tibiletti et al., 1998). The minimal interval of this deletion has been determined to contain only three genes, one of which is *MPC1* (Bignone et al., 2007; Liu et al., 2002). Colon and rectal cancer risk associates strongly with various haplotypes that include the *MPC1* locus (Slattery et al., 2011). In addition, this region is frequently deleted in ulcerative colitis patients with neoplastic transformation (Chen et al., 2005). Low *MPC1* expression correlates with poor survival in almost all cancers examined, including colon, kidney, lung, bladder, and brain (Figures 1B and S1B) (Aguirre-Gamboa et al., 2013). The correlation of survival with *MPC2* expression was more variable but was associated with poor prognosis in kidney and colon cancers (Figure S1C). The correlation of low *MPC1* expression with poor survival is more significant (Hazard Ratio [HR] = 3.16, $p = 0.02575$) than a number of metabolic genes with validated roles in the cancer phenotype, including low *PDHA1* ($p = 0.1603$), high *PKM2* ($p = 0.1232$), high *LDHA* ($p = 0.2442$), high *MCT1* ($p = 0.09482$), and high *MCT4* ($p = 0.1115$).

We next investigated whether *MPC1* or *MPC2* gene expression is altered in a variety of cancers. *MPC2* was inconsistent, being underexpressed in some cancers and overexpressed in others (Figure 1C) (Rhodes et al., 2004). *MPC1*, however, was underexpressed in all cancers examined with the exception of the hematologic malignancies, leukemia and lymphoma (Figure 1C). The data were particularly striking for colon adenocarcinoma, wherein the *MPC1* and *MPC2* mRNAs are both at much lower abundance in tumor compared to normal tissue (Figure 1D). MPC1 protein was also decreased in colon adenocarcinoma (Figure 1E). When we examined the statistical relationships between *MPC1* and *MPC2* expression along with a variety of other tumor suppressors, oncogenes, and metabolic genes in colorectal cancer, we found that *MPC1* and *MPC2* expression was positively correlated as expected (Figure 1F). The expression of *MPC1* was negatively correlated with the *MYC* oncogene and positively correlated with the colon tumor suppressor *APC* (Figure 1F) (Cerami et al., 2012; Gao et al., 2013; Network, 2012).

These data demonstrate that *MPC1*, and perhaps *MPC2*, associate with cancer risk, with deletion or underexpression being strongly correlated with cancer onset and poor prognosis (Figure S1D) (Hong et al., 2007). Reductions in *MPC1* expression were not general to the locus, as the adjacent gene, *RPS6KA2*, was increased in early onset colorectal cancer (Figure S1D). To begin to address the functional relevance of these findings, *MPC1* and *MPC2* expressions were assessed in a variety of transformed and untransformed cell lines. We found consistently low expression among colon cancer cell lines, particularly as compared to leukemia and lymphoma. Embryonal carcinoma cells were the only cancer type that exhibited levels of *MPC1* and *MPC2* expression consistently lower than those found in colon cancer (Figure 1G).

Based on the consistent observation of reduced MPC expression, we employed a re-expression system to test the necessity of low MPC expression for the metabolic and proliferative phenotypes in colon cancer. We expressed *MPC1, MPC2,* or both in four different colon cancer cell lines: HCT116, HCT15, DLD1, and HT29. When expressed alone, MPC1 and MPC2 did not accumulate (Figure 2A), despite robust mRNA expression (Figure 2B). When both genes were expressed, however, both MPC1 and MPC2 accumulated in all cell lines (Figure 2A). We also expressed a combination of *MPC2* and the R97W mutant of *MPC1*, which we previously described in a human patient (Bricker et al., 2012). This mutant MPC1 protein appeared to be unstable, as it did not accumulate, despite wild-type mRNA abundance (Figures 2A and 2B). We had hoped that MPC1-R97W would be an appropriate negative control, but the lack of stability limits its utility, and therefore, we did not use it for subsequent experiments. While MPC1 and MPC2 protein abundance is greatly increased over endogenous expression in colon cancer cells, it is similar to higher MPC-expressing cancers and less than normal heart tissue (Figure 2C).

Both proteins colocalize with mitochondria as expected (Figure 2D), and subsequent experiments focused on the effects of *MPC1* and *MPC2* coexpression. When expressed together, MPC1 and MPC2 assembled into an intact MPC complex, identical to what we previously observed for the native MPC (Figures 2E and S2A) (Bricker et al., 2012). The re-expression of MPC1 and MPC2 had no consistent effect on the abundance of a variety of mitochondrial proteins or on a variety of enzymes relevant to pyruvate metabolism, including LDHA and PDH (Figures 2F and S2B). There was also no effect on mitochondrial morphology (Figure S2C), suggesting that increased MPC abundance does

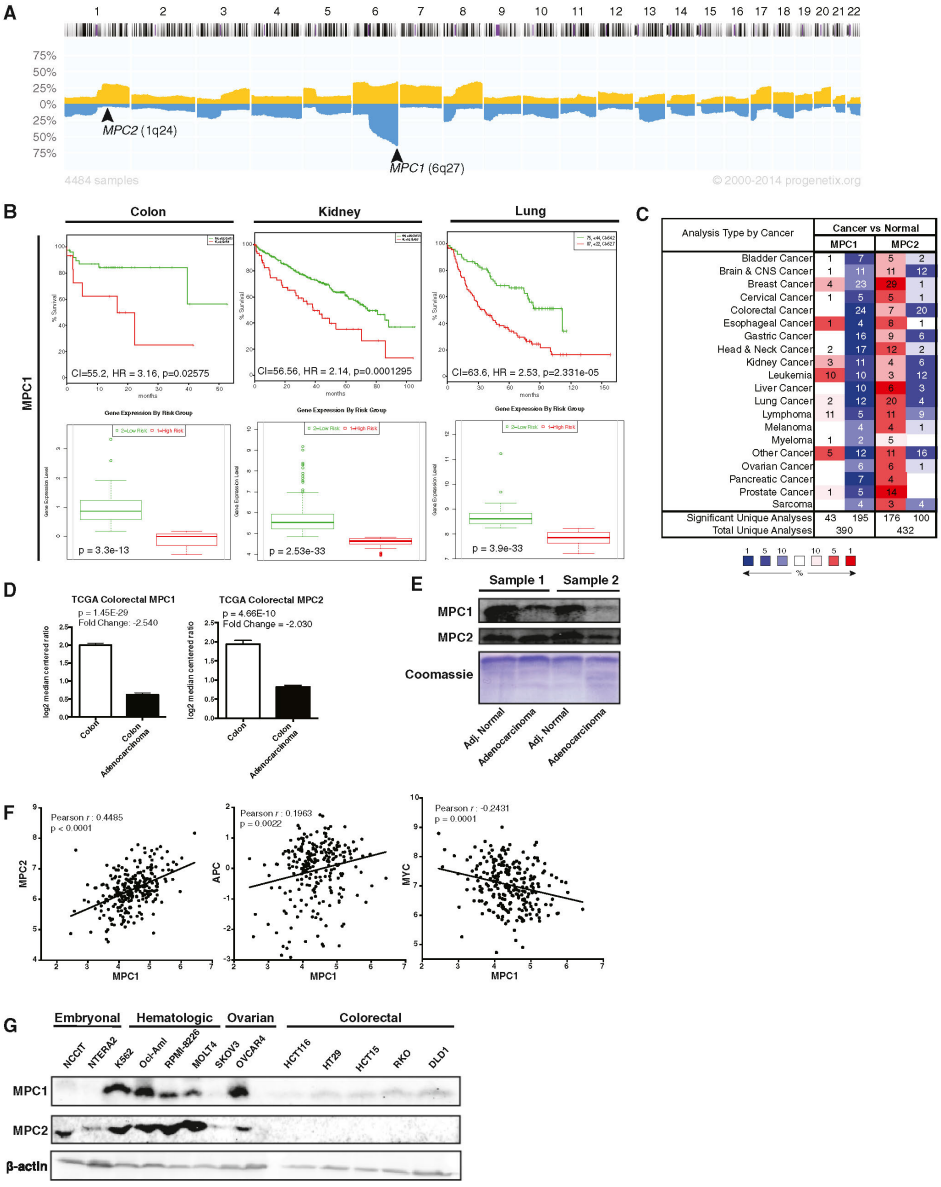

(legend on next page)

not grossly alter metabolic gene expression, or mitochondrial biogenesis or removal.

We next sought to assess the metabolic effects of MPC re-expression, focusing on the HCT15 and HT29 cell lines. MPC re-expression caused increased pyruvate oxidation, as measured by oxygen consumption with pyruvate as the sole substrate (Figure 3A). The magnitude of the effect was enhanced when measuring maximally stimulated pyruvate oxidation in the presence of FCCP (Figure 3A). We also performed isotope tracing to determine the fate of glucose-derived carbon (Figure 3B). After culture with D-[U-^{13}C]glucose, unlabeled citrate (m+0) was modestly reduced in cells re-expressing MPC, while higher-order citrate labeling (m+3, m+4, and m+5) was modestly increased (Figure 3C). Species that contain higher order labeling result from transfer of glucose-derived pyruvate into the mitochondria, followed by activity of PDH, pyruvate carboxylase, and TCA cycling (Figure 3C). Labeling differences were more pronounced at shorter labeling times; however, stable reductions in m+0 citrate suggest an increased rate of glucose contribution to the TCA cycle (Figure S3A). These data were further supported by in silico modeling experiments that varied pyruvate transport through the MPC (Figures S3B and S3C). In these experiments, m+0 citrate decreases significantly with increasing MPC flux due to the accumulation of ^{13}C in citrate resulting in higher abundances of m+3, m+4, and m+5, but with very small changes in the abundance of m+2 citrate. The modeled citrate abundances mirror closely the observed data upon MPC re-expression. As expected, we also observed a decrease in lactate production and extracellular acidification rate (ECAR) (Figures 3D and S3D). These data are all consistent with MPC expression increasing pyruvate flux into mitochondria for oxidation via the TCA cycle.

After pyruvate enters the mitochondria it is converted to acetyl-CoA by PDH, which is phosphorylated and inactivated by PDH kinases, including PDK1. Upon MPC expression, HT29 cells exhibited decreased PDK1 expression, decreased PDH phosphorylation, and increased PDH activity (Figures 3E and 3F). We did not observe the same effects in HCT15 cells, although we did observe increased $^{14}CO_2$ production from [1-^{14}C]-pyruvate (Figures 3F and S3E). In neither case did we observe a change in the activity of the TCA cycle enzyme citrate synthase (CS) (Figure 3G). Mitochondrial membrane potential was elevated upon MPC expression (Figure 3H), while reactive oxygen species (ROS) decreased in these cells (Figure 3I). As increased oxidative metabolism is often associated with increased generation of ROS, this result was surprising. Therefore, we also tested ROS levels in HCT116 and DLD1 cells with and without MPC re-expression and observed a similar effect (Figure S3F). While the mechanism remains to be determined, perhaps MPC re-expression leads to increased mitochondrial pyruvate, which is known to act as an antioxidant (Bassenge et al., 2000; Huang et al., 2013; Kang et al., 2001; Wang et al., 2007).

We next assessed the role of the MPC in cancer cell proliferation. MPC re-expression neither affected proliferation rate in adherent cell culture conditions (Figure 4A) nor altered cell viability, apoptosis, or necrosis (Figure 4B). We examined cell-cycle progression using an EdU pulse-chase and observed no difference in the timing or quantity of S phase entry or progression across a 24 hr time course (Figures 4C and S4A). We also assessed the effect of MPC re-expression on proliferation under nonadherent conditions, which are often used to model tumor initiation and metastasis. Interestingly, we found that *MPC1* and *MPC2* expression significantly suppressed colony formation in soft agar in both HCT15 and HT29 cells under a variety of different media conditions, from multiple independently derived biological replicates (Figure 4D; Table S1). As a complementary measure, we plated HCT15 and HT29 cells in low attachment dishes and monitored spheroid formation (Carpentino et al., 2009; Takaishi et al., 2009). MPC re-expression was maintained in low attachment culture (Figure S4B) and decreased the number and size of spheroids in both cell lines (Figures 4E and S4C). To confirm the specific role of pyruvate transport by the MPC in these effects, we treated cells with the MPC inhibitor UK5099 (Halestrap, 1975) and found that it rescued spheroid formation ability in both cell lines (Figure 4F).

We extended these studies to xenograft assays in nude mice. In both HCT15 and HT29 cell lines, MPC re-expression slowed tumor growth across the 40-day course of the experiment (Figures 5A and 5B). Upon completion of the experiment, we examined MPC1 and MPC2 protein content and found it to be similar to the parental cells (Figure 5C). We did, however, observe changes that reflect adaptation to the enhanced metabolic demand in the xenograft system. The content of PK-M2 and LDHA, both of which tend to exhibit increased expression in cancer cells and promote aerobic glycolysis, were decreased in MPC-expressing HT29 xenografts (Figure 5C). In all experiments, we observed that MPC expression reduced the phosphorylation of PDH, consistent with pyruvate inhibition of PDH kinase (Figure 5C) (Pratt and Roche, 1979; Whitehouse et al., 1974).

Figure 1. MPC Expression Is Altered in Cancer

(A) Progenetix histoplot of copy number across all chromosomes for 4,484 cancer samples.

(B) *Top*: Kaplan-Meier survival curves of censored Cox analysis for Director's Challenge NCI60 Lung, TCGA Colon Adenocarcinoma, and TCGA Kidney Clear Cell Carcinoma stratified by maximized *MPC1* expression risk group. *Bottom*: *MPC1* expression levels stratified by risk group (SurvExpress).

(C) *MPC1* and *MPC2* expression profiles across multiple cancer types, compared to normal tissue (Oncomine). The number of studies in which overexpression or underexpression was observed is indicated in red or blue boxes, respectively. Color intensity corresponds to the magnitude of expression differences (threshold [p value] set to 0.05, threshold [fold change] to all, threshold [gene rank] set to all; *MPC1* queried as *BRP44L* and *MPC2* as *BRP44*).

(D) *MPC1* and *MPC2* mRNA abundance in TCGA colorectal adenocarcinoma, compared to normal tissue (Oncomine).

(E) Western blot of MPC1 and MPC2 in human colon adenocarcinoma samples versus adjacent normal/grossly uninvolved tissue.

(F) Coexpression analysis for *MPC1* in colorectal cancer versus *MPC2*, *MYC*, and *APC*. Plotted data are $\log_2$ mRNA expression from RNA Seq RPKM (Data from TCGA Research Network).

(G) Western blot of MPC1 and MPC2 across a panel of cancer cell lines.

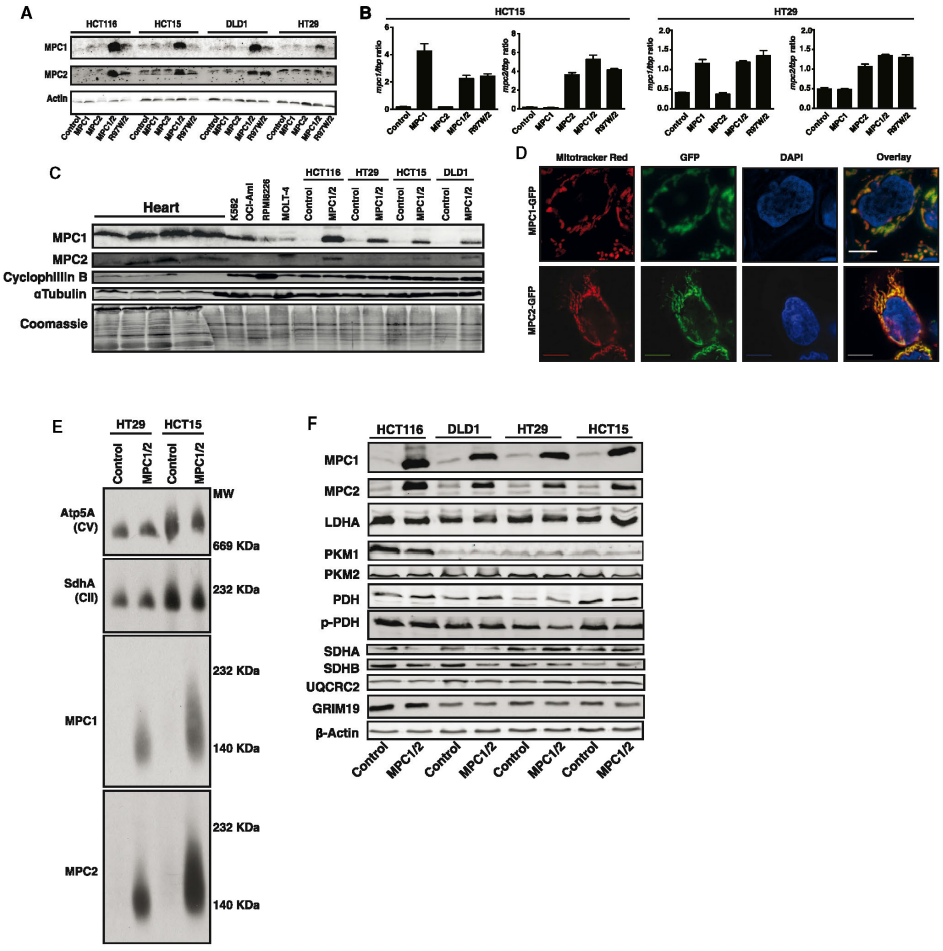

Figure 2. Re-Expressed MPC1 and MPC2 Form a Mitochondrial Complex

(A and B) (A) Western blot and (B) qRT-PCR analysis of the indicated colon cancer cell lines with retroviral expression of MPC1 (or MPC1-R97W) and/or MPC2.

(C) Western blots of human heart tissue, hematologic cancer cells, and colon cancer cell lines with and without MPC1 and MPC2 re-expression.

(D) Fluorescence microscopy of MPC1-GFP and MPC2-GFP overlaid with Mitotracker Red in HCT15 cells. Scale bar: 10 μm.

(E) Blue-native PAGE analysis of mitochondria from control and MPC1/2-expressing cells.

(F) Western blots of metabolic and mitochondrial proteins across four colon cancer cell lines with or without MPC1/2 expression.

Because our first experiment with control and MPC-expressing HCT15 cells showed profound effects using a low number of mice per group (n = 4), we repeated the experiment after additional passaging of the cells. In the second xenograft experiment (n = 10), we again observed that MPC-expressing tumors grew slower than control tumors (Figure 6A). In this experiment, however, the effects were more modest, and by the end, the tumor volume of MPC-expressing tumors had "caught up" to the controls. Puzzled by this discrepancy, we examined the protein levels in the harvested tumor samples. Unlike HT29 tumors, we

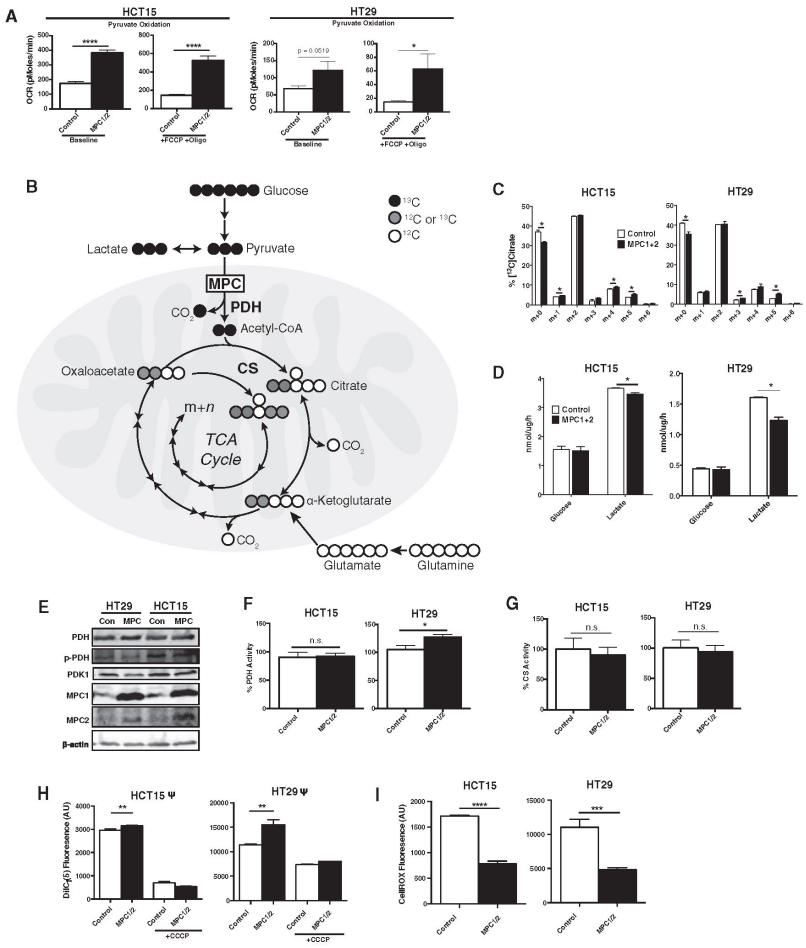

Figure 3. MPC Re-Expression Alters Mitochondrial Pyruvate Metabolism

(A) OCR at baseline and maximal respiration in HCT15 (n = 7) and HT29 (n = 13) with pyruvate as the sole carbon source (mean ± SEM).

(B and C) Schematic and citrate mass isotopomer quantification in cells cultured with D-[U-^{13}C]glucose and unlabeled glutamine for 6 hr (mean ± SD, n = 2).

(D) Glucose uptake and lactate secretion normalized to protein concentration (mean ± SD, n = 3).

(E–G) (E) Western blots of PDH, phospho-PDH, and PDK1; (F) PDH activity assay and (G) CS activity assay with or without MPC1 and MPC2 expression (mean ± SD, n = 4).

(H and I) Effects of MPC1/2 re-expression on mitochondrial membrane potential and ROS production (mean ± SD, n = 3). *p < 0.05; **p < 0.01; ***p < 0.001; ****p < 0.0001.

found that MPC1 protein levels were ~5-fold lower in the tumor sample relative to the parental MPC-expressing cell line. There was no difference in the MPC2 protein level between the tumor and cells cultured in vitro (Figure 6B). Compared to the control xenografts, MPC-expressing xenografts also had lower c-Myc, Grim19, and PCNA (Figure S5A). These data are consistent with a selection against MPC1 protein expression in the context of xenograft tumors.

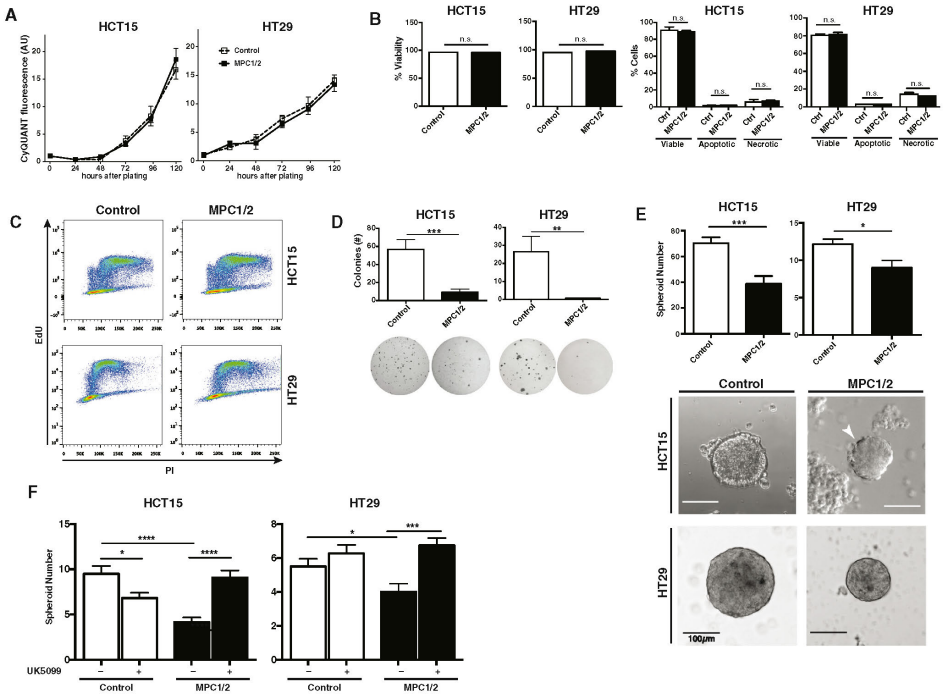

Figure 4. MPC Re-Expression Alters Growth under Low-Attachment Conditions

(A) Cell number of control and MPC1/2 re-expressing cell lines in adherent culture (mean ± SD, n = 7).

(B) Cell viability determined by trypan blue exclusion and Annexin V/PI staining (mean ± SD, n = 3).

(C–F) (C) EdU incorporation of MPC re-expressing cell lines at 3 hr post EdU pulse. Growth in 3D culture evaluated by (D) soft agar colony formation (mean ± SD, n = 12, see also Table S1) and by ([E] and [F]) spheroid formation ± MPC inhibitor UK5099 (mean ± SEM, n = 12). *p < 0.05; **p < 0.01; ***p < 0.001; ****p < 0.0001.

This adaptation was recapitulated in vitro after serial passaging of spheroids. Bicistronic vectors were used to express MPC1 and GFP from the same transcript and MPC2 and mCherry from a distinct transcript. Maintenance of GFP and mCherry expression were used as surrogate markers of MPC1 and MPC2 expression, respectively, after eight spheroid passages. As in xenografts, we observed little evidence of decreased MPC1 or MPC2 expression after spheroid passaging in HT29 cells (Figure 6C). On the other hand, we observed a ~60% decrease in GFP/mCherry double-positive HCT15 cells. As in the xenografts, this was due almost completely to a loss of GFP/MPC1 expression; we observed a doubling of the mCherry-positive, GFP-negative population (Figure 6C). These surrogate observations were confirmed by western blots, showing a loss of MPC1 protein in passaged HCT15 spheroids (Figure 6D). In contrast, MPC1 expression remained stable after eight passages in adherent culture (Figures S5B and S5C). These data suggest a selective pressure against high *MPC1* expression in cancer cells grown in anchorage-free conditions in vitro or in vivo.

When MPC is re-expressed at levels comparable to differentiated cells and tissues, these cancer cells lose oncogenic potential, without signs of impaired cell health or viability. The first clue as to a potential mechanism came from examination of western blots from the xenograft experiments displayed in Figure 5. We found that aldehyde dehydrogenase, ALDHA, was significantly decreased in the MPC-expressing tumors relative to controls (Figures 5C and 7A). ALDHA is a stem cell marker and is a regulator of differentiation through its control of retinoic acid synthesis (Chute et al., 2006). The expression of this marker has also been shown to associate with more aggressive cancers and is commonly used to isolate cancer stem cells (Deng et al., 2014; Ginestier et al., 2007; Wang et al., 2012). Similarly, the LIN28A stem cell marker was also decreased in the MPC-expressing tumors relative to controls (Figures 7A and 5C). This led us to hypothesize that the defects in soft agar, spheroid, and xenograft

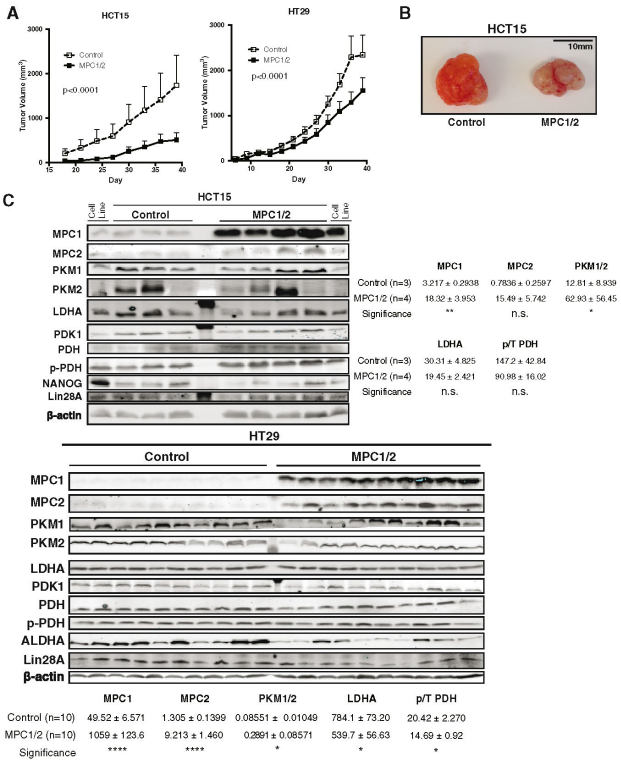

Figure 5. MPC Re-Expression Reduces Tumor Growth In Vivo

(A and B) Tumor growth of HCT15 (n = 4) and HT29 (n = 10) xenografts as determined by caliper measurement (mean ± SEM) and representative HCT15 xenograft tumor images.

(C) Western blots of excised tumors and band quantification after normalization to β-actin.

growth upon *MPC1* and *MPC2* re-expression were a consequence of impaired stem cell properties. We went back to HCT15 and HT29 cells grown in adherent culture and examined whether the decrease in ALDH activity was present prior to injection into mice. Indeed, we found that the ALDH^{hi} population was depleted in both HCT15 and HT29 cells upon *MPC1* and *MPC2* expression (Figures 7B and S6A). Similarly, FACS-based analysis of CD44^{hi} (stem-cell-like) versus CD44^{lo} (non-stem-cell-like) cells showed MPC expression decreased the CD44^{hi} population in both cell lines also (Figures 7C and S6B). We also performed western blots of additional stem cell markers and found that LGR5 and LIN28A protein levels were decreased in adherent cells upon MPC expression in both cell lines, and NANOG was decreased in HCT15 cells (Figures 7D and S6C).

We next isolated the top and bottom 5% of cells based on ALDH activity (ALDH^{hi} and ALDH^{lo}) from control and MPC-expressing HCT15 cells. Exogenous *MPC1* expression was markedly suppressed in the stem cell population relative to the non-stem cell population (Figure 7E). Expression of *MPC2* was also lower, albeit to a lesser extent (Figure 7E). We examined the proliferation rate of these cell populations; in all experiments, the number of cells entering the assay was normalized across all groups. As observed previously, MPC expression had no effect on proliferation when assessed in the entire cell population (Figure 7F) or in the ALDH^{lo} population (Figure 7G). We observed impaired proliferation in MPC-expressing ALDH^{hi} cells, however (Figure 7G). We next isolated stem cells using a complementary parameter, the ability to efflux Hoechst 33342 (Haraguchi et al., 2006; Patrawala et al., 2005; Wu et al., 2007). As with ALDH-selected stem cells, we observed no difference in HCT15 proliferation upon MPC expression in the main (non-stem cell) population (Figures 7H and S6D). In the side (stem cell) population, we observed decreased proliferation in the MPC-expressing cells (Figure 7H). When these same cells were assessed for ability to form spheroids, the results were more profound. Side population control cells exhibited a ~5-fold increased frequency of spheroid formation relative to the main population, and this difference was markedly blunted in the MPC-expressing cells (Figure 7I). MPC re-expression had no effect on the proficiency of spheroid formation in main population cells (Figure 7I).

DISCUSSION

The Warburg effect, wherein cells oxidize carbohydrates at a reduced rate even in the presence of oxygen, is now recognized as a common feature of cancer. Otto Warburg's observations in the early 20th century led him to conclude that cancer cells contain defective mitochondria. While mitochondria have subsequently been shown to be vital for cancer growth (Cavalli et al., 1997; Morais et al., 1994), we show herein that impaired import of pyruvate via loss of the MPC enforces the Warburg effect and MPC re-expression impacts the metabolic and growth properties of cancer cells. The oxidative machinery of cancer cells, at least those that were studied herein, is capable of effective oxidative metabolism (Zu and Guppy, 2004); pyruvate simply must be provided through increased expression and activity of the MPC. It is quite surprising that solely expressing *MPC1*

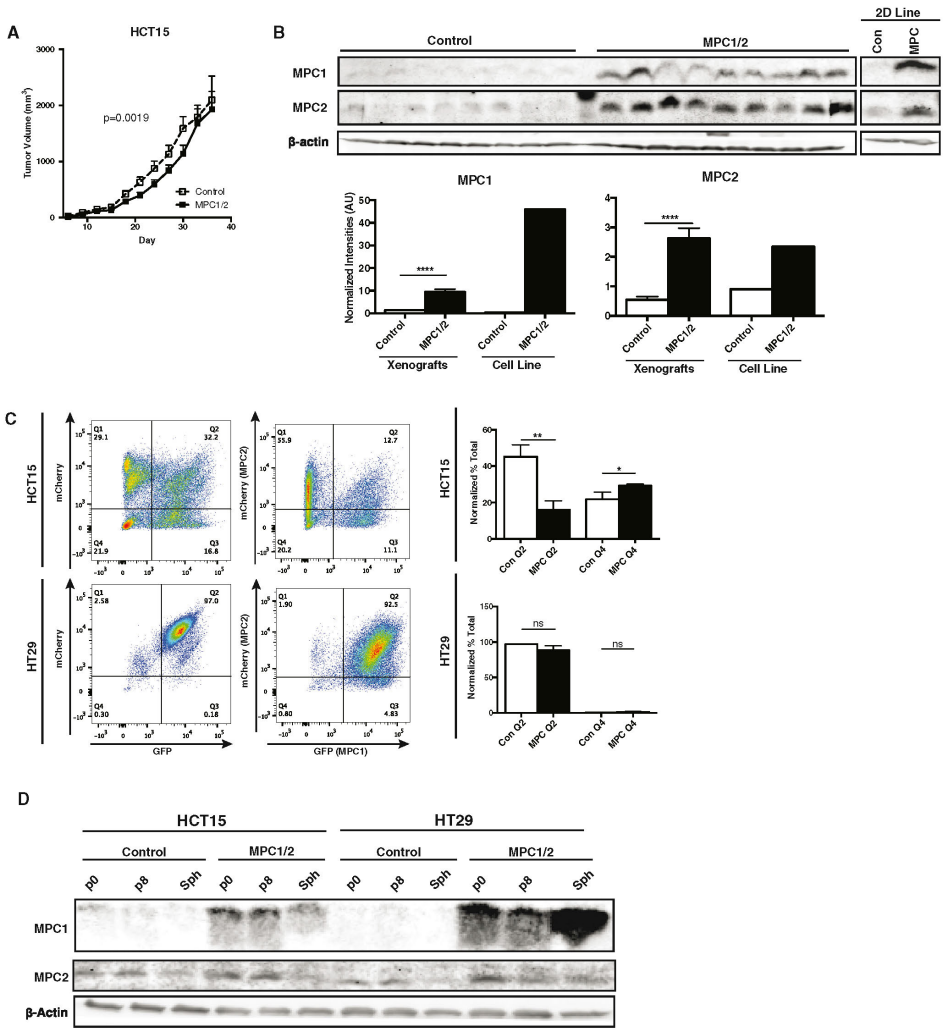

Figure 6. Adaptation to MPC Re-Expression in Xenograft and Spheroids

(A) Tumor growth of HCT15 xenografts as determined by caliper measurement (n = 10, mean ± SEM).

(B) Western blots of excised HCT15 tumors versus parental cell line and band quantification after normalization to β-actin (mean ± SEM).

(C) Dissociated spheroid FACS plot of GFP and mCherry fluorescence after eight passages in low-attachment culture. Fractions plotted of high-high (Q2) versus low-low (Q4) expressers (mean ± SD, n = 6.).

(D) Western blot of 8-passage cells in 2D and 3D culture. *p < 0.05; **p < 0.01.

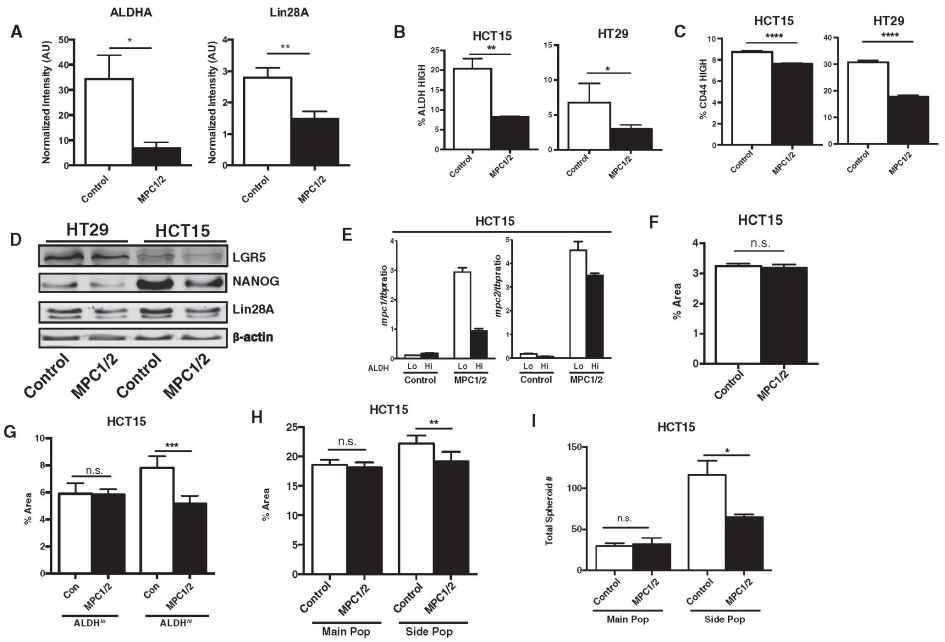

Figure 7. MPC Re-Expression Alters the Cancer Initiating Cell Population

(A) Western blot quantification of ALDHA and Lin28A from control or MPC re-expressing HT29 xenografts (mean ± SEM, n = 10).

(B and C) Percentage of ALDH^{hi} (n = 3) and CD44^{hi} (n = 5) cells as determined by flow cytometry (mean ± SEM).

(D) Western blot analysis of stem cell markers in control and MPC re-expressing cell lines.

(E) Relative *MPC1* and *MPC2* mRNA levels in ALDH sorted HCT15 cells (n = 4, mean ± SEM). 2D growth of (F) whole-population HCT15 cells and (G) ALDH sorted cells. Area determined by ImageJ after crystal violet staining (mean ± SD, n = 6).

(H and I) (H) Adherent and (I) spheroid growth of main population (MP) versus side population (SP) HCT15 cells. (mean ± SD, n = 6). *p < 0.05; **p < 0.01; ***p < 0.001; ****p < 0.0001.

and *MPC2* to generate more intact MPC complexes is sufficient to alter the metabolic program of cancer cells given the numerous, redundant, and efficacious mechanisms in place to limit pyruvate oxidation in cancer cells. In the face of these counteracting mechanisms, the metabolic effects of MPC expression are impressive.

Our demonstration that the MPC is lost or underexpressed in many cancers might provide clarifying context for earlier attempts to exploit metabolic regulation for cancer therapeutics. The PDH kinase inhibitor dichloroacetate, which impairs PDH phosphorylation and increases pyruvate oxidation, has been explored extensively as a cancer therapy (Bonnet et al., 2007; Olszewski et al., 2010). It has met with mixed results, however, and has typically failed to dramatically decrease tumor burden as a monotherapy (Garon et al., 2014; Sánchez-Aragó et al., 2010; Shahrzad et al., 2010). Is one possible reason for these failures that the MPC has been lost or inactivated, thereby limiting the metabolic effects of PDH activity? The inclusion of the MPC adds additional complexity to targeting cancer metabolism for therapy but has the potential to explain why treatments may be more effective in some studies than in others (Fulda et al., 2010; Hamanaka and Chandel, 2012; Tennant et al., 2010; Vander Heiden, 2011).

The redundant measures to limit pyruvate oxidation make it easy to understand why expression of the MPC leads to relatively modest metabolic changes in cells grown in adherent culture conditions. While subtle, we observed a number of changes in metabolic parameters, all of which are consistent with enhanced mitochondrial pyruvate entry and oxidation. There are at least two possible explanations for the discrepancy that we observed between the impact on adherent and nonadherent cell proliferation. One hypothesis is that the stress of nutrient deprivation and detachment combines with these subtle metabolic effects to impair survival and proliferation. It is also possible, however, that the metabolic effects themselves become much more profound during anchorage-independent

growth. Regardless of the magnitude of the metabolic effect of MPC expression, it seems clear that the effects of MPC expression on stemness are indeed metabolic, as they are reversed by an inhibitor of pyruvate transport. There is precedent for mitochondrial metabolism affecting stemness as HT29 cells differentiate following replacement of glucose with galactose, which promotes mitochondrial oxidative metabolism (Pinto et al., 1982). The mechanism(s) underlying the loss of stem cell markers and behavior that we observed, however, remains unknown. Filling this gap will be very important, as these mechanisms likely constitute a key vulnerability in cancer cells and a critical defining feature of stem cells.

Not surprisingly, cancer cells appear to select against MPC expression, principally through deleting or suppressing *MPC1* gene expression. This is most convincingly demonstrated by the strong correlation of low *MPC1* expression with poor prognosis across a wide variety of cancers. We also observed the same phenomenon in our ectopic *MPC1* and *MPC2* expression system. We found that both serial spheroid passage and xenograft growth appeared to suppress *MPC1* gene expression in HCT15 cells. The disproportionate and consistent suppression of *MPC1* is surprising, given that we have previously shown that both MPC1 and MPC2 are absolutely required for formation of a functional MPC complex. Moreover, in the present study, we have shown stable accumulation of either protein to be completely dependent on expression of the other. These data raise the interesting possibility that a decrease in the MPC1:MPC2 ratio has a functional consequence beyond just decreased intact MPC complexes and pyruvate transport.

Our attempts to define the molecular mechanism for the context-dependent impairment of cell proliferation upon MPC re-expression culminated in the observation of decreases in multiple measures of stemness. Interestingly, this occurs in cells growing in adherent culture, where we see no effect on proliferation, viability, apoptosis, or necrosis. We measured six different markers of the stem cell compartment, and each showed a decrease in both HCT15 and HT29 cells except the side population assay, which is a measure of the activity of the ATP-dependent drug transporters ABCG1, ABCC1-5, and ABCG2 to efflux Hoechst 33342 (Goodell et al., 1996). It is possible that the perturbation of metabolism by the MPC, perhaps through ATP production, somehow disconnects the side population assay from other measures of stem cell content (Liu et al., 2014). We see it as significant that, in spite of this, the side population is exclusively affected by MPC expression. Similarly, when selecting stem cells based on high ALDH activity, we also only observed effects of MPC expression on proliferation in the stem cell population. The data strongly suggest that the effects of MPC expression on proliferation in multiple contexts are related to its effects on the stem cell compartment.

This seemingly intimate connection between the MPC and stemness is consistent with recent observations that most stem cell populations exhibit a glycolytic metabolic phenotype similar to cancer cells (Folmes et al., 2012; Ito and Suda, 2014; Wanet et al., 2012). Our preliminary analysis of publically available data sets suggests that the MPC might be involved. Both *MPC1* and *MPC2* are expressed at a very low level in embryonic stem cells, and their expression increases upon differentiation (for example, *MPC1*, $p = 4.8 \times 10^{-6}$; *MPC2*, $p = 6.3 \times 10^{-5}$ for cardiomyocyte differentiation [Cao et al., 2008], and *MPC1*, $p < 0.0001$; *MPC2*, $p = 0.0061$ for neurons [Fathi et al., 2011]). This leads us to speculate that modulation of pyruvate metabolism via the MPC is vital for the maintenance of stem cell populations (Mandal et al., 2011; Schieke et al., 2008). In addition, glycolysis supports numerous biosynthetic pathways that may be altered by enhanced pyruvate oxidation, including the pentose phosphate pathway and one-carbon pools, which may in turn alter stemness (Shyh-Chang et al., 2013). Therefore, the studies of cancer cell metabolism described herein might also be informative as to the metabolic requirements for stem cell maintenance.

In conclusion, we propose that suppression of *MPC1* expression and the concomitant decrease in mitochondrial pyruvate uptake and oxidation is an important mediator of the Warburg effect in colon cancer cells, and most likely in many cancer settings. It is well documented that, in many cancers, the extent of this glycolytic metabolism correlates with a poorer prognosis—consistent with the prognostic impact of *MPC1* expression shown herein. We suggest that the data presented herein begin to establish a more complete framework for understanding and therapeutically exploiting cancer metabolism. We have shown that loss of MPC activity, and the concomitant loss of pyruvate supply to the TCA cycle, is required for the normal oncogenic function of cancer cells. It is possible that this metabolic inflexibility will confer enhanced sensitivity to agents that prevent anapleurotic contribution of other substrates, such as glutamine, to the TCA cycle. Therefore, placing the MPC properly in the metabolic network of cancer cells might enable a more personalized and sophisticated approach to target this axis for therapeutic benefit.

EXPERIMENTAL PROCEDURES

Additional details can be found in Supplemental Experimental Procedures.

Mammalian Cell Culture

Unless otherwise stated, all cell lines were maintained in Dulbecco's modified Eagle's medium +2 mM Glutamax (Invitrogen) with 10% FBS (Sigma Aldrich) and 1% primocin at 37°C in 5% CO_2. Cells were obtained from the National Cancer Institute (Bethesda) and ATCC (Manassas). All retroviral transductions were performed with pseudotyped retroviral supernatants generated by cotransfection of 293T cells with Vsv-G, Gag-Pol, and a retroviral targeting vector (pQCXIP/B/Z) harboring cDNA for the gene of interest. All lentiviral transductions were performed with pseudotyped third-generation lentiviral supernatants generated by cotransfection of 293T cells with vectors pMD2.G (Addgene #12259), pMDLG/pRRE (Addgene #12251), pRSV-Rev (Addgene #12253), and a lentiviral targeting vector (LeGO iG2/iC2) harboring cDNA for the gene of interest. Stable cell lines were generated by selection with appropriate antibiotic Blasticidin (6 μg/ml), Puromycin (6 μg/ml), Zeocin (400 μg/ml), or by fluorescence sorting.

Xenografts

One million cells were injected for HCT15, and two million cells for HT29. Control and MPC overexpression cells were injected to each side of the same nude mouse. Tumor sizes were measured at indicated times by caliper.

Blue-Native PAGE

Blue-native PAGE was performed as described previously (Bricker et al., 2012). Mitochondria were resuspended in lysis buffer (50 mM NaCl, 5 mM 6-aminocaproic acid, 50 mM imidazole, 1 mM AEBSF, and protease inhibitor cocktail). Mitochondria were solubilized with ~1.5% digitonin. Lysates were

resolved on a 3%–13% gradient native gel using a PROTEAN II xi Cell gel running system (Bio-Rad). Western blot performed as described elsewhere using a Trans-Blot transfer cell (Bio-Rad) and PVDF membranes.

Fluorescence Microscopy

Stable cell lines with empty vector, MPC1 and MPC2, MPC1-GFP, or MPC2-GFP were plated at 1,000/cells per well and grown for at least 24 hr prior to imaging. The cells were then treated with 25 nM Mitotracker Red CMXRos (Life Technologies) and 16.2 μM Hoechst 33342 and incubated for 5 min prior to imaging. Cells were imaged on the Axio Observer Z1 imaging system (Carl Zeiss) equipped with 10×, 40×, and 100× objectives (oil immersion). Digital fluorescence and differential interference contrast images were acquired using a monochrome digital camera (AxioCam MRm, Carl Zeiss). Z stacks were obtained and deconvolved using the AxioVision software (Version 4.8, Carl Zeiss). 2D projection of the z stacks was performed using the ImageJ software (summation – average intensity). The final images were adjusted and assembled using Adobe Photoshop CS5. Brightness and contrast were adjusted only using linear operation on the entire image.

Oxygen Consumption Studies; Seahorse

Metabolic measurements were carried out in standard 24-well Seahorse microplates on a Seahorse XF24 analyzer. Glycolysis was measured per the glycolysis stress test kit and displayed as ECAR. Pyruvate oxidation was measured using oxygen consumption rate (OCR) when cells were incubated in unbuffered Seahorse media containing 10 mM sodium pyruvate as the only respiratory substrate. For all experiments 80,000 cells per well were plated 16–18 hr prior to analysis.

Statistical Methods

Statistical analyses were performed using Graphpad Prism 6. Unless otherwise noted, data were analyzed by Student's t test and considered significant at $p < 0.05$.

SUPPLEMENTAL INFORMATION

Supplemental Information includes six figures, one table, and Supplemental Experimental Procedures and can be found with this article online at http://dx.doi.org/10.1016/j.molcel.2014.09.026.

AUTHOR CONTRIBUTIONS

J.C.S., K.A.O., and J.R. wrote the manuscript. J.C.S., K.A.O., L.J., A.J.H., and R.J.D. edited the manuscript. J.C.S., K.A.O., L.J., A.J.H., J.G.V., R.A.E., R.J.D., and J.R. designed experiments. J.C.S., K.A.O., L.J., A.J.H., J.G.V., R.A.E., and E.G.E. performed experiments. J.X. developed proprietary antibodies essential to this work.

ACKNOWLEDGMENTS

The authors would like to acknowledge the following individuals for their contribution to this work: James Marvin for his consultation and flow cytometry training and Chris Leukel for lively discussion regarding flow cytometry. We thank Janet Bassett and our fellow students in the MD/PhD Program including Dr. Jess Maddox, Joe Cho, Jon Downie, and Alex Keefe. We thank Dr. Dave Jones for reviewing this manuscript. We thank Drs. Dean Tantin, Sue Hammoud, Don Ayer, Janet Shaw, Sihem Boudina, James Cox, Jerry Kaplan, Janet Lindsley, Amnon Schlegel, Adam Frost, Rich Dorsky, Jody Rosenblatt, Ed Levine, Joe Yost, Charlie Murtaugh, Carl Thummel, and members of the Rutter Lab for discussion and insight. We thank Drs. Nikolaos Diakos, Stavros Drakos, and Dean Li for human heart tissue samples and the Huntsman Cancer Institute Biorepository for the human colon tissue samples. We thank the Metabolic Phenotyping Core for their expertise and services. This project was supported by the Nora Eccles Treadwell Foundation (to J.R.) and NIH R01 GM094232 (to J.R.), NIH Developmental Biology Training Grant 5T32HD07491 (to J.C.S.), NIH Hematology Training Grant 5T32DK007115-40 (to K.A.O.), NIH R01 CA157996 (to R.J.D.), CPRIT: RP130272 (to R.J.D.); NCI P30CA042014 (to HCI Biorepository), and NCRR 1S10RR026802-01 (to Utah Flow Cytometry Core). A.J.H. was supported by an American Cancer Society-Daiichi Sankyo, Inc. Postdoctoral Fellowship, grant number PF-13-363-01-TBE.

Received: May 30, 2014
Revised: August 8, 2014
Accepted: September 25, 2014
Published: October 30, 2014

REFERENCES

Aguirre-Gamboa, R., Gomez-Rueda, H., Martínez-Ledesma, E., Martínez-Torteya, A., Chacolla-Huaringa, R., Rodriguez-Barrientos, A., Tamez-Peña, J.G., and Treviño, V. (2013). SurvExpress: an online biomarker validation tool and database for cancer gene expression data using survival analysis. PLoS ONE *8*, e74250.

Azuma, M., Shi, M., Danenberg, K.D., Gardner, H., Barrett, C., Jacques, C.J., Sherod, A., Iqbal, S., El-Khoueiry, A., Yang, D., et al. (2007). Serum lactate dehydrogenase levels and glycolysis significantly correlate with tumor VEGFA and VEGFR expression in metastatic CRC patients. Pharmacogenomics *8*, 1705–1713.

Bassenge, E., Sommer, O., Schwemmer, M., and Bünger, R. (2000). Antioxidant pyruvate inhibits cardiac formation of reactive oxygen species through changes in redox state. Am. J. Physiol. Heart Circ. Physiol. *279*, H2431–H2438.

Bayley, J.P., and Devilee, P. (2012). The Warburg effect in 2012. Curr. Opin. Oncol. *24*, 62–67.

Bignone, P.A., Lee, K.Y., Liu, Y., Emilion, G., Finch, J., Soosay, A.E.R., Charnock, F.M.L., Beck, S., Dunham, I., Mungall, A.J., and Ganesan, T.S. (2007). RPS6KA2, a putative tumour suppressor gene at 6q27 in sporadic epithelial ovarian cancer. Oncogene *26*, 683–700.

Bonnet, S., Archer, S.L., Allalunis-Turner, J., Haromy, A., Beaulieu, C., Thompson, R., Lee, C.T., Lopaschuk, G.D., Puttagunta, L., Bonnet, S., et al. (2007). A mitochondria-K+ channel axis is suppressed in cancer and its normalization promotes apoptosis and inhibits cancer growth. Cancer Cell *11*, 37–51.

Bricker, D.K., Taylor, E.B., Schell, J.C., Orsak, T., Boutron, A., Chen, Y.C., Cox, J.E., Cardon, C.M., Van Vranken, J.G., Dephoure, N., et al. (2012). A mitochondrial pyruvate carrier required for pyruvate uptake in yeast, *Drosophila*, and humans. Science *337*, 96–100.

Cai, H., Kumar, N., Ai, N., Gupta, S., Rath, P., and Baudis, M. (2014). Progenetix: 12 years of oncogenomic data curation. Nucleic Acids Res. *42* (Database issue), D1055–D1062.

Cao, F., Wagner, R.A., Wilson, K.D., Xie, X., Fu, J.D., Drukker, M., Lee, A., Li, R.A., Gambhir, S.S., Weissman, I.L., et al. (2008). Transcriptional and functional profiling of human embryonic stem cell-derived cardiomyocytes. PLoS ONE *3*, e3474.

Carpentino, J.E., Hynes, M.J., Appelman, H.D., Zheng, T., Steindler, D.A., Scott, E.W., and Huang, E.H. (2009). Aldehyde dehydrogenase-expressing colon stem cells contribute to tumorigenesis in the transition from colitis to cancer. Cancer Res. *69*, 8208–8215.

Cavalli, L.R., Varella-Garcia, M., and Liang, B.C. (1997). Diminished tumorigenic phenotype after depletion of mitochondrial DNA. Cell Growth Differ. *8*, 1189–1198.

Cerami, E., Gao, J., Dogrusoz, U., Gross, B.E., Sumer, S.O., Aksoy, B.A., Jacobsen, A., Byrne, C.J., Heuer, M.L., Larsson, E., et al. (2012). The cBio cancer genomics portal: an open platform for exploring multidimensional cancer genomics data. Cancer Disc. *2*, 401–404.

Chen, R., Bronner, M.P., Crispin, D.A., Rabinovitch, P.S., and Brentnall, T.A. (2005). Characterization of genomic instability in ulcerative colitis neoplasia leads to discovery of putative tumor suppressor regions. Cancer Genet. Cytogenet. *162*, 99–106.

Christofk, H.R., Vander Heiden, M.G., Harris, M.H., Ramanathan, A., Gerszten, R.E., Wei, R., Fleming, M.D., Schreiber, S.L., and Cantley, L.C. (2008a). The M2 splice isoform of pyruvate kinase is important for cancer metabolism and tumour growth. Nature *452*, 230–233.

Christofk, H.R., Vander Heiden, M.G., Wu, N., Asara, J.M., and Cantley, L.C. (2008b). Pyruvate kinase M2 is a phosphotyrosine-binding protein. Nature *452*, 181–186.

Chute, J.P., Muramoto, G.G., Whitesides, J., Colvin, M., Safi, R., Chao, N.J., and McDonnell, D.P. (2006). Inhibition of aldehyde dehydrogenase and retinoid signaling induces the expansion of human hematopoietic stem cells. Proc. Natl. Acad. Sci. USA *103*, 11707–11712.

Colca, J.R., McDonald, W.G., Cavey, G.S., Cole, S.L., Holewa, D.D., Brightwell-Conrad, A.S., Wolfe, C.L., Wheeler, J.S., Coulter, K.R., Kilkuskie, P.M., et al. (2013). Identification of a mitochondrial target of thiazolidinedione insulin sensitizers (mTOT)–relationship to newly identified mitochondrial pyruvate carrier proteins. PLoS One *8*, e61551.

Deng, Y., Zhou, J., Fang, L., Cai, Y., Ke, J., Xie, X., Huang, Y., Huang, M., and Wang, J. (2014). ALDH1 is an independent prognostic factor for patients with stages II-III rectal cancer after receiving radiochemotherapy. Br. J. Cancer *110*, 430–434.

Divakaruni, A.S., Wiley, S.E., Rogers, G.W., Andreyev, A.Y., Petrosyan, S., Loviscach, M., Wall, E.A., Yadava, N., Heuck, A.P., Ferrick, D.A., et al. (2013). Thiazolidinediones are acute, specific inhibitors of the mitochondrial pyruvate carrier. Proc. Natl. Acad. Sci. USA *110*, 5422–5427.

Eboli, M.L., Paradies, G., Galeotti, T., and Papa, S. (1977). Pyruvate transport in tumour-cell mitochondria. Biochim. Biophys. Acta *460*, 183–187.

Fathi, A., Hatami, M., Hajihosseini, V., Fattahi, F., Kiani, S., Baharvand, H., and Salekdeh, G.H. (2011). Comprehensive gene expression analysis of human embryonic stem cells during differentiation into neural cells. PLoS ONE *6*, e22856.

Folmes, C.D., Nelson, T.J., Dzeja, P.P., and Terzic, A. (2012). Energy metabolism plasticity enables stemness programs. Ann. N Y Acad. Sci. *1254*, 82–89.

Fulda, S., Galluzzi, L., and Kroemer, G. (2010). Targeting mitochondria for cancer therapy. Nat. Rev. Drug Discov. *9*, 447–464.

Gao, J., Aksoy, B.A., Dogrusoz, U., Dresdner, G., Gross, B., Sumer, S.O., Sun, Y., Jacobsen, A., Sinha, R., Larsson, E., et al. (2013). Integrative analysis of complex cancer genomics and clinical profiles using the cBioPortal. Sci. Signal. *6*, pl1–pl1.

Garon, E.B., Christofk, H.R., Hosmer, W., Britten, C.D., Bahng, A., Crabtree, M.J., Hong, C.S., Kamranpour, N., Pitts, S., Kabbinavar, F., et al. (2014). Dichloroacetate should be considered with platinum-based chemotherapy in hypoxic tumors rather than as a single agent in advanced non-small cell lung cancer. J. Cancer Res. Clin. Oncol. *140*, 443–452.

Ginestier, C., Hur, M.H., Charafe-Jauffret, E., Monville, F., Dutcher, J., Brown, M., Jacquemier, J., Viens, P., Kleer, C.G., Liu, S., et al. (2007). ALDH1 is a marker of normal and malignant human mammary stem cells and a predictor of poor clinical outcome. Cell Stem Cell *1*, 555–567.

Goodell, M.A., Brose, K., Paradis, G., Conner, A.S., and Mulligan, R.C. (1996). Isolation and functional properties of murine hematopoietic stem cells that are replicating in vivo. J. Exp. Med. *183*, 1797–1806.

Gotanda, Y., Akagi, Y., Kawahara, A., Kinugasa, T., Yoshida, T., Ryu, Y., Shiratsuchi, I., Kage, M., and Shirouzu, K. (2013). Expression of monocarboxylate transporter (MCT)-4 in colorectal cancer and its role: MCT4 contributes to the growth of colorectal cancer with vascular endothelial growth factor. Anticancer Res. *33*, 2941–2947.

Halestrap, A.P. (1975). The mitochondrial pyruvate carrier. Kinetics and specificity for substrates and inhibitors. Biochem. J. *148*, 85–96.

Hamanaka, R.B., and Chandel, N.S. (2012). Targeting glucose metabolism for cancer therapy. J. Exp. Med. *209*, 211–215.

Olszewski, U., Poulsen, T.T., Ulsperger, E., Poulsen, H.S., Geissler, K., and Hamilton, G. (2010). In vitro cytotoxicity of combinations of dichloroacetate with anticancer platinum compounds. Clin. Pharmacol. *2*, 177–183.

Haraguchi, N., Utsunomiya, T., Inoue, H., Tanaka, F., Mimori, K., Barnard, G.F., and Mori, M. (2006). Characterization of a side population of cancer cells from human gastrointestinal system. Stem Cells *24*, 506–513.

Herzig, S., Raemy, E., Montessuit, S., Veuthey, J.L., Zamboni, N., Westermann, B., Kunji, E.R., and Martinou, J.C. (2012). Identification and functional expression of the mitochondrial pyruvate carrier. Science *337*, 93–96.

Hong, Y., Ho, K.S., Eu, K.W., and Cheah, P.Y. (2007). A susceptibility gene set for early onset colorectal cancer that integrates diverse signaling pathways: implication for tumorigenesis. Clin. Cancer Res. *13*, 1107–1114.

Huang, C.Y., Kuo, W.T., Huang, Y.C., Lee, T.C., and Yu, L.C. (2013). Resistance to hypoxia-induced necroptosis is conferred by glycolytic pyruvate scavenging of mitochondrial superoxide in colorectal cancer cells. Cell Death Dis. *4*, e622.

Ito, K., and Suda, T. (2014). Metabolic requirements for the maintenance of self-renewing stem cells. Nat. Rev. Mol. Cell Biol. *15*, 243–256.

Kang, Y.H., Chung, S.J., Kang, I.J., Park, J.H., and Bünger, R. (2001). Intramitochondrial pyruvate attenuates hydrogen peroxide-induced apoptosis in bovine pulmonary artery endothelium. Mol. Cell. Biochem. *216*, 37–46.

Kaplon, J., Zheng, L., Meissl, K., Chaneton, B., Selivanov, V.A., Mackay, G., van der Burg, S.H., Verdegaal, E.M., Cascante, M., Shlomi, T., et al. (2013). A key role for mitochondrial gatekeeper pyruvate dehydrogenase in oncogene-induced senescence. Nature *498*, 109–112.

Kim, J.W., Tchernyshyov, I., Semenza, G.L., and Dang, C.V. (2006). HIF-1-mediated expression of pyruvate dehydrogenase kinase: a metabolic switch required for cellular adaptation to hypoxia. Cell Metab. *3*, 177–185.

Koukourakis, M.I., Giatromanolaki, A., Sivridis, E., Bougioukas, G., Didilis, V., Gatter, K.C., and Harris, A.L.; Tumour and Angiogenesis Research Group (2003). Lactate dehydrogenase-5 (LDH-5) overexpression in non-small-cell lung cancer tissues is linked to tumour hypoxia, angiogenic factor production and poor prognosis. Br. J. Cancer *89*, 877–885.

Le Floch, R., Chiche, J., Marchiq, I., Naiken, T., Ilc, K., Murray, C.M., Critchlow, S.E., Roux, D., Simon, M.P., and Pouysségur, J. (2011). CD147 subunit of lactate/H+ symporters MCT1 and hypoxia-inducible MCT4 is critical for energetics and growth of glycolytic tumors. Proc. Natl. Acad. Sci. USA *108*, 16663–16668.

Li, C.L., Wang, M., Ma, X.Y., and Zhang, W. (2014). NRGA1, a putative mitochondrial pyruvate carrier, mediates ABA regulation of guard cell ion channels and drought stress responses in Arabidopsis. Mol. Plant *7*, 1508–1521.

Liu, Y., Emilion, G., Mungall, A.J., Dunham, I., Beck, S., Le Meuth-Metzinger, V.G., Shelling, A.N., Charnock, F.M.L., and Ganesan, T.S. (2002). Physical and transcript map of the region between D6S264 and D6S149 on chromosome 6q27, the minimal region of allele loss in sporadic epithelial ovarian cancer. Oncogene *21*, 387–399.

Liu, P.P., Liao, J., Tang, Z.-J., Wu, W.-J., Yang, J., Zeng, Z.-L., Hu, Y., Wang, P., Ju, H.-Q., Xu, R.-H., and Huang, P. (2014). Metabolic regulation of cancer cell side population by glucose through activation of the Akt pathway. Cell Death Differ. *21*, 124–135.

Luo, W., and Semenza, G.L. (2011). Pyruvate kinase M2 regulates glucose metabolism by functioning as a coactivator for hypoxia-inducible factor 1 in cancer cells. Oncotarget *2*, 551–556.

Mandal, S., Lindgren, A.G., Srivastava, A.S., Clark, A.T., and Banerjee, U. (2011). Mitochondrial function controls proliferation and early differentiation potential of embryonic stem cells. Stem Cells *29*, 486–495.

McFate, T., Mohyeldin, A., Lu, H., Thakar, J., Henriques, J., Halim, N.D., Wu, H., Schell, M.J., Tsang, T.M., Teahan, O., et al. (2008). Pyruvate dehydrogenase complex activity controls metabolic and malignant phenotype in cancer cells. J. Biol. Chem. *283*, 22700–22708.

Michelakis, E.D., Sutendra, G., Dromparis, P., Webster, L., Haromy, A., Niven, E., Maguire, C., Gammer, T.L., Mackey, J.R., Fulton, D., et al. (2010). Metabolic modulation of glioblastoma with dichloroacetate. Sci. Transl. Med. *2*, 31ra34.

Morais, R., Zinkewich-Péotti, K., Parent, M., Wang, H., Babai, F., and Zollinger, M. (1994). Tumor-forming ability in athymic nude mice of human cell lines devoid of mitochondrial DNA. Cancer Res. *54*, 3889–3896.

Network, T.C.G.A.; Cancer Genome Atlas Network (2012). Comprehensive molecular characterization of human colon and rectal cancer. Nature *487*, 330–337.

Papa, S., and Paradies, G. (1974). On the mechanism of translocation of pyruvate and other monocarboxylic acids in rat-liver mitochondria. Eur. J. Biochem. *49*, 265–274.

Paradies, G., Capuano, F., Palombini, G., Galeotti, T., and Papa, S. (1983). Transport of pyruvate in mitochondria from different tumor cells. Cancer Res. *43*, 5068–5071.

Patrawala, L., Calhoun, T., Schneider-Broussard, R., Zhou, J., Claypool, K., and Tang, D.G. (2005). Side population is enriched in tumorigenic, stem-like cancer cells, whereas ABCG2+ and ABCG2- cancer cells are similarly tumorigenic. Cancer Res. *65*, 6207–6219.

Patterson, J.N., Cousteils, K., Lou, J.W., Manning Fox, J.E., MacDonald, P.E., and Joseph, J.W. (2014). Mitochondrial metabolism of pyruvate is essential for regulating glucose-stimulated insulin secretion. J. Biol. Chem. *289*, 13335–13346.

Pinheiro, C., Longatto-Filho, A., Scapulatempo, C., Ferreira, L., Martins, S., Pellerin, L., Rodrigues, M., Alves, V.A.F., Schmitt, F., and Baltazar, F. (2008). Increased expression of monocarboxylate transporters 1, 2, and 4 in colorectal carcinomas. Virchows Arch. *452*, 139–146.

Pinto, M., Appay, M.D., Simon-Assmann, P., Chevalier, G., Dracopoli, N., Fogh, J., and Zweibaum, A. (1982). Enterocytic Differentiation of cultured human colon cancer cells by replacement of glucose by galactose in the medium. Biol. Cell *44*, 193–196.

Pratt, M.L., and Roche, T.E. (1979). Mechanism of pyruvate inhibition of kidney pyruvate dehydrogenasea kinase and synergistic inhibition by pyruvate and ADP. J. Biol. Chem. *254*, 7191–7196.

Rhodes, D.R., Yu, J., Shanker, K., Deshpande, N., Varambally, R., Ghosh, D., Barrette, T., Pandey, A., and Chinnaiyan, A.M. (2004). ONCOMINE: a cancer microarray database and integrated data-mining platform. Neoplasia *6*, 1–6.

Rohatgi, N., Aly, H., Marshall, C.A., McDonald, W.G., Kletzien, R.F., Colca, J.R., and McDaniel, M.L. (2013). Novel insulin sensitizer modulates nutrient sensing pathways and maintains β-cell phenotype in human islets. PLoS One *8*, e62012.

Sánchez-Aragó, M., Chamorro, M., and Cuezva, J.M. (2010). Selection of cancer cells with repressed mitochondria triggers colon cancer progression. Carcinogenesis *31*, 567–576.

Schieke, S.M., Ma, M., Cao, L., McCoy, J.P., Jr., Liu, C., Hensel, N.F., Barrett, A.J., Boehm, M., and Finkel, T. (2008). Mitochondrial metabolism modulates differentiation and teratoma formation capacity in mouse embryonic stem cells. J. Biol. Chem. *283*, 28506–28512.

Shahrzad, S., Lacombe, K., Adamcic, U., Minhas, K., and Coomber, B.L. (2010). Sodium dichloroacetate (DCA) reduces apoptosis in colorectal tumor hypoxia. Cancer Lett. *297*, 75–83.

Shyh-Chang, N., Locasale, J.W., Lyssiotis, C.A., Zheng, Y., Teo, R.Y., Ratanasirintrawoot, S., Zhang, J., Onder, T., Unternaehrer, J.J., Zhu, H., et al. (2013). Influence of threonine metabolism on S-adenosylmethionine and histone methylation. Science *339*, 222–226.

Slattery, M.L., Lundgreen, A., Herrick, J.S., and Wolff, R.K. (2011). Genetic variation in RPS6KA1, RPS6KA2, RPS6KB1, RPS6KB2, and PDK1 and risk of colon or rectal cancer. Mutat. Res. *706*, 13–20.

Takaishi, S., Okumura, T., Tu, S., Wang, S.S.W., Shibata, W., Vigneshwaran, R., Gordon, S.A.K., Shimada, Y., and Wang, T.C. (2009). Identification of gastric cancer stem cells using the cell surface marker CD44. Stem Cells *27*, 1006–1020.

Tennant, D.A., Durán, R.V., and Gottlieb, E. (2010). Targeting metabolic transformation for cancer therapy. Nat. Rev. Cancer *10*, 267–277.

Tibiletti, M.G., Trubia, M., Ponti, E., Sessa, L., Acquati, F., Furlan, D., Bernasconi, B., Fichera, M., Mihalich, A., Ziegler, A., et al. (1998). Physical map of the D6S149-D6S193 region on chromosome 6Q27 and its involvement in benign surface epithelial ovarian tumours. Oncogene *16*, 1639–1642.

Timón-Gómez, A., Proft, M., and Pascual-Ahuir, A. (2013). Differential regulation of mitochondrial pyruvate carrier genes modulates respiratory capacity and stress tolerance in yeast. PLoS ONE *8*, e79405.

Vander Heiden, M.G. (2011). Targeting cancer metabolism: a therapeutic window opens. Nat. Rev. Drug Discov. *10*, 671–684.

Vander Heiden, M.G., Cantley, L.C., and Thompson, C.B. (2009). Understanding the Warburg effect: the metabolic requirements of cell proliferation. Science *324*, 1029–1033.

Wanet, A., Arnould, T., Renard, P., Lou, P.H., and Peterson, N. (2012). Mitochondrial involvement in stemness and stem cell differentiation. In Cellular Bioenergetics in Health and Disease: New Perspective in Mitochondrial Biology, P.-H. Lou and N. Petersen, eds. (Kerala: Research Signpost), pp. 195–215.

Wang, X., Perez, E., Liu, R., Yan, L.J., Mallet, R.T., and Yang, S.H. (2007). Pyruvate protects mitochondria from oxidative stress in human neuroblastoma SK-N-SH cells. Brain Res. *1132*, 1–9.

Wang, Y.-C., Yo, Y.-T., Lee, H.-Y., Liao, Y.-P., Chao, T.-K., Su, P.-H., and Lai, H.-C. (2012). ALDH1-bright epithelial ovarian cancer cells are associated with CD44 expression, drug resistance, and poor clinical outcome. Am. J. Pathol. *180*, 1159–1169.

Warburg, O., Wind, F., and Negelein, E. (1927). The Metabolism of Tumors in the Body. J. Gen. Physiol. *8*, 519–530.

Whitehouse, S., Cooper, R.H., and Randle, P.J. (1974). Mechanism of activation of pyruvate dehydrogenase by dichloroacetate and other halogenated carboxylic acids. Biochem. J. *141*, 761–774.

Wu, C., Wei, Q., Utomo, V., Nadesan, P., Whetstone, H., Kandel, R., Wunder, J.S., and Alman, B.A. (2007). Side population cells isolated from mesenchymal neoplasms have tumor initiating potential. Cancer Res. *67*, 8216–8222.

Yang, W., Xia, Y., Ji, H., Zheng, Y., Liang, J., Huang, W., Gao, X., Aldape, K., and Lu, Z. (2011). Nuclear PKM2 regulates β-catenin transactivation upon EGFR activation. Nature *480*, 118–122.

Yeh, C.-S., Wang, J.-Y., Chung, F.-Y., Lee, S.-C., Huang, M.-Y., Kuo, C.-W., Yang, M.-J., and Lin, S.-R. (2008). Significance of the glycolytic pathway and glycolysis related-genes in tumorigenesis of human colorectal cancers. Oncol. Rep. *19*, 81–91.

Zu, X.L., and Guppy, M. (2004). Cancer metabolism: facts, fantasy, and fiction. Biochem. Biophys. Res. Commun. *313*, 459–465.

Molecular Cell, Volume *56*

Supplemental Information

A Role for the Mitochondrial Pyruvate Carrier as a Repressor of the Warburg Effect and Colon Cancer Cell Growth

John C. Schell, Kristofor A. Olson, Lei Jiang, Amy J. Hawkins, Jonathan G. Van Vranken, Jianxin Xie, Robert A. Egnatchik, Espen G. Earl, Ralph J. DeBerardinis, and Jared Rutter

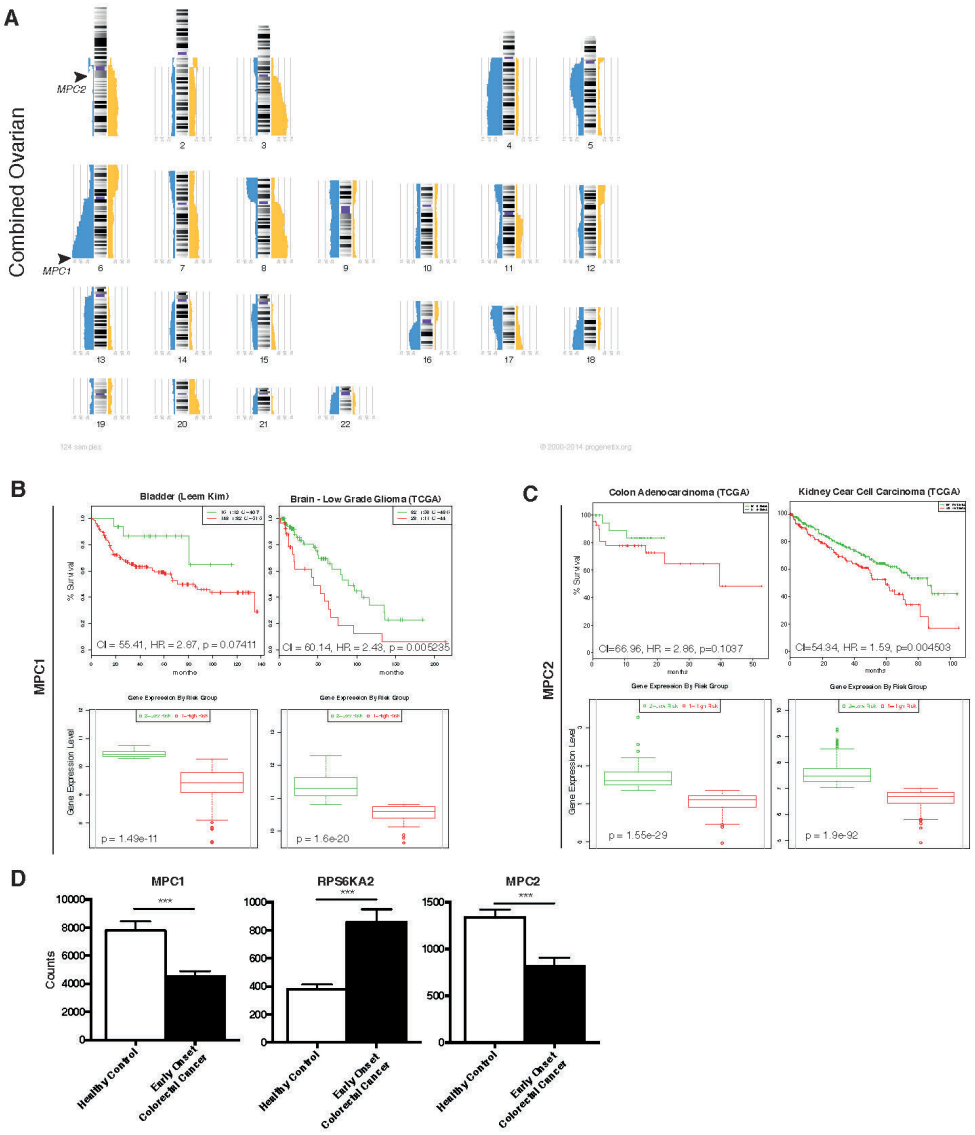

Figure S1 – Additional Bioinformatics related to Figure 1.

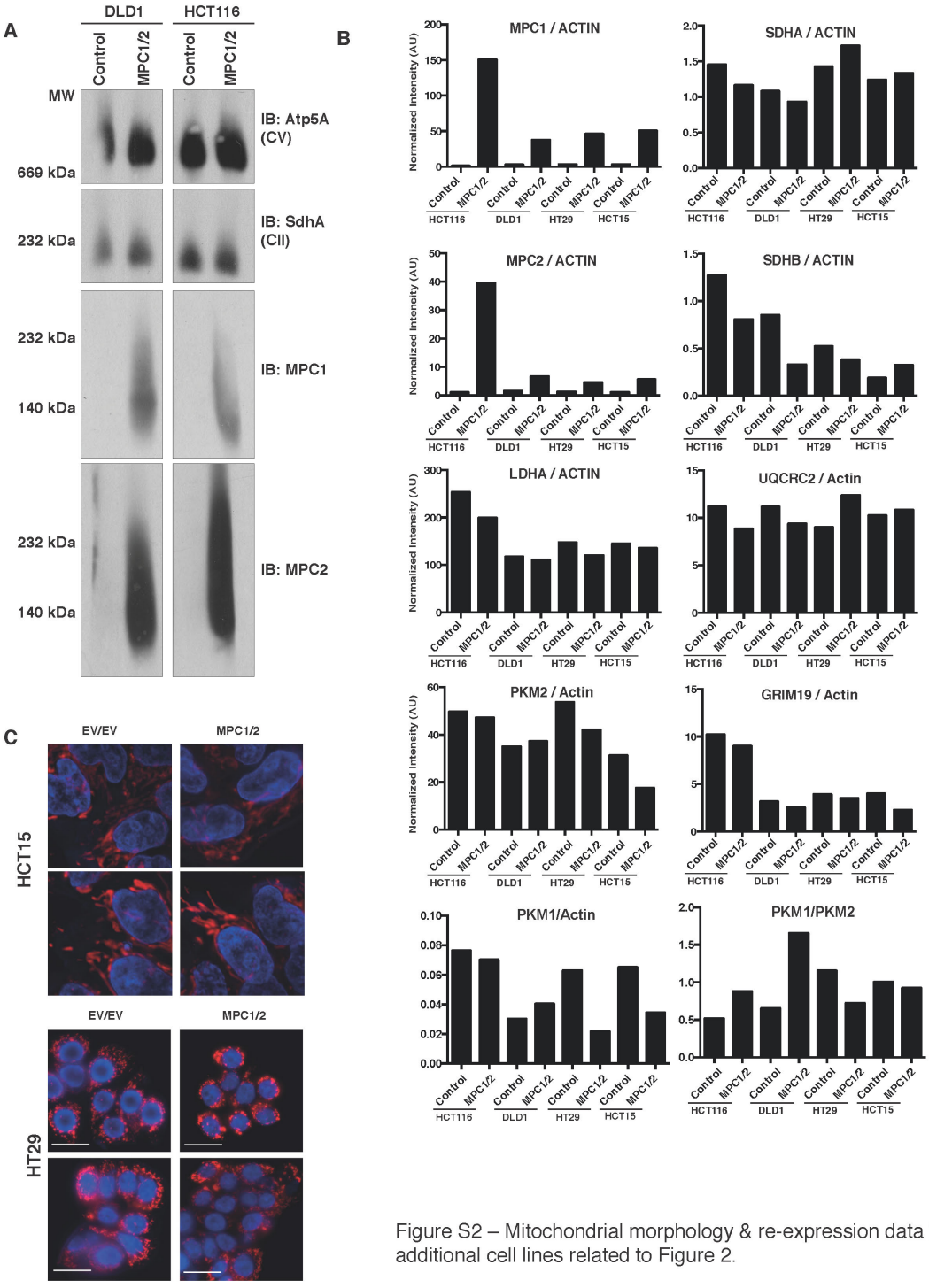

Figure S2 – Mitochondrial morphology & re-expression data in additional cell lines related to Figure 2.

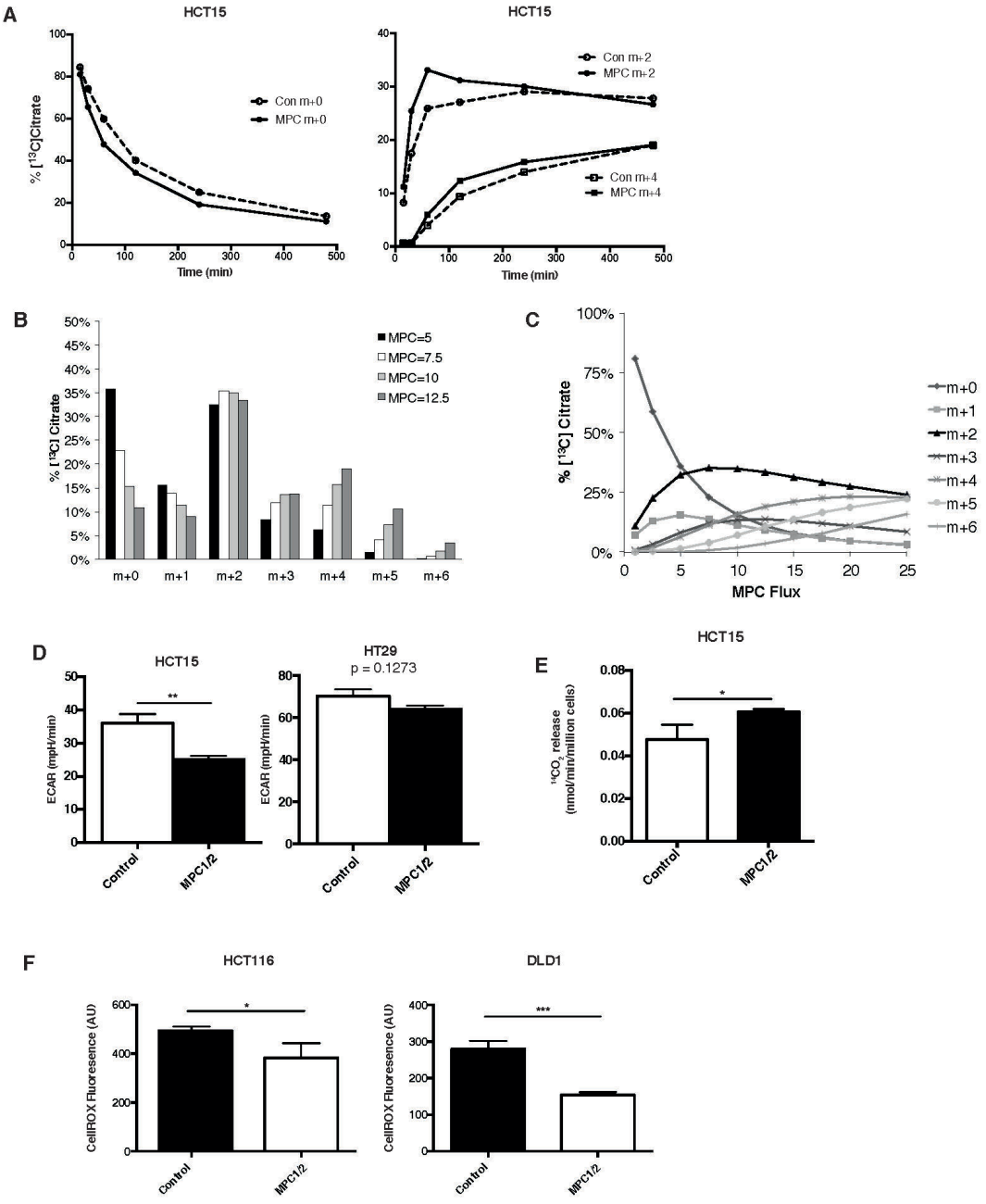

Figure S3 – Supplemental metabolic data and flux modeling related to Figure 3.

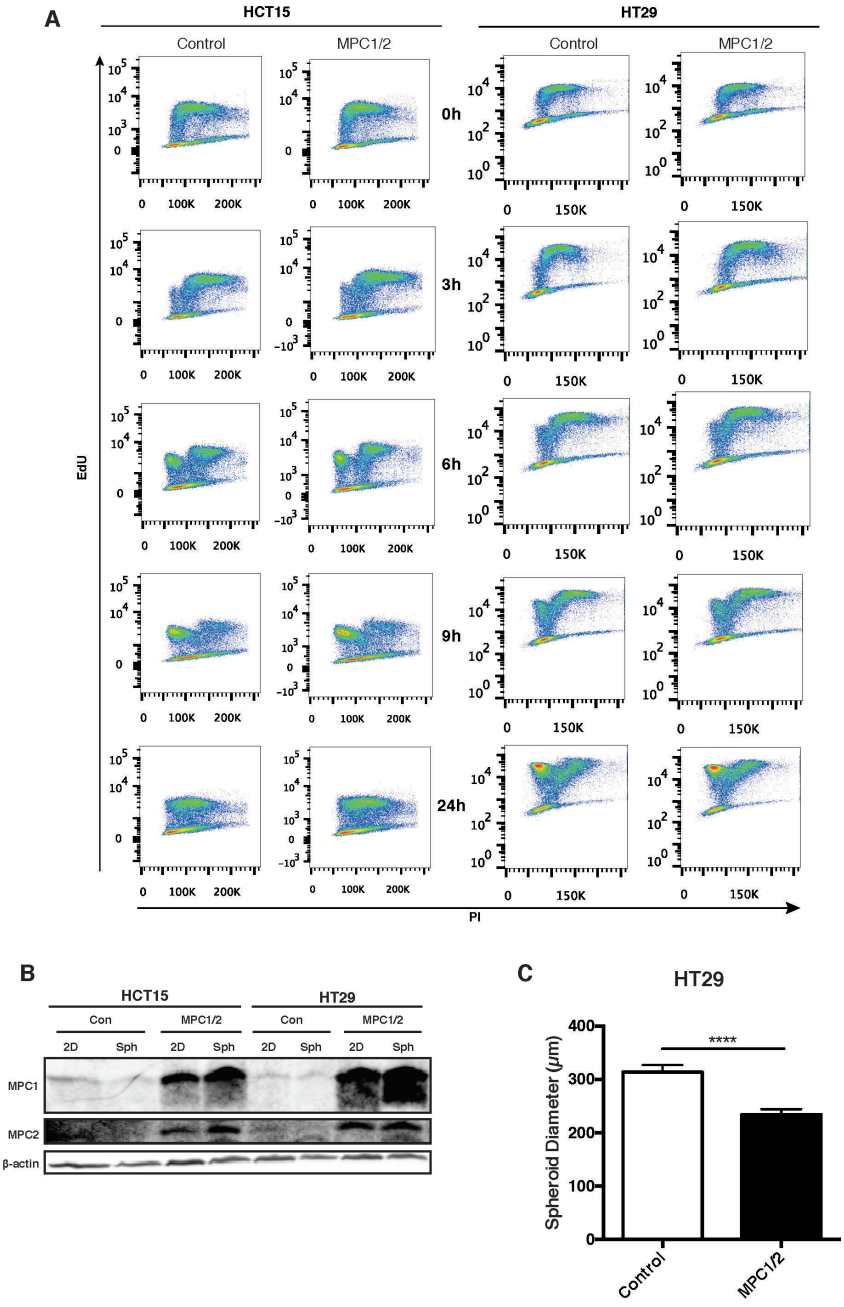

Figure S4 - Additional cell cycle and growth data related to Figure 4.

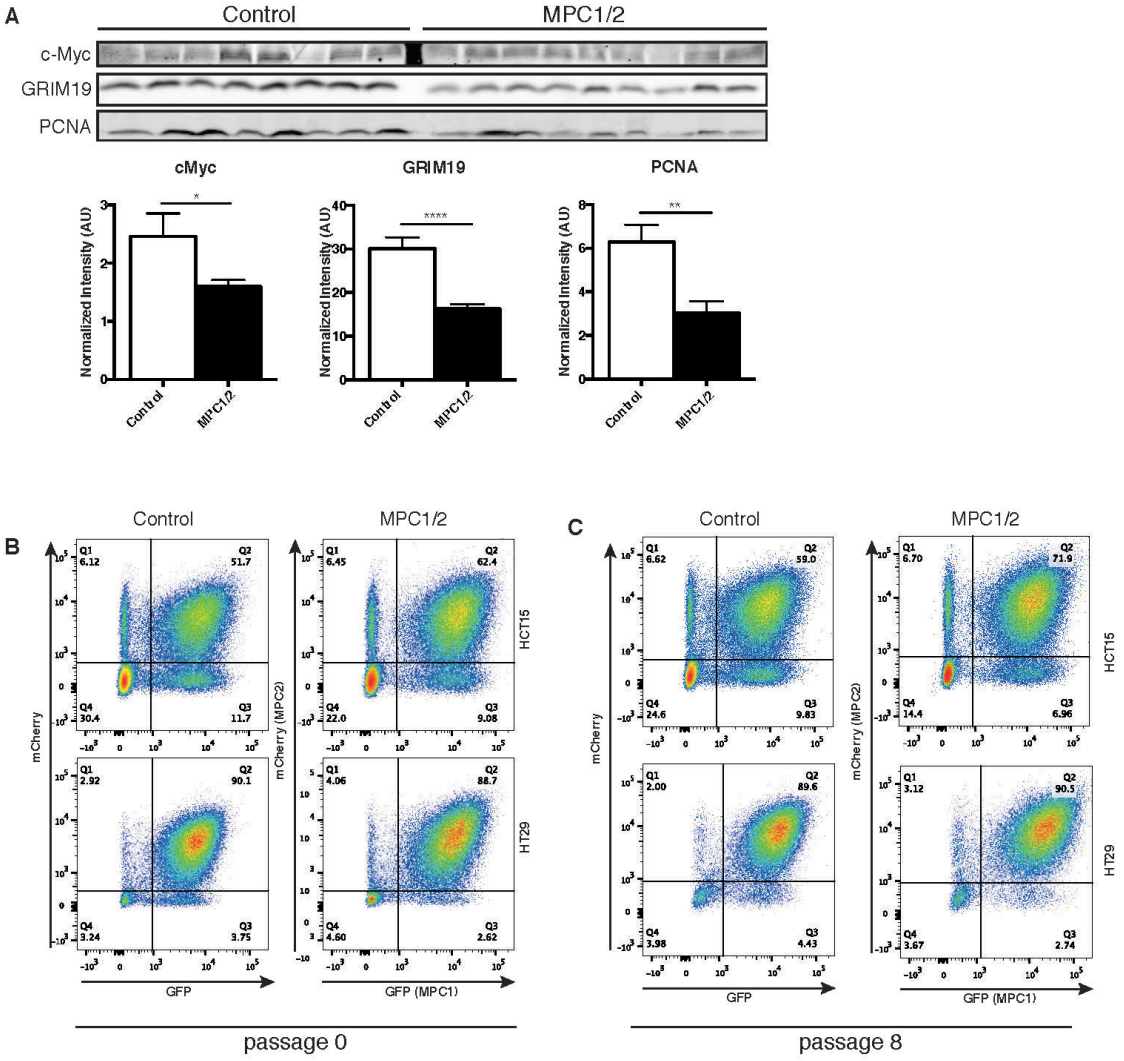

Figure S5 – Additional data illustrating the HCT15 adaptation phenotype related to Figure 6.

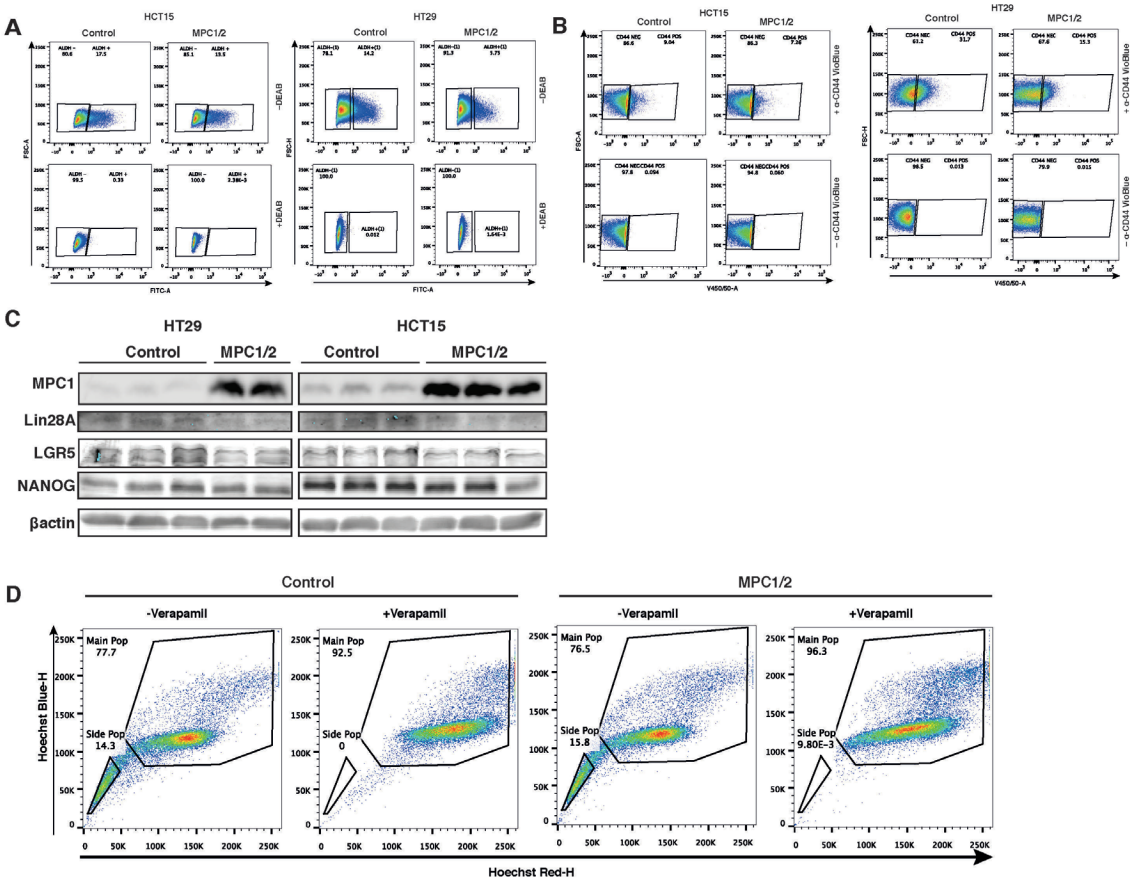

Figure S6 - Additional stem cell data and FACS dotplots related to Figure 7

Figure S1 – Additional Bioinformatics related to Figure 1.

(A) Genomic analysis of Ovarian Cancers according to Progenetix dataset (www.progenetics.org) across 124 samples. Arrows indicate *MPC1* (6q27) and *MPC2* (1q24) loci (B)*Top*- Kaplan-Meier survival curves of censored Cox analysis for Leem Kim Bladder, and TCGA Low Grade Glioma stratified by *MPC1* Expression risk group (SurvExpress, TCGA Research Network). *Bottom* – Gene expression level stratified by risk group. (C)*Top* Kaplan-Meier survival curves of censored Cox analysis for Director's Challenge NCI60 Lung, TCGA Colon Adenocarcinoma, and TCGA Kidney Clear Cell Carcinoma stratified by maximized *MPC2* expression risk group. *Bottom MPC2* expression levels stratified by risk group (SurvExpress, TCGA Research Network). (D) Total counts from GEO dataset GDS2609 showing expression of MPC1, MPC2, and RPS6KA2 (6q27) relative to healthy control tissue (n=10) in early-onset colorectal cancer (n=12). Data presented are mean ± SEM. ***, $p<0.001$

Figure S2 – Mitochondrial morphology & re-expression data in additional cell lines related to Figure 2.

(A) Western blot & Blue-native PAGE analysis of empty vector control vs. MPC1 & MPC2 co-expressing cell lines DLD1 and HCT116. (B) Quantification of MPC1/2, metabolic, and mitochondrial proteins across a panel of four colon cancer cell lines. Data presented are band intensities normalized to β-actin. (C) Fluorescence microscopy of mitochondrial morphology in empty vector control and MPC re-

expressing colon cancer cell lines HT15 and HT29. Two representative images per condition shown. Cells stained with DAPI (Blue) and Mitotracker (Red). Scale is 10μm.

Figure S3 – Supplemental metabolic data and flux modeling related to Figure 3.

(A) Time course mass isotopomer analysis of HCT15 control and re-expressing cell lines. (B and C) Simulated citrate MID from [U-^{13}C]glucose as a function of MPC flux. (D) Maximally-stimulated extracellular acidification rate (ECAR) on glucose with oligomycin (n=3, mean ± SEM). (E) ^{14}CO2 release in HCT15 cells. (mean ± SD, n=3) Effects of MPC1/2 on reactive oxygen species. (F) Median fluorescence values for CellROX Deep Red (mean ± SD, n=3) *, p<0.05; **,p<0.01; ***, p<0.001

Figure S4 – Additional cell cycle and growth data related to Figure 4.

(A) Full time course FACS dotplots of HCT15 and HT29 EdU pulse-chase. (B) Western blot of MPC1 and MPC2 in re-expressing cell lines in 2D and 3D culture. (C) HT29 spheroid size in control (n=129) and MPC (n=120) re-expressing cells. (mean ± SEM). ***, p<0.001

Table S1 – Summary of Soft Agar Growth Assays

Figure S5 – Additional data illustrating the HCT15 adaptation phenotype, related to Figure 6.

(A) Additional HCT15 Adaptation Xenograft Western Blots for c-Myc, GRIM19, and PCNA. Data presented are band intensities normalized to actin, mean ± SEM. (B-C) FACS dot-plots of HCT15 cell lines grown in 2D culture at initial passage and after 8 serial passages.*, $p<0.05$; **, $p < 0.01$; ***, $p < 0.001$

Figure S6 - Additional stem cell data and FACS dotplots related to Figure 7

(A) Representative FACS dot-plots and gating of Aldafluor assay for MPC re-expressing cell lines HCT15 and HT29. DEAB was used as a negative control. (B) Representative FACS dot-plots and gating of CD44 for MPC re-expressing cell lines HCT15 and HT29. Antibody-free sample was used as a negative control. (C) Additional western blots illustrating the change in stem cell markers between control (HT29 n=3, HCT15 n=3) and MPC re-expressing (HT29 n=2, HCT15 n=3) cell lines. (D) Side population assay analysis of HCT15 cell lines with empty vector control or MPC1/2 expression. Verapamil was used as a negative control.

Table S1 – Summary of HCT15/HT29 soft agar assay data (Related to Figure 4)

Soft agar assays are presented chronologically as they were performed, with the respective viral expression systems ("Biological Derivation") noted. Each growth assay was conducted with an n=12 per media condition. Significance values (Student's t-test) of colony formation between Control (GFP/tdT) vs. MPC1/2 expressing lines presented below. Unless marked otherwise, all control samples formed significantly more colonies than the MPC1/2 lines. For more information see Supplemental Experimental Procedures.

HCT15		Media Conditions				
Assay #	Biological Derivation	DMEM	RPMI	McCoy's 5A	DMEF/12	Iscove's
HCT15-1	pQCXIP-GFP/MPC1 pBabeHygro-tdT/MPC2	p = 0.0006	p < 0.0001	p < 0.0001	p = 0.0005	p < 0.0001
HCT15-2	pQCXIP-GFP/MPC1 pQCXIZ-tdT/MPC2	p < 0.0001	p = 0.0005	p = 0.0033	n.s.	p = 0.0081
HCT15-3	pQCXIP-GFP/MPC1 pQCXIZ-tdT/MPC2	p < 0.0001	p < 0.0001	p = 0.0429	p = 0.0002	n.s.

HT29		Media Conditions				
Assay #	Biological Derivation	DMEM	RPMI	McCoy's 5A	DMEF/12	Iscove's
HT29-1	pQCXIP-GFP/MPC1 pQCXIZ-tdT/MPC2	p = 0.0015	p < 0.0001	p = 0.0022	n.s.	p = 0.0003
HT29-2	pQCXIP-GFP/MPC1 pQCXIZ-tdT/MPC2	p = 0.033	p = 0.0072	p = 0.0097	p = 0.0464	p = 0.0012

Supplemental Experimental Procedures

Bioinformatic analyses

Publically available and curated resources were used to explore potential alterations of *MPC1* and *MPC2* in various normal and disease states including Survexpress, Oncomine, TCGA, Progenetix, cBioprotal, and Gene Expression Omnibus. Survexpress was utilized to compared survival profiles for individuals segregated based on high and low MPC expression with risk groups maximized and censored for survival in months (Aguirre-Gamboa et al., 2013). Oncomine was used to compared studies in which both cancer and adjacent normal samples were present to determine if patterns in *MPC1* and *MPC2* expression existed across multiple studies and investigate genes that were commonly co-expressed (Rhodes et al., 2004). Compilation data in figure 1C was generated using a p value cutoff of 0.05, no threshold fold change and all gene ranking criteria to summarize the maximum number of available studies. The Tumor Cancer Genome Atlas studies on colon and rectal adenocarcinoma were used for gene expression of *MPC1* and *MPC2* as well as survival statistics, and correlation investigations with other genes of interest throughout the paper. For figures 1B, 1C, 1D, 1F, and table S1 the results shown are in whole or part based upon data generated by the TCGA Research Network: http://cancergenome.nih.gov/. Analysis of chromosomal copy number aberrations was carried out using Progenetix.org for all cancer datasets available (Figure 1A) and specific cancer datasets (Figure S1) (Cai et al., 2014). cBioPortal was used as the source for co-expression analysis within the TCGA colorectal cancer dataset (Figure 1F). Gene Expression Omnibus was queried for datasets in which *MPC1* and *MPC2* expression was significantly altered.

Plasmids

Human *MPC1*, *MPC2* and the R97W mutant were cloned from pQCXIP-MPC1 & pQCXIP-MPC2 (Bricker, 2014) into either pQCXIB (Addgene #17475), pQCXIZ (Addgene #22801), LeGO iG2 (Addgene #27341), or LeGO iC2 (Addgene#27345).

Fluorescent MPC1 & MPC2 fusion proteins were generated by ligation into pQCXIP-GFP. Control constructs were empty vectors or expressed GFP or tdTomato.

Side population assay

Side population assays were performed as previously described with minor changes (Goodell et al., 1996). Trypsinized cultured cells were resuspended in media to $1x10^6$cell/mL. After a 10 minute pre-incubation, with or without 50μM Verapamil (Abcam), cells were labeled with 16.2μM Hoechst 33342 for 90 minutes at 37˚C. Cells were counterstained with Fixable Viability Dye eFluor 780 (eBioscience) and counted and sorted on BD FACSAria II (BD Biosciences San Jose, CA). Cells were gated using the strategy published for the assay's critical review.(Golebiewska et al., 2011) The Hoechst dye was excited with the ultraviolet laser and was measured at two wavelengths using optical filters 450/50 (Hoechst Blue) and 670LP (Hoechst Red). Data were analyzed and presented with FlowJo vX (TreeStar Inc Ashland, OR).

Fluoresence assisted cell sorting

Cultured cells were trypsinized, resuspended, and incubated with VioBlue-conjugated antibody against CD44 (Miltenyi Biotech) as per the manufacturer's recommendations. Single, live cells were sorted on BD FACSAria II after excitation with the 408nm laser and read with the 450/50 optical filter. The top and bottom 5% of cells were sorted as $CD44^{hi}/CD44^{lo}$. Similarly, cells were analyzed for ALDH activity using the Aldefluor assay (Stemcell Technologies) as per the manufacturer's recommendations, and sorted on FACSAria II after excitation with the 488nm laser and read with the 530/30 filter set. The top and bottom 5% of cells were sorted as $ALDH^{hi}/ALDH^{lo}$ for subsequent experiments. Data were analyzed and presented with FlowJo vX.

Cell Viability Assays

Cell viability was determined by exclusion of 0.2% Trypan Blue (Sigma-Aldrich) and counting with Cellometer Auto T4 (Nexelcom). Apoptosis & necrosis was

determined by Annexin V Alexa Fluor 647 and propidium iodide staining (Life Technologies). Data were acquired on BD FACSCanto (BD Biosciences San Jose, CA) with the 640nm laser (670/30 filter set) and 488nm laser (685/40 filter set).

Mitochondrial membrane potential and ROS

Mitochondrial membrane potential was determined using MitoProbe $DiIC_5$ (Life Technologies) as per the manufacturer's recommendations. Cells were treated with CCCP as a control. Data were acquired on BD FACSCanto (BD Biosciences San Jose, CA) with the 640nm laser and 670/30 filter. Reactive oxygen species were evaluated utilizing CellROX Deep Red (Life Technologies) as per the manufacturer's recommendations. As controls, cells were treated with *N*-acetylcysteine and menadione. Data were acquired on BD FACSCanto with the 640nm laser and 750/LP optical filter. Data were analyzed and presented with FlowJo vX.

EdU cell-cycle assay

Cells were initially passaged into 10cm dishes. At 50% confluence, cells were pulsed for 30 minutes with 10mM 5-ethynyl-2′-deoxyuridine (EdU) (Life Technologies). Media was then replaced and cells were harvested at 0, 3, 6, 9, and 24h; fixed, and permeabilized as per the manufacturer's protocol. Click-iT AlexaFluor 647 was conjugated to the EdU as per the manufacturer's protocol, and DNA content was simultaneously measured with with propidium iodide. Data were acquired on BD FACSCanto with the 640nm laser (670/3 filter set) and 488nm laser (685/40 filter set). Data were analyzed and presented with FlowJo vX.

Fluoresence adaptation assay

We utilized the LeGO vector system (Weber et al., 2008) to allow us a fluorescent "surrogate" mark, encoded by a bicistronic mRNA, to evaluate population-wide shifts of MPC expression over time. After infection, cells were sorted on BD FACSAriaII with 488nm laser (525/50 filter set) and 561nm laser (610/20 filter set) for only those GFP/mCherry double-positives. These cells were then plated in 10cm dishes or low-attachment plates. After serial passaging in 2D or 3D (see "Spheroid

growth assay"), cells were scanned on the BD FACSCanto with the 488nm laser (530/30 optical filter) and 561nm laser (610/20 optical filter) for GFP/mCherry fluorescence, respectively. Data were analyzed and presented with FlowJo vX.

Cell proliferation assay

Cell proliferation in 2D culture was performed by sorting 5,000 single cells per well in a 96-well plate. Plates were harvested every 24 hours for 5 days by aspirating media and washing 2X with PBS before storing at -80°C. Proliferation was determined using a CyQuant Cell Proliferation assay kit (Life Technologies) and fluorescence was determined using a Varioskan Flash plate-reader (Thermo Scientific).

Anchorage independent cell growth assay

Soft agar assays were carried out as described by: http://www.nature.com/protocolexchange/protocols/2611#/procedure with the following modifications. Single cells were sorted on a BD FACSAria II to ensure precise cell number and consistent size between control and MPC expressing groups into collection tubes containing media and plated at 2,500 cells per well. For each biological replicate experiment, assays were performed in 12-well plates, in 5 different media conditions: DMEM, RPMI 1560, McCoy's 5A, DMEF/12, & Iscove's; each with 2mM Glutamax (Invitrogen), 10% FBS (Sigma Aldrich) and 1% primocin. Plates were monitored for colony formation, and fixed in ice-cold methanol, followed by 3x wash in 70% ethanol. Colonies were visualized by backlight illumination, and imaged with a Panasonic Lumix DMC-ZS10 on macro mode. Images were cropped, normalized to 2000x2000pixels, desaturated using Adobe Photoshop CS5, and colonies were counted using ImageJ and verified by eye. Data were analyzed by Student's t-test with unequal variances.

Spheroid growth assay

Single cells were sorted on a BD FACSAria II directly into 24-well Costar Ultra-Low Attachment plates (Corning) containing media at 5,000 cells per well. Plates were

monitored eye and dissecting microscope for the formation of spheroids and growth was assessed over the course of 2 weeks followed by imaging and quantification. For the rescue experiment, cells were grown with and without 5μM UK5099 (Sigma Aldrich). Serial passaging of spheroids for adaptation studies were carried out in 6-well ultra-low attachment plates (Corning). Briefly, cells were vigorously resuspended and transferred to conical tubes followed by centrifugation at 600 x g for 5 minutes. Spheroids were then washed in PBS, re-pelleted, and incubated in 0.25% Trypsin EDTA until dissociated. Trypsin was then neutralized with media containing serum and the cell mixture was filtered through a 0.35μm cell strainer. These dissociated cells were then used to re-seed ultra-low attachment dishes. Spheroid number was determined per well by manual counting with Olympus SZ61 dissecting microscope. Spheroids were imaged by treating spheroids with 16.2μM Hoechst 33342 and imaged with Axio Observer Z1 imaging system (Carl Zeiss) equipped with 4X objective and DAPI filter or DIC.

Immunoblotting

Antibodies were obtained from Cell Signalling Technologies (CS), Abcam (ab), Sigma. Antibodies used were: PKM2 (ab100841), PKM1 (CS7067), SDHA (ab14715), SDHB (ab14714), ALDH1A1 (ab52492), GPCR GPR49-LGR5 (ab71225), LDHA (CS2102), UQCRC2 (ab14745), GRIM19 (ab110240), beta-actin (Sigma A5441), PCNA (CS2586), c-Myc (CS5605), Lin28A (CS3695), NANOG (CS4903), Phospho PDH (ab9296), Total PDH (ab67592), PDK1 (CS3820) Cyclophilin B (ab74173), & alpha-Tubulin (CS3873). MPC1 and MPC2 antibodies were developed and tested in collaboration with Cell Signaling Technologies. Secondary antibodies were as follows Alexa-Fluor 680 donkey anti-rabbit (A10043, Invitrogen) and IRDye 800 donkey anti-mouse (RL610-732-002, VWR).

Cell line pellets and xenograft derived tumor samples were prepared in tissue lysis buffer (50mM HEPES, 150 mM NaCl, 10% Glycerol, 1% Triton X-100, 1.5 mM MgCl, 1.0 mM EGTA, 10 mM Sodium Pyrophosphate, 100 mM Sodium Fluoride, 1 mM phenylmethylsulfonyl fluoride (PMSF), 1x mammalian Protease Inhibitor Cocktail (Sigma P8340), and 1x Phosphatase Inhibitor Cocktail (Sigma P5726). Sample

protein concentrations were quantified by BCA assay (Thermo Scientific/Pierce) and normalized to ensure constant sample loading between wells. Samples were then subjected to SDS-polyacrylamide gel electrophoresis (PAGE) and immunoblotting. Specifically, MPC1 and MPC2 were resolved using 18% acrylamide gels and transferred to methanol activated 0.45 um Immobilon FL PVDF membranes (EMD Millipore). Following one hour of blocking in 2.5% milk the membranes were washed and probed with specific antibodies diluted in a solution of 5% BSA made in TBS containing 0.1% Tween-20. Membranes were washed and probed with fluorescent conjugated secondary antibodies and scanned using the LI-COR Biosciences Odyssey system. Analysis of band intensities was carried out using the LI-COR imaging software with background method set to average of all surrounding pixels with beta-Actin or Cyclophilin B as a loading control.

Mitochondrial enzyme activity assays

Citrate synthase assays were performed on whole cell lysates as previously described (Riehle et al., 2013), utilizing 50 and 100ng of total protein. Pyruvate dehydrogenase activity assays were performed using PDH Enzyme Activity Assay kit (Abcam) as per the manufacturer's recommendations loading 50ng, 100ng, and 150ng of cell lysate. Bands were scanned and quantified using ImageJ.

Quantitative RT-PCR

Total RNA was extracted and purified from cells using the RNeasy Mini Kit (Qiagen) according to manufacturer instructions. cDNA was synthesized using the High Capacity cDNA Reverse Transcription Kit (Applied Biosystems). For RNA extracted from cells sorted in the ALDH assay, total RNA was extracted and purified using the Arcturus PicoPure RNA Isolation Kit, and cDNA was synthesized using PrimeScript RT Master Mix (Takara). Subsequently, real time PCR was performed with LightCycler 480 SYBR Green I Master Mix (Applied Biosystems) using a LightCycler 480 (Roche). All reactions were performed at least four times. Sequences of RT-PCR primers are as follows.

MPC1 Fwd1 (GTGCGGAAAGCGGCGGACTA)

MPC1 Rev1 (GGCAGCAATGGGAAGACCCCA
MPC1 Fwd2 (CGCGTTGGTGCGGAAAGCG)
MPC1 Rev2 (GGCAAATGTCATCCGCCCACTGA)
TBP Fwd (AGCCTGCCACCTTACGCTCAG)
TBP Rev (TGCTGCCTTTGTTGCTCTTCC)
36B4 Fwd (AGATGCAGCAGATCCGCAT)
36B4 (GTTCTTGCCCATCAGCACC).
The following primer sequences were obtained and verified from the Harvard PrimerBank (Cai et al., 2014):
MPC2 Fwd (TACCACCGGCTCCTCGATAAA)
MPC2 Rev (TATCAGCCAATCCAGCACACA).

Mass isotopomer analysis

Nutrients labeled with ^{13}C were purchased from Cambridge Isotope Laboratories. All ^{13}C studies were performed in medium containing 10% dialyzed FBS and prepared so that 100% of either the glucose or glutamine pool was labeled with ^{13}C, and the other pool was unlabeled. DMEM lacking both glucose and glutamine was prepared from powder (Sigma), then supplemented with 15 mM D[U-^{13}C]glucose. Cells were grown in 60- or 100-mm dishes until 80% confluent, then rinsed with PBS and cultured with ^{13}C-containing medium for the indicated time (usually 6 h). The cells were then extracted by freeze-thawing three times in 0.5 ml of a cold 1:1 mixture of methanol:water. Macromolecules and debris were removed by centrifugation, an internal standard was added (50 nmol of 2-oxobutyrate), and the supernatants with aqueous metabolites were evaporated completely and derivatized for 30 min at 42 °C in 100 µl of a trimethylsilyl donor (Tri-Sil, Thermo). Metabolites were analyzed using an Agilent 6970 gas chromatograph networked to an Agilent 5973 mass selective detector. Retention times and mass fragmentation signatures of all metabolites were validated using pure standards. To determine relative metabolite abundance across samples, the area of the total ion current peak for the metabolite of interest was compared to that of the internal standard and normalized for protein content. The mass isotopomer distribution analysis

measured the fraction of each metabolite pool that contained every possible number of ^{13}C atoms; that is, a metabolite could contain 0, 1, 2, … n ^{13}C atoms, where n = the number of carbons in the metabolite. For each metabolite, an informative fragment ion containing all carbons in the parent molecule was analyzed using MSDChem software (Agilent), integrating the abundance of all mass isotopomers from m+0 to m+n, where m = the mass of the fragment ion without any ^{13}C. The abundance of each mass isotopomer was then corrected mathematically to account for natural abundance isotopes and finally converted into a percentage of the total pool.

Simulation of citrate labeling as a function of MPC flux.

Simulations of the steady state citrate labeling from [U-^{13}C]glucose as a function of MPC flux were performed using the INCA software package (Young, 2014). Briefly, a simple metabolic network of glycolysis, pyruvate transport, anaplerosis and cataplerosis was constructed as detailed in "**Reactions and Atom Transitions for the Simulation of Citrate Labeling as a Function of Pyruvate Transport**" below. In order to examine how MPC activity would affect citrate labeling, the following reactions were set to fixed values. Glutamate entry into the TCA cycle was maintained at a constant value (10% of glucose uptake) to have the same rate of dilution on modeled citrate pools. Pyruvate carboxylase activity was assumed to be minimal. Lastly, cataplerotic demand for lipid synthesis through ATP citrate lyase was fixed based upon the observation that adherent cells overexpressing MPC have similar growth rates in adherent culture. Lastly, the lactate secretion flux was allowed to decrease as the MPC flux increased. Assuming that all incoming glucose would be 100% [U-^{13}C]glucose, the mass isotopomer distribution of citrate was then calculated using these parameter estimates. MPC fluxes as arbitrary flux units relative to a fixed glucose uptake of 100. An MPC flux of 5 therefore indicates that the MPC flux is 5% of the glucose uptake and 2.5% of the carbon is oxidized in the TCA cycle.

Reactions and Atom Transitions for the Simulation of Citrate Labeling as a Function of Pyruvate Transport.

Dot suffixes for metabolites indicate distinct metabolite populations: .t, ^{13}C tracer: .c, cytosol: .m, mitochondria: .f, fat.

Cytosolic Pyruvate Metabolism			Notes	Name
Glc.t (abcdef)	→	Pyr.c (cba) + Pyr.c (def)	Fixed to 100	PK
Pyr.c (abc)	→	Lac.x (abc)		LDH
Pyruvate Transport				
Pyr.c (abc)	→	Pyr.m (abc)	Manually Varied	MPC
Mitochondrial Metabolism				
Pyr.m (abc)	→	AcCoA (bc) + CO_2 (a)		PDH
AcCoA (ab) + Mal (cdef)	→	Cit (fedbac)		CS
Cit (abcdef)	→	αKG (abcde) + CO2 (f)		IDH
αKG (abcde)	→	Suc (bcde) + CO2 (a)		ADH
Suc (½ abcd + ½ dcba)	→	Fum (½ abcd + ½ dcba)		SDH
Fum (abcd)	←→	Mal (abcd)		FUM
Anaplerosis/Cataplerosis				
Glu (abcde)	←→	αKG (abcde)	Fixed to 10	GDH
Mal (abcd)	→	Pyr.m (abc) + CO2 (d)	Fixed to 0.1	ME
Pyr.m (abc) + CO2 (d)	→	Mal (abcd)		PC
Cit (abcdef)	→	Mal (fcba) + AcCoA.f	Fixed to 5	ACL

CO_2 production assay

Trypsinized and resuspended HCT15 cells ($0.5x10^6$) were cultured with [1-^{14}C]Pyruvate in warm Krebs buffer for 20 minutes. Released $^{14}CO_2$ was measured by scintillation counting.

Supplemental References

Aguirre-Gamboa, R., Gomez-Rueda, H., Martínez-Ledesma, E., Martínez-Torteya, A., Chacolla-Huaringa, R., Rodriguez-Barrientos, A., Tamez-Peña, J.G., and Treviño, V. (2013). SurvExpress: an online biomarker validation tool and database for cancer gene expression data using survival analysis. PLoS ONE *8*, e74250.

Bricker, D.K., Taylor, E.B., Schell, J.C., Orsak, T., Boutron, A., Chen, Y.C., Cox, J.E., Cardon, C.M., Van Vranken, J.G., Dephoure, N., et al. (2012). A Mitochondrial Pyruvate Carrier Required for Pyruvate Uptake in Yeast, Drosophila, and Humans. Science *337*, 96–100.

Cai, H., Kumar, N., Ai, N., Gupta, S., Rath, P., and Baudis, M. (2014). Progenetix: 12 years of oncogenomic data curation. Nucleic Acids Research *42*, D1055–D1062.

Golebiewska, A., Brons, N.H.C., Bjerkvig, R., and Niclou, S.P. (2011). Critical Appraisal of the Side Population Assay in Stem Cell and Cancer Stem Cell Research. Cell Stem Cell *8*, 136–147.

Goodell, M.A., Brose, K., Paradis, G., Conner, A.S., and Mulligan, R.C. (1996). Isolation and functional properties of murine hematopoietic stem cells that are replicating in vivo. *183*, 1797–1806.

Rhodes, D.R., Yu, J., Shanker, K., Deshpande, N., Varambally, R., Ghosh, D., Barrette, T., Pandey, A., and Chinnaiyan, A.M. (2004). ONCOMINE: a cancer microarray database and integrated data-mining platform. Neoplasia (New York, N.Y.) *6*, 1–6.

Riehle, C., Wende, A.R., Sena, S., Pires, K.M., Pereira, R.O., Zhu, Y., Bugger, H., Frank,

D., Bevins, J., Chen, D., et al. (2013). Insulin receptor substrate signaling suppresses neonatal autophagy in the heart. J. Clin. Invest. *123*, 5319–5333.

Tibiletti, M.G., Trubia, M., Ponti, E., Sessa, L., Acquati, F., Furlan, D., Bernasconi, B., Fichera, M., Mihalich, A., Ziegler, A., et al. (1998). Physical map of the D6S149-D6S193 region on chromosome 6Q27 and its involvement in benign surface epithelial ovarian tumours. Oncogene *16*, 1639–1642.

Weber, K., Bartsch, U., Stocking, C., and Fehse, B. (2008). A Multicolor Panel of Novel Lentiviral "Gene Ontology" (LeGO) Vectors for Functional Gene Analysis. Mol Ther *16*, 698–706.

Young, J.D. (2014). INCA: a computational platform for isotopically non-stationary metabolic flux analysis. Bioinformatics *30*, 1333–1335.

CHAPTER 4

IN VIVO STUDY OF THE MPC IN MOUSE COLON EPITHELIUM

4.1 Abstract

Deregulated cellular energetics is now firmly established as a hallmark of cancer,[1] and much work is being done to dissect the mechanisms enforcing aerobic glycolysis, or the Warburg effect. Similar to glycolytic cancer cells, many stem cells limit mitochondrial oxidation of carbons in favor of glycolysis. Within the colon, crypt stem cells have been shown to be the cell of origin for many colon adenocarcinomas. The mitochondrial pyruvate carrier (MPC) is sufficient to repress the Warburg effect in colon cancer cells in vitro, and its expression decreases tumor growth, owing to the metabolic inflexibility of this type of cancer. Here we investigate whether forcing the Warburg effect, via deletion of the MPC in colon stem cells, metabolically "primes" cells for transformation, or promotes stemness by limiting the mitochondrial oxidation necessary for differentiation.

4.2 Introduction

The metabolic derangements of cancer were first examined nearly a century ago, when it was observed that cancers perform glycolysis irrespective of oxygen tension, and at the expense of complete mitochondrial oxidation of carbon sources.[2] This phenomenon is known as the "Warburg effect." Over the past two decades, there has been resurgence of research on cancer metabolism,[3-5] with the hope that understanding the metabolic phenotype of cancer can lead do the development of novel chemotherapeutics.[6-10]

Central to the "Warburg effect" is the fate of pyruvate; whether it is transported into the mitochondrion for further oxidation or reduced to lactate and excreted from the cell.[11] Each of the proteins surrounding pyruvate have been shown to be deregulated in some fashion or another in cancer, including pyruvate kinase,[12-17] lactate dehydrogenase,[18-23] and pyruvate dehydrogenase kinase (PDK),[24-26] as well as the mitochondrial pyruvate carrier (MPC).[27] The extent of regulation of pyruvate formation and destruction in normal and disease physiology underlines the importance of this three carbon molecule.

Proliferative cells, including stem cells, exhibit a similar metabolic paradigm as the "Warburg effect," where mitochondrial oxidation is reduced in favor of increased glycolysis.[28-31] Stem cells, much like cancer cells, have an increased requirement for biosynthetic building blocks[32,33] for the construction of nucleotides, lipids, and amino acids, many of which are

intermediates of glycolysis.[3,33,34] During the process of differentiation, stem cells generally undergo a shift from glycolytic to more mitochondrial carbon oxidation, owing to an increased energetic demand of the differentiated tissue.[35,36]

Previous work in colon cancer showed that reexpression of the mitochondrial pyruvate carrier was sufficient to repress the "Warburg effect" and decrease xenograft tumor growth.[37] These deleterious effects manifest in the "stem cell like" or cancer stem cell compartment, suggesting that the MPC may also play an important role in the metabolism, maintenance, and/or differentiation of stem cells.

Several questions remained after the *Molecular Cell* paper in 2014 regarding the connection between the MPC, stem cells, and cancer.[37] Is the MPC required for differentiation, or conversely is its absence required for the maintenance of stemness? Is *MPC1* a tumor suppressor gene? In sum, these questions address whether metabolism itself is simply a bystander, responding passively to cellular energetic needs, or whether modulation of metabolism, and metabolism alone is sufficient to drive proliferation and tumorigenesis. This chapter highlights some preliminary data towards answering these fundamental questions.

4.3 Results

4.3.1 Generation of Colon Stem Cell MPC1 Conditional Knockout Mouse

This study begins by obtaining a transgenic mouse harboring an *Mpc1*$^{tm1a(EUCOMM)Wtsi}$ targeted allele from the Wellcome Trust Sanger Institute (Figure 4.1). Mice were crossed with germline FLP-Cre mice to remove the reporter and selection cassette. Homozygous *Mpc1* and *Mpc2* knockout mice are embryonic lethal,[38] so the conditional allele was validated by generating MEF lines from a heterozygous *Mpc1*$^{flox/wt}$ cross. After transient transfection with GFPCre,[39] recombination and loss of MPC1 was validated by western blot (Figure 4.2). The loss of MPC2 protein is consistent with previous studies[40-42] that have shown knockdown of either *Mpc1* or *Mpc2* is sufficient to lose the complex in mitochondria.

Stem cells reside in the base of the colon crypt, and are generally stratified into a rapid-cycling (Lgr5)[43,44] or slow-cycling/quiescent (Lrig1)[45] component (Figure 4.3A). Previous work identified Lrig1 stem cells within the colon crypt as a cell-of-origin for colon adenocarcinoma.[46] To assess the role of the MPC in maintaining stemness and/or its potential function as a tumor suppressor, we crossed *Mpc1*^{flox} mice with *Lrig1*^{CreERT2} mice (Figure 4.3B). Mice were harvested 30 days after tamoxifen injection and Swiss-rolled, fixed, and sectioned colons were analyzed by IHC.

Turnover of the colon epithelium occurs approximately every 4-5

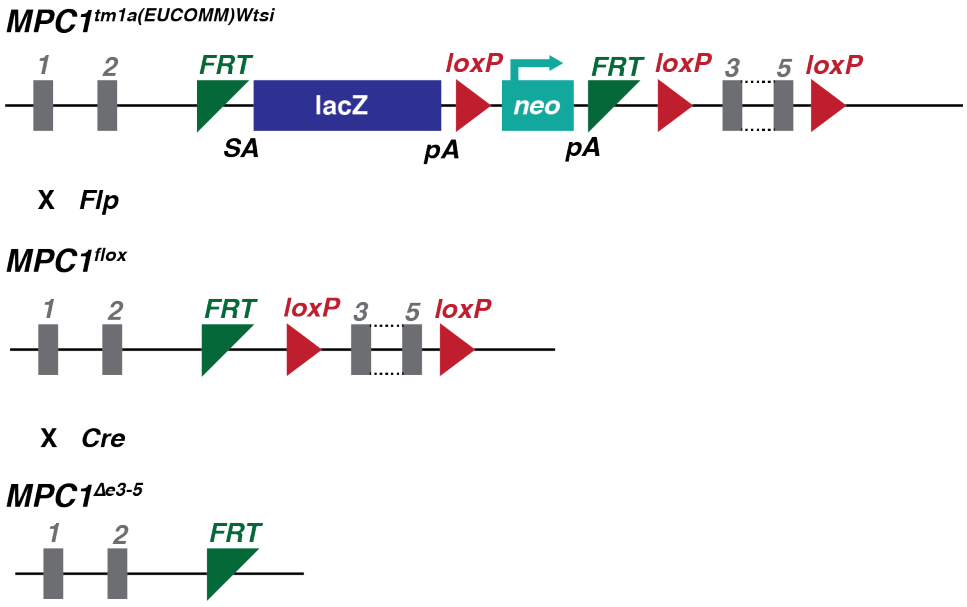

Figure 4.1 *Mpc1* Knockout Mouse Generation. Allele diagrams of targeted *Mpc1* transgenic and generation of *Mpc1* knockout mouse. Cross with Flp recombinase removed the reporter and selection cassette. Cre-mediated recombination removes exons 3-5.

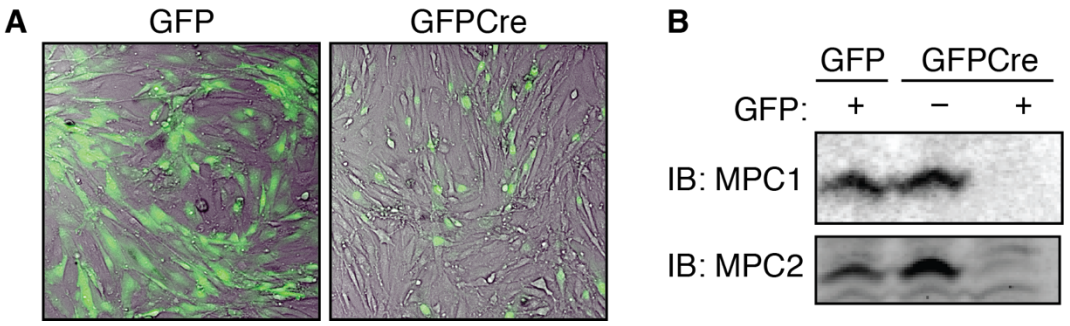

Figure 4.2 MPC1 Knockout Validation. **A)** Transient transfection of *MPC1*$^{flox/flox}$ MEFs with plasmids encoding GFP or GFPCre (note cytoplasmic versus nuclear localization). **B)** Western blot of FACS sorted GFP positive cells. Note loss of MPC1 and MPC2 protein in GFPCre positive cells.

Figure 4.3 Validation of *Mpc1* Colon Stem Cell Knockout. A) Schematic diagram of the colon crypt. From bottom to top: rapid-cycling Lgr5+ crypt base columnar cells (CBCC) at the bottom, slow-cycling Lrig1+ "+4 cells," transient amplifying (TA) cells and differentiated cells. During differentiation, crypt cells transition from glycolytic to OXPHOS as they move up the crypt. **B)** Diagram of transgenic *Lrig1*$^{tm1.1(Cre/ERT2)Rjc/J}$ allele. CreER^{T2} transcript begins at the endogenous start site for Lrig1. **C)** Immunohistochemistry staining of wild-type, heterozygous, and homozygous knockout colon sections. Note the loss of dark, punctate MPC1 staining (top) in the heterozygous and homozygous floxed animals. VDAC staining performed as a positive control for mitochondria. Similar to the schematic in **A**, cells near the crypt base have less MPC1 and VDAC than those further up the crypt. Scale bars are 100μm.

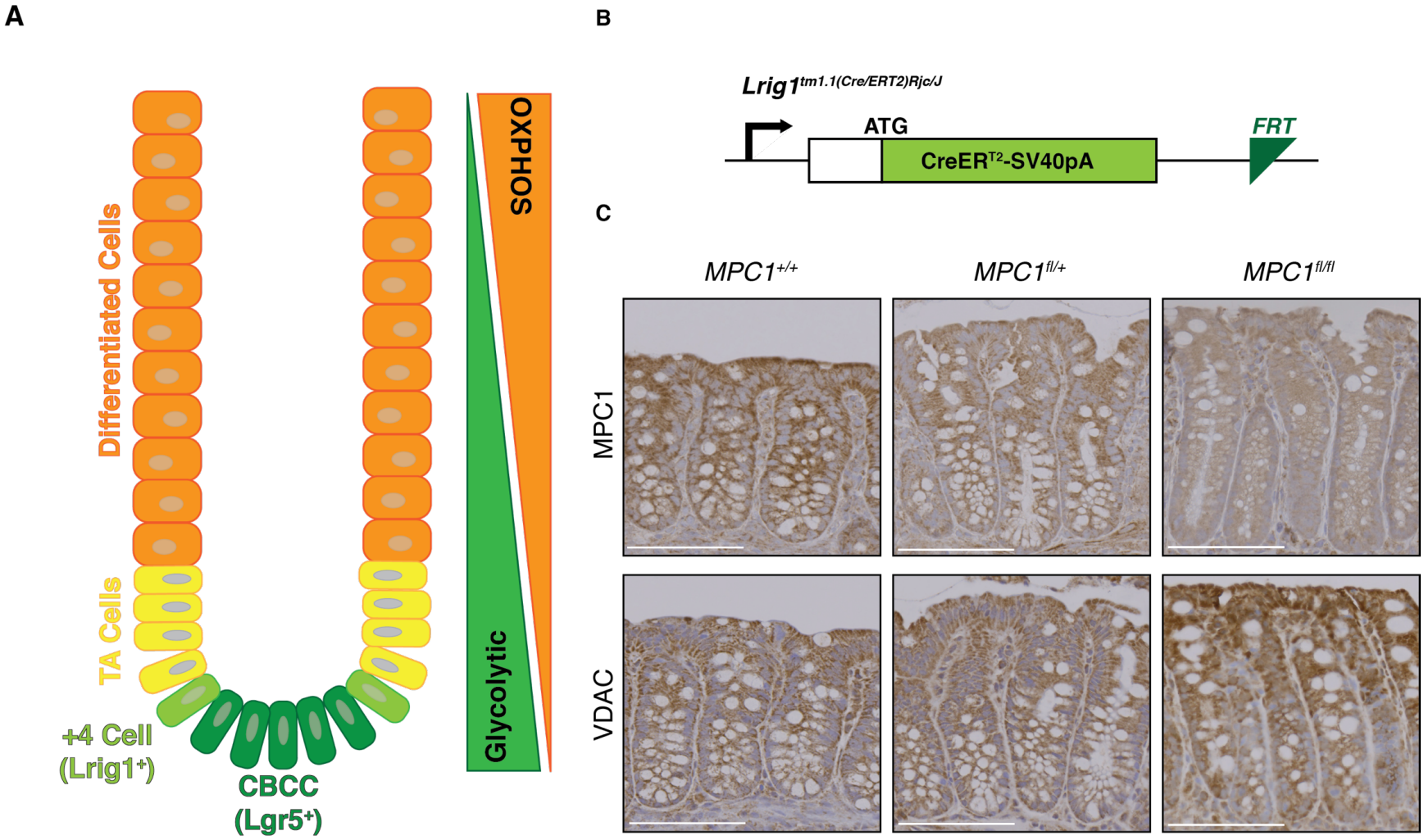
A
Differentiated Cells
TA Cells
+4 Cell
(Lrig1+)
CBCC
(Lgr5+)
OXPHOS
Glycolytic
B
Lrig1tm1.1(Cre/ERT2)Rjc/J
ATG
CreERT2-SV40pA
FRT
C
MPC1+/+
MPC1fl/+
MPC1fl/fl
MPC1
VDAC

days,[44] and at 30 days we observed a loss of MPC1 staining in the entirety of the crypt in *Mpc1*$^{fl/fl}$*Lrig1*^{CreERT2} mice (Figure 4.3C). Of interesting note is the gradient of MPC1 staining from the bottom to the top of the crypt in *Mpc1*$^{+/+}$ control mice. The staining pattern is the inverse of that previously reported for PDK1 in the colon crypt,[47] and is consistent with a metabolic shift from glycolysis to OXPHOS as cells differentiate and move up the crypt.

4.3.2 *Mpc1* Knockout Promotes Proliferation in Colon Stem Cells

We hypothesized that MPC1 is necessary for the glycolysis to OXPHOS transition during differentiation, and sought to assess its impact on the colon epithelium over time. After 3 days of IP tamoxifen, we harvested a cohort of mice at 30-day intervals out to 120 days, and noted no significant morphologic change of the colon epithelium by hematoxylin & eosin (H&E) staining (Figure 4.4). Similarly, *Mpc1*$^{fl/fl}$ mice did not have a decrease in weight gain compared to control mice (data not shown), suggesting normal physiologic function of the colon epithelium.

However, when we stained for Ki67, a marker of cell proliferation, we observed an increased percentage of Ki67 positive nuclei in the knockout versus control crypts (Figure 4.5A), which remained throughout the time-course (Figure 4.4). We also observed an increase in cells with a higher nuclear to cytoplasmic ratio by H&E, suggesting that there may be an

Figure 4.4 Time Course of *Mpc1* Knockout Crypts. Homozygous wild type and knockout mice were treated with tamoxifen and harvested at 30 day intervals post-injection for dissection and analysis by IHC. H&E staining shows no epithelial collapse or histologic changes between wild-type and knockout animals. Ki67 is increased at 30 days in the MPC1 knockout animals, and continues to stay increased throughout the time course. MPC1 knockout mice also show an increase in Lrig1 positive staining, suggesting an expansion of the stem cell compartment. At 30 days the MPC1 knockout animals lack the characteristic dark punctate MPC1 staining pattern, which remains absent throughout the time course. Boxes dimensions are 220μm per side.

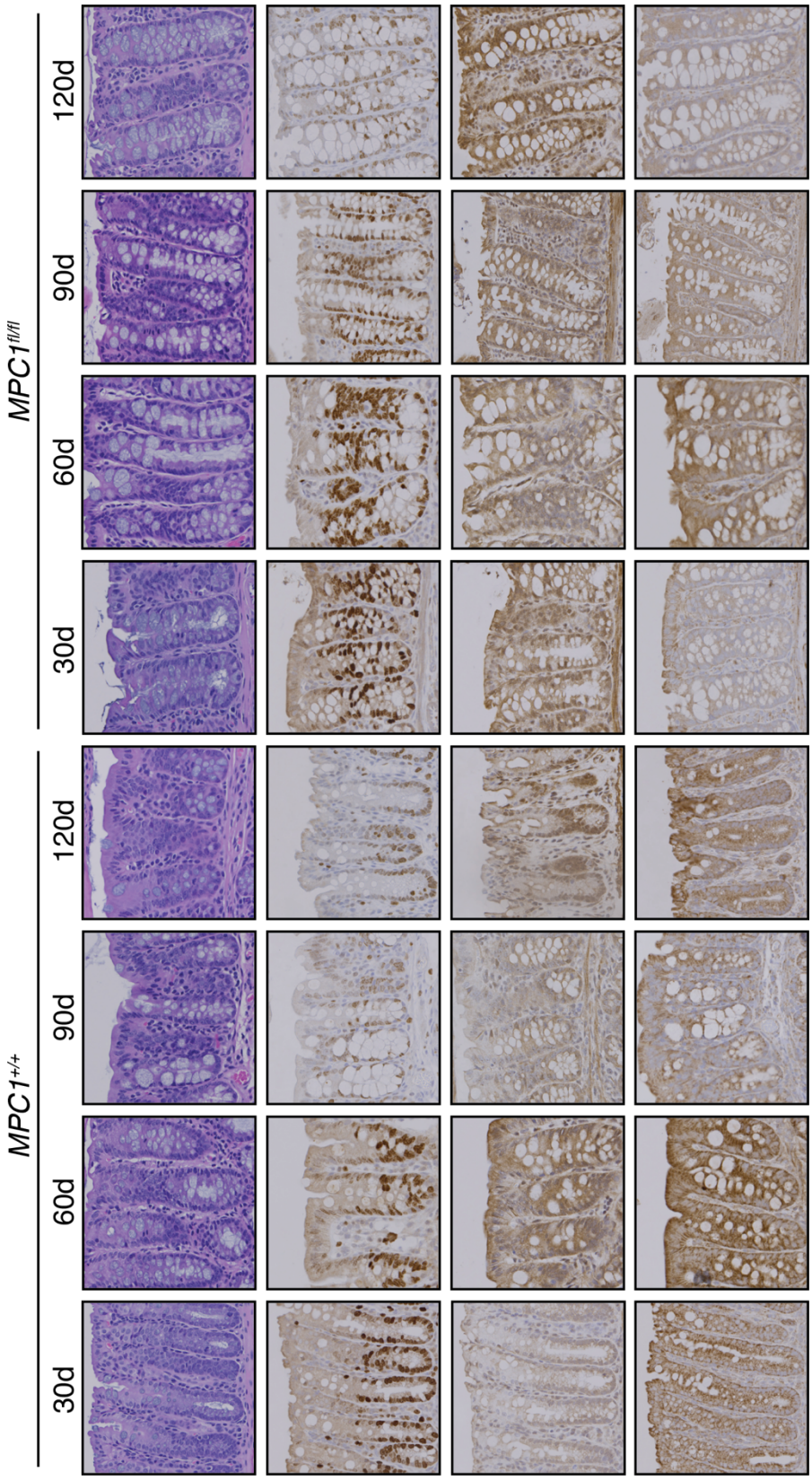
MPC1+/+
MPC1fl/fl
30d
60d
90d
120d
30d
60d
90d
120d
H&E
Ki67
Lrig1
MPC1

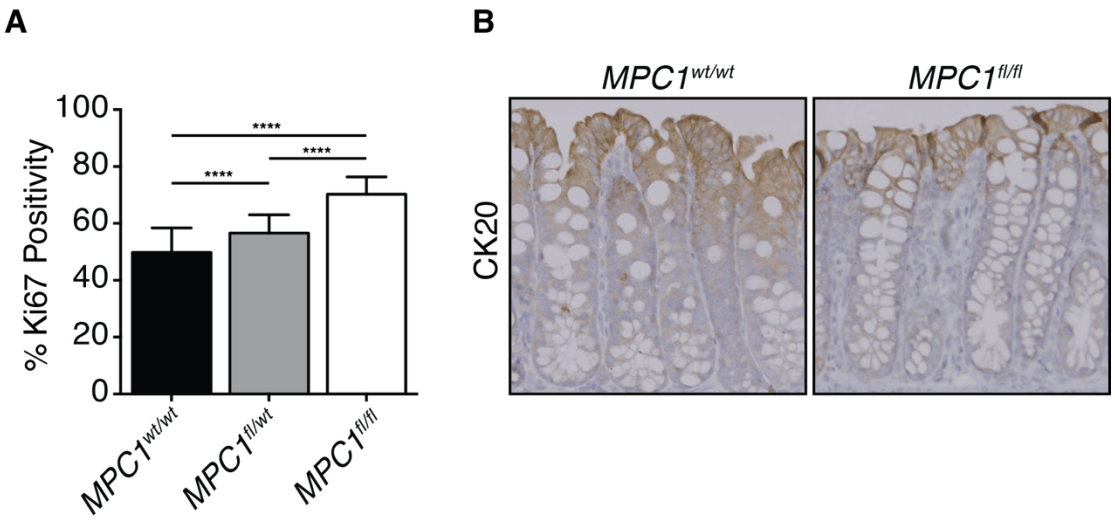

Figure 4.5 Proliferation Is Dose-Dependent and Associated with Decreased Differentiation. A quantification of % Ki67+ cells in wild type (*n*=69), heterozygous (*n*=85), and homozygous (*n*=73) *MPC1* knockout crypts. ****; p < 0.0001. **B** Cytokeratin 20 staining of MPC1 wild type and knockout crypts. Boxes are 220µm per side.

expansion of the stem cell compartment. Indeed, knockout crypts appear to contain more Lrig1 cells than wild type controls. MPC1 staining remains absent in the knockout cells through 120 days, suggesting that the Ki67+, Lrig1+ cells arise from MPC1 negative, Lrig1+ cells and that the crypts are not repopulated by daughter cells from another stem cell compartment. We further observe a decrease in cytokeratin 20 (CK20) positive cells (Figure 4.5), a marker of differentiation, reinforcing the notion that MPC knockout causes a hyperplasia of the stem cell compartment.

4.3.3 Does Loss of MPC1 Metabolically Prime Cells for Transformation?

While the lack of dysplasia, adenoma, or adenocarcinoma at 120 days suggests that *Mpc1* itself does not have a tumor suppressor function, hyperplasia and hyperproliferation within the colon epithelium is an established precursor lesion to colon cancer.[48] Previous work showed that conditional knockout of one allele of the adenomatous polyposis coli gene (*Apc1)* in Lrig1 cells results in multiple, fulminant tumors in the distal colon within 100 days.[46] To test whether *Mpc1* knockout metabolically "primes" or accelerates cells for transformation, we crossed $Mpc1^{flox}Lrig1^{CreERT2}$ mice with mice harboring a floxed *Apc* allele,[49] Apc^{tm1Tyj} (Figure 4.6) mice to generate the $Mpc1^{flox}Apc^{flox/+}Lrig1^{CreERT2}$ conditional knockout line.

Similar to the $Mpc1^{flox}Lrig1^{CreERT2}$ mice, we injected with tamoxifen

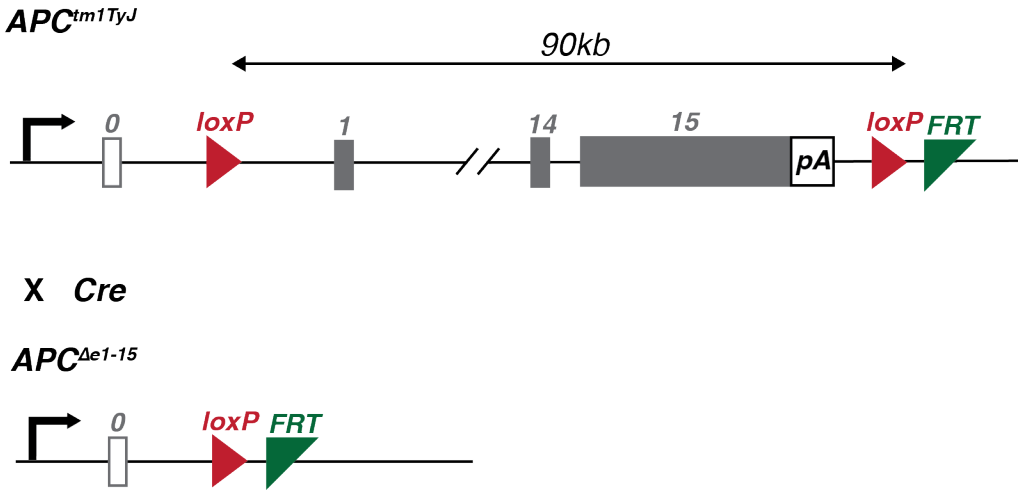

Figure 4.6 Diagram of *Apc* Conditional Knockout Allele. Conditional *Apc* knockout allele obtained from Jackson Laboratories. Upon Cre-mediated recombination, all 15 exons of APC (a 90kb genomic region) are deleted.

and harvested a cohort of mice at 30-day intervals out to 120 days. To our surprise, none of the wild type nor the *Mpc1* knockout mice carrying the Apc^{flox} allele had obvious tumors on gross dissection anywhere in the GI tract, as had previously been reported in the literature. Analysis of IHC sections showed loss of MPC1 in the $Mpc1^{fl/fl}$ mice, suggesting functional recombination machinery was still intact. APC promotes the degradation of beta-catenin,[50] and we expect an increase in beta-catenin staining in the $Apc^{flox/+}$ mice. However, there was no change in beta-catenin staining patterns or intensity between $Apc^{+/+}$ and $Apc^{flox/+}$ mice across the time-course (data not shown). In combination with the lack of tumors, dysplasia, and normal colon histology, we suspected that the $Apcf^{lox}$ allele was simply not recombining.

To determine if the floxed *Apc* allele is able recombine in vivo, crypts were isolated from tamoxifen treated $Mpc1^{flox/+}Apc^{flox/+}$ mice. We genotyped DNA isolated from the colon crypts and confirmed that while the floxed *Apc* allele was present, there was no indication of recombination (Figure 4.7). In sum, these data confirmed our suspicion that this Apc^{flox} allele is non-functional in our system, and data remain inconclusive as to whether *Mpc1* loss promotes or accelerates tumor formation.

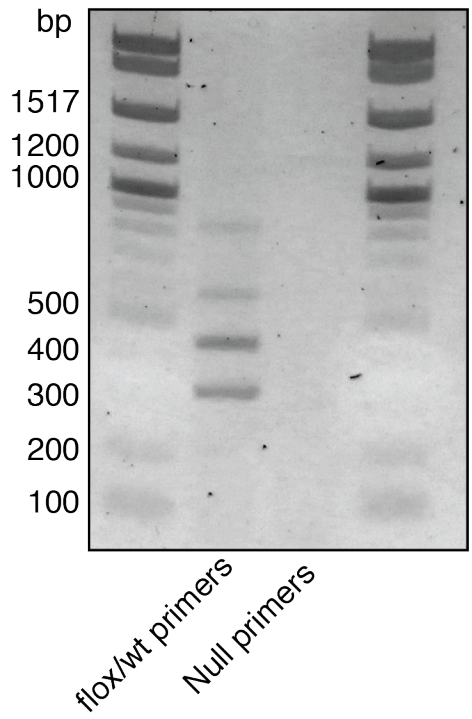

Figure 4.7 Floxed *Apc* Allele Does Not Recombine In Vivo. PCR genotyping of DNA from isolated crypts from tamoxifen treated $MPC^{flox/+}APC^{flox/+}Lrig1^{Cre\text{-}ERT2}$ mouse. Genotyping primers used to detect the presence of the floxed allele show the anticipated wild-type (340bp) and floxed (471bp) bands. A second set of primers did not amplify the 1250kb null/recombined allele.

4.4 Discussion

Previous work over the past several decades have established the connection between cancer and metabolic perturbations. Our current and previous work focuses on the mechanisms enforcing aerobic glycolysis, and means to exploit the metabolic inflexibility of this restrictive paradigm.[11] Similar to glycolytic cancers, many stem cells also reduce mitochondrial oxidation in favor of glycolysis. In many cases, the machinery regulating the metabolism of both cancers and stem cells is similar, if not the same.[29,51-53]

The recent discovery of the genes encoding the MPC,[54,55] and its connection to the Warburg effect[37] is yet another chapter in this continuing series. *Mpc1* resides at the distal end of chromosome 6, the most frequently lost genomic region across all cancers.[37,56] The mechanism behind the frequency of this genomic loss is not known, however data suggest that deletions in the *Mpc1* locus occur very early in the development of preneoplastic lesions.[57,58]

With the frequent and early loss of *Mpc1*, and its function as a metabolic "gatekeeper" between cytosolic and mitochondrial pyruvate metabolism, we inquired whether genomic deletion of *Mpc1*, and concomitant induction of the Warburg effect, can be a precipitating event in oncogenesis. In essence, is metabolism a passive bystander, affected by and responding to cellular energetic demands, or can a fixed metabolic program determine cell fate and/or promote oncogenesis?

Similarly, it is well appreciated that the stem cells within the colon crypt accumulate mutations and serve as the cell of origin for most colon cancers.[48] Colon crypt stem cells, during the process of differentiation, switch from glycolytic to oxidative metabolism, and we hypothesize that the MPC may play an important role in differentiation as well.

To address both hypotheses, we generated an in vivo model of MPC loss in colon crypt stem cells. Initially, we suspected that deleting *Mpc1* in the colon stem cells would result in epithelial collapse, as the stem cells would fail to differentiate to their more oxidative daughter cells. However, throughout our 120-day time course we did not observe any collapsed epithelium nor the associated physiologic changes such as weight loss in our knockout mice. We also did not observe dysplasia, adenoma, or adenocarcinoma over the time course, suggesting that the MPC does not function as a tumor suppressor, at least in the canonical sense.

We did, however, observe a surprising dose-dependent increase in Ki67 positivity in *Mpc1* knockouts as early as 30 days, which remained throughout the time course. If *Mpc1* is necessary for differentiation, perhaps loss of *Mpc1* in the stem cell compartment causes an accumulation of progenitor cells within the colon. While the precise identity of these cells is still to be determined, IHC staining for stem cell markers and an increased number of cells with a low nuclear to cytoplasmic ratio suggests that the Ki67+ cells may indeed be stem cells.

An expansion of the stem cell compartment, and an increase in proliferative cells is an important observation. Canonically, hyperproliferation within the colon crypt is one of the earliest identifiable lesions in the classical adenoma-carcinoma sequence. Given the stochastic model of DNA mutation and the Knudson hypothesis,[59] this logically makes sense. A dividing cell simply has more opportunities to accumulate mutations than a quiescent cell, and an increased number of dividing cells per crypt may further enhance the rate of transformation.

To assess whether MPC1 loss, and concomitant hyperproliferation and expansion of the stem cell compartment increases the rate of tumor formation, we chose to use an APC loss-of-heterozygosity model. The *Lrig1*^{CreERT2}*Apc*$^{flox/+}$ model previously has been shown to have multiple large tumors in the distal colon by 100 days.[46]

Unfortunately, by 120 days we did not observe any tumors on gross dissection, nor any dysplasia or microadenomas by histology. Genomic PCR analysis of isolated crypts from tamoxifen treated *Apc*$^{flox/+}$ mice detected the presence of floxed and wild-type alleles, but not a recombined allele.

The previous literature which showed tumor formation in an *Lrig1*^{CreERT2}*Apc*^{flox} mouse utilized an *Apc* allele with loxP sites flanking only exon 14 (*Apc*^{e14}), whereas the *APC* allele used in this study (*Apc*^{tm1Tyj}) possesses loxP sites flanking all 15 *Apc* exons, a distance of 90kb. A paper published in 2010 compared these two *Apc* alleles, and showed that they

shared similar pathology when crossed with a germ-line Cre mouse.[49] Upon further review of the literature, there is a conspicuous absence of publications utilizing this specific *APC*^{tm1Tyj} floxed allele, and no studies published using this allele in a CreERT2 driven system.

While the data from our APC study are inconclusive, the logic still applies that metabolically forcing a "Warburg" program, via knockout of MPC1, may still "prime" the cell for transformation. Ultimately this study must be repeated, either using the APC floxed allele at exon 14, or another mutagenic system such as azoxymethane/dextran sulfate sodium (AOM-DSS) treatment.[60] The latter may be the more favorable option, as it would directly test whether the hyperproliferative stem cell compartment (induced by *Mpc1* deletion) is more susceptible to accumulating DNA damage (by AOM treatment) and progressing to adenoma/adenocarcinoma than wild-type, metabolically flexible tissue. Furthermore, it would avoid confounding results should it be shown that the MPC is regulated by APC/Wnt/beta-catenin signaling.

4.5 Methods

4.5.1 Mouse Breeding and Animal Husbandry

All mouse work conducted herein was approved and monitored by the University of Utah Institutional Animal Care and Use Committee, protocol number 14-10002. *Mpc1*$^{tm1a(EUCOMM)Wtsi}$ ES cells were obtained from the

Wellcome Trust Sanger Institute. Microinjection into blastocysts was performed by the University of Utah Transgenic and Gene Targeting Core. Germ-line Flp mice were obtained from the University of Utah Transgenic and Gene Targeting Core. *Apc* flox (Apc^{tm1Ty}, strain #009045) and *Lrig1-CreERT2* ($Lrig1^{tm1.1(Cre/ERT2)Rjc}$, strain # 018418) mice were obtained from The Jackson Laboratory. Experimental cohorts for $Mpc1^{flox}Lrig1^{CreERT2}$ mice were generated by crossing $Mpc1^{flox/flox}$ mice with $Lrig1^{CreERT2/+}$ mice. $Mpc1^{flox/+}Lrig1^{CreERT2/+}$ mice were then crossed with $Mpc1^{flox/+}$ mice to generate the *Mpc1* allelic series experimental cohort. $Mpc1^{flox}Apc^{flox}Lrig1^{CreERT2}$ mice were generated by crossing $Mpc1^{flox/flox}$ mice with $Apc^{flox/flox}$ mice. The resulting $Mpc1^{flox/+}Apc^{flox/+}$pups were crossed with $Mpc1^{flox/+}Lrig1^{CreERT2/+}$ to generate the experimental cohort. Recommended genotyping protocols for *Apc* and *Lrig1* were followed from the JAX website. *Mpc1* genotyping was performed as previously described.[40]

4.5.2 Tissue Harvest and Swiss roll

Experimental animals were injected intraperitoneally with 100μL 20mg/mL tamoxifen for 3 days at 8 weeks of age, and sacrificed at either 30, 60, 90, 120, 150, or 180 days after injection. Mice were fasted for 24h prior to sacrifice under isoflurane anesthesia by cervical dislocation and bilateral thoracotomy. The lungs, liver, and kidneys were rinsed with PBS, hemisectioned, and fixed in 10% buffered formalin for 48 h. The

mesentery/pancreas were dissected from the small and large intestine, rinsed with cold PBS, and fixed in 10% buffered formalin for 48 h.

The intestines were prepared for Swiss roll[61] by removing from the abdomen by cutting at the pylorus and the rectum. Small and large intestines were separated by cutting at the iliocecal valve. Small and large intestines were split open using ball-tip artery scissors, moving from proximal to distal. Opened intestinal sections were then rinsed thoroughly in PBS to remove feces, and length and weight were measured. Intestines were briefly submerged in 10% buffered formalin prior to pinning the distal end to moist cork board, lumen side down. Approximately 10cm intestinal segments were wound around a pipette tip, moving proximal to distal (proximal intestine inside center of Swiss roll). Rolls were carefully placed inside a cassette and fixed in 10% buffered formalin for 48 h. After 48 h, all tissues were transferred to 70% ethanol. Paraffin embedding and sectioning, and H&E staining was performed by the Huntsman Cancer Institute Research Histology core. All tissues from each mouse were sectioned and H&E stained.

4.5.3 Immunohistochemistry

Colon and small intestine Swiss roll sections from each mouse were stained for MPC1, Ki67, beta-catenin, Lrig1, VDAC, CK20, and CD44. IHC staining was performed by ARUP Research Histology, using the following protocol: Cut tissue sample at 3-4 microns on positively charged slides. Let

slides air dry. Melt slides in a 60°C oven for 30 min. Place slides on automated stainer (Ventana Medical Systems). De-paraffin slides with EZ Prep solution (Ventana Medical Systems). Pretreat slides with CC1 (Cell Conditioning 1, pH 8.5) for 4 min at 95°C (VDAC1), or for 32 min 95°C (Ki-67) or 60 min at 95°C (CK20, Beta-catenin, MPC1) or digest with Protease 3 (Ventana Medical Systems) for 36 min at 37°C (LRIG1). (Beta-catenin only): Apply Mouse Detective (mouse protein blocker) for 40 min at 37°C. Primary antibody is applied for 1 h at 37°C (VDAC1 at a 1:300 dilution). Primary antibody is applied for 1 h at room temperature (Ki-67 at a 1:600 dilution). Primary antibody is applied for 1 h at 37°C (CK20 at a 1:500 dilution). Primary antibody is applied for 1 h at 37°C (MPC1 at a 1:200 dilution). Primary antibody is applied for 1 h at 37°C (Beta-catenin at a 1:200 dilution). Primary antibody is applied for 1 h at room temperature (LRIG1 at a 1:700 dilution). Apply the secondary antibody (rabbit anti-mouse Fab, Dako, catalog # E0413) at a dilution of 1:100 for 24 min at 37°C (Beta-catenin). Apply the secondary antibody (goat anti-rabbit IgG, Sigma, catalog #B8895) at a dilution of 1:100 for 32 min at 35°C (Ki-67 and LRIG1) or 40 min at 37°C (VDAC1 and CK20). Detection of slides was performed on the Ventana BenchMark™ Discovery automated system using the DAB Map detection kit which incorporates a peroxidase inhibitor (3% H_2O_2), a blocker to reduce background staining, a streptavidin horseradish peroxidase conjugate, 3-3, diaminobenzidine/H_2O_2 as the chromogen and a copper sulfate enhancer

(Ventana Medical Systems). Counterstain slides with hematoxylin for 8 min (Ventana Medical Systems). Blue slides for 4 min (Ventana Medical Systems). Remove slides from the autostainer and placed in a mixture of DAWN/dH_2O. Wash slides in the DAWN/dH_2O to remove any oil applied by the autostainer. Rinse slides in dH_2O. Place slides in Iodine to remove any precipitate from fixation. Place slides in Sodium Thiosulfate to clear Iodine. Rinse slides in dH_2O. De-hydrate slides in graded alcohols (70% x1, 95% x2 and 100% x2) 30 s each. Clear slides in 4 changes of xylene 10 dips each. Coverslip slides.

The following antibodies were used for IHC analysis: Lrig1 (Abcam, ab36707, rabbit polyclonal antibody); CK20 (Abcam, ab118574, rabbit polyclonal antibody); VDAC1 (Abcam, ab34726, rabbit polyclonal antibody); Beta-catenin (BD Transduction Laboratories, 610154, clone 14); Ki-67 (Abcam, ab15580, rabbit polyclonal antibody); MPC1 (Sigma, HPA045119, rabbit polyclonal antibody).

4.5.4 Slide Imaging and Histology

Slides were imaged on an Axioscan Z.1 slide scanner (Carl Zeiss Optics) using the "Medium Size, Medium Stain" scan wizard profile for H&E sections and the "Medium Size, Faint Stain" scan wizard profile for IHC sections. Fine focus map was calculated using "onion skin" method at 0.5. Slides were scanned using 40x objective. Slide scans were viewed using Zen

Pro 2 (Carl Zeiss), and regions of interest were exported for further analysis by ImageJ.

4.5.5 MEF Isolation

Heterozygous *Mpc1*^{flox} mice were intercrossed to generate pups with the *Mpc1* allelic series. Male and female mice were placed together for 3 days in harem breeding before removing the male. Observation of a vaginal plug was noted and female weights were monitored for the subsequent 9 days. Pregnant females were then sacrificed, and MEFs were generated following the Jacks lab protocol (http://web.mit.edu/jacks-lab/protocols/Making_MEFs_tables.html). MEFs were maintained in Dulbecco's modified Eagle's medium +2mM Glutamax (Invitrogen) with 15% FBS (Sigma Aldrich) and 1% primocin at 37˚C in 5% CO_2.

4.5.6 Transfection/Microscopy/FACS

MEFs were transfected using Lipofectamine 3000 (Invitrogen) and plasmids encoding either GFP[54] or GFPCre[39] (Addgene #11920). Cells were imaged on the Axio Observer Z1 imaging system (Carl Zeiss) equipped with 10x, 40x, and 100x objectives (oil immersion). Digital fluorescence and differential interference contrast (DIC) images were acquired using a monochrome digital camera (AxioCam Mrm, Carl Zeiss). The final images were adjusted and assembled using Adobe Photoshop CC 2015. Brightness

and contrast were adjusted only using linear operations across the entire image.

Cells were sorted 48h after transfection for GFP positive cells on BD FACSAria II after excitation with the 488nm laser and read with the 530/30 optical filter set.

4.5.7 Immunoblotting

Samples were prepared, and immunoblotting conducted as described previously.[37] Proprietary MPC1 and MPC2 antibodies were developed and tested in collaboration with Cell Signaling Technologies.

4.5.8 Statistical Methods

Statistical analyses were performed using Graphpad Prism 6. Unless otherwise noted, data were analyzed by Student's t test and considered significant at $p < 0.05$.

4.6 References

(1) Hanahan, D.; Weinberg, R. A. Hallmarks of Cancer: the Next Generation. *Cell* **2011**, *144*, 646–674.

(2) Warburg, O.; Wind, F.; Negelein, E. The Metabolism of Tumors in the Body. *J. Gen. Physiol.* **1927**, *8*, 519–530.

(3) Boroughs, L. K.; deberardinis, R. J. Metabolic Pathways Promoting Cancer Cell Survival and Growth. *Nat. Cell Biol* **2015**, *17*, 351–359.

(4) DeNicola, G. M.; Cantley, L. C. Cancer's Fuel Choice: New Flavors for

a Picky Eater. *Mol. Cell* **2015**, *60*, 514–523.

(5) Pavlova, N. N.; Thompson, C. B. The Emerging Hallmarks of Cancer Metabolism. *Cell Metab.* **2016**, *23*, 27–47.

(6) Jang, M.; Kim, S. S.; Lee, J. Cancer Cell Metabolism: Implications for Therapeutic Targets. *Exp. Mol. Med.* **2013**, *45*, e45.

(7) Granchi, C.; Fancelli, D.; Minutolo, F. An Update on Therapeutic Opportunities Offered by Cancer Glycolytic Metabolism. *Bioorg. Med. Chem. Lett.* **2014**, *24*, 4915-4925.

(8) Vander Heiden, M. G. Targeting Cancer Metabolism: A Therapeutic Window Opens. *Nat. Rev. Drug Discov.* **2011**, *10*, 671–684.

(9) Wise, D. R.; Thompson, C. B. Glutamine Addiction: A New Therapeutic Target in Cancer. *Trends Biochem. Sci.* **2010**, *35*, 427–433.

(10) Tennant, D. A.; Durán, R. V.; Gottlieb, E. Targeting Metabolic Transformation for Cancer Therapy. *Nat. Rev. Cancer* **2010**, *10*, 267–277.

(11) Olson, K. A.; Schell, J. C.; Rutter, J. Pyruvate and Metabolic Flexibility: Illuminating a Path Toward Selective Cancer Therapies. *Trends Biochem. Sci.* **2016**, *41,* 219–230.

(12) Li, Z.; Yang, P.; Li, Z. The Multifaceted Regulation and Functions of PKM2 in Tumor Progression. *Biochim. Biophys. Acta* **2014**, *1846*, 285–296.

(13) Desai, S.; Ding, M.; Wang, B.; Lu, Z.; Zhao, Q.; Shaw, K.; Yung, W. K. A.; Weinstein, J. N.; Tan, M.; Yao, J. Tissue-Specific Isoform Switch and DNA Hypomethylation of the Pyruvate Kinase PKM Gene in Human Cancers. *Oncotarget* **2013**, *5*, 8202–8210.

(14) Christofk, H. R.; Vander Heiden, M. G.; Wu, N.; Asara, J. M.; Cantley, L. C. Pyruvate Kinase M2 Is a Phosphotyrosine-Binding Protein. *Nature* **2008**, *452*, 181–186.

(15) Christofk, H. R.; Vander Heiden, M. G.; Harris, M. H.; Ramanathan, A.; Gerszten, R. E.; Wei, R.; Fleming, M. D.; Schreiber, S. L.; Cantley, L. C. The M2 Splice Isoform of Pyruvate Kinase Is Important for Cancer Metabolism and Tumour Growth. *Nature* **2008**, *452*, 230–233.

(16) Bettaieb, A.; Bakke, J.; Nagata, N.; Matsuo, K.; Xi, Y.; Liu, S.; AbouBechara, D.; Melhem, R.; Stanhope, K.; Cummings, B.; et al. Protein Tyrosine Phosphatase 1B Regulates Pyruvate Kinase M2 Tyrosine Phosphorylation. *J. Biol. Chem.* **2013**, *288*, 17360–17371.

(17) Anastasiou, D.; Yu, Y.; Israelsen, W. J.; Jiang, J.-K.; Boxer, M. B.; Hong, B. S.; Tempel, W.; Dimov, S.; Shen, M.; Jha, A.; et al. Pyruvate Kinase M2 Activators Promote Tetramer Formation and Suppress Tumorigenesis. *Nat. Chem. Biol.* **2012**, *8*, 839–847.

(18) Miao, P.; Sheng, S.; Sun, X.; Liu, J.; Huang, G. Lactate Dehydrogenase A in Cancer: a Promising Target for Diagnosis and Therapy. *IUBMB Life* **2013**, *65*, 904–910.

(19) Le, A.; Cooper, C. R.; Gouw, A. M.; Dinavahi, R.; Maitra, A.; Deck, L. M.; Royer, R. E.; Vander Jagt, D. L.; Semenza, G. L.; Dang, C. V. Inhibition of Lactate Dehydrogenase A Induces Oxidative Stress and Inhibits Tumor Progression. *Proc. Natl. Acad. Sci. U.S.A.* **2010**, *107*, 2037–2042.

(20) Fantin, V. R.; St-Pierre, J.; Leder, P. Attenuation of LDH-A Expression Uncovers a Link Between Glycolysis, Mitochondrial Physiology, and Tumor Maintenance. *Cancer Cell* **2006**, *9*, 425–434.

(21) Xie, H.; Hanai, J.-I.; Ren, J.-G.; Kats, L.; Burgess, K.; Bhargava, P.; Signoretti, S.; Billiard, J.; Duffy, K. J.; Grant, A.; et al. Targeting Lactate Dehydrogenase-A Inhibits Tumorigenesis and Tumor Progression in Mouse Models of Lung Cancer and Impacts Tumor-Initiating Cells. *Cell Metab.* **2014**, *19*, 795–809.

(22) Sheng, S. L.; Liu, J. J.; Dai, Y. H.; Sun, X. G.; Xiong, X. P.; Huang, G. Knockdown of Lactate Dehydrogenase A Suppresses Tumor Growth and Metastasis of Human Hepatocellular Carcinoma. *FEBS J* **2012**, *279*, 3898–3910.

(23) Wang, J.; Wang, H.; Liu, A.; Fang, C.; Hao, J.; Wang, Z. Lactate Dehydrogenase a Negatively Regulated by miRNAs Promotes Aerobic Glycolysis and Is Increased in Colorectal Cancer. *Oncotarget* **2015**, *6*, 19456–19468.

(24) Fujiwara, S.; Kawano, Y.; Yuki, H.; Okuno, Y.; Nosaka, K.; Mitsuya, H.; Hata, H. PDK1 Inhibition Is a Novel Therapeutic Target in Multiple Myeloma. *Br. J. Cancer* **2013**, *108*, 170–178.

(25) Hitosugi, T.; Fan, J.; Chung, T.-W.; Lythgoe, K.; Wang, X.; Xie, J.; Ge,

Q.; Gu, T.-L.; Polakiewicz, R. D.; Roesel, J. L.; et al. Tyrosine Phosphorylation of Mitochondrial Pyruvate Dehydrogenase Kinase 1 Is Important for Cancer Metabolism. *Mol. Cell* **2011**, *44*, 864–877.

(26) Kaplon, J.; Zheng, L.; Meissl, K.; Chaneton, B.; Selivanov, V. A.; Mackay, G.; van der Burg, S. H.; Verdegaal, E. M. E.; Cascante, M.; Shlomi, T.; et al. A Key Role for Mitochondrial Gatekeeper Pyruvate Dehydrogenase in Oncogene-Induced Senescence. *Nature* **2013**, *498*, 109–112.

(27) Bender, T.; Martinou, J.-C. The Mitochondrial Pyruvate Carrier in Health and Disease: to Carry or Not to Carry? *Biochim. Biophys. Acta*. [Online early access]. DOI: 10.1016/j.bbamcr.2016.01.017. Published Online: Jan 26, 2016. http://www.sciencedirect.com/science/article/pii/S0167488916300076 (accessed Mar 2, 2016).

(28) Ito, K.; Suda, T. Metabolic Requirements for the Maintenance of Self-Renewing Stem Cells. *Nat. Rev. Mol. Cell Biol.* **2014**, *15*, 243–256.

(29) Folmes, C. D. L.; Terzic, A. Energy Metabolism in the Acquisition and Maintenance of Stemness. *Semin. Cell Dev. Biol.* **2016,** *52*, 68-75.

(30) Suda, T.; Takubo, K.; Semenza, G. L. Metabolic Regulation of Hematopoietic Stem Cells in the Hypoxic Niche. *Cell Stem Cell* **2011**, *9*, 298–310.

(31) Ushio-Fukai, M.; Rehman, J. Redox and Metabolic Regulation of Stem/Progenitor Cells and Their Niche. *Antioxid. Redox Signal.* **2014**, *21*, 1587–1590.

(32) Lunt, S. Y.; Muralidhar, V.; Hosios, A. M.; Israelsen, W. J.; Gui, D. Y.; Newhouse, L.; Ogrodzinski, M.; Hecht, V.; Xu, K.; Acevedo, P. N. M.; et al. Pyruvate Kinase Isoform Expression Alters Nucleotide Synthesis to Impact Cell Proliferation. *Mol. Cell* **2015**, *57*, 95–107.

(33) Jiang, L.; DeBerardinis, R. J. Cancer Metabolism: When More Is Less. *Nature* **2012**, *489,* 511–512.

(34) Vander Heiden, M. G.; Cantley, L. C.; Thompson, C. B. Understanding the Warburg Effect: the Metabolic Requirements of Cell Proliferation. *Science* **2009**, *324*, 1029–1033.

(35) Tamai, M.; Yamashita, A.; Tagawa, Y.-I. Mitochondrial Development

of the in Vitro Hepatic Organogenesis Model with Simultaneous Cardiac Mesoderm Differentiation from Murine Induced Pluripotent Stem Cells. *J. Biosci. Bioeng.* **2011**, *112*, 495–500.

(36) Pereira, S. L.; Grãos, M.; Rodrigues, A. S.; Anjo, S. I.; Carvalho, R. A.; Oliveira, P. J.; Arenas, E.; Ramalho-Santos, J. Inhibition of Mitochondrial Complex III Blocks Neuronal Differentiation and Maintains Embryonic Stem Cell Pluripotency. *PLoS ONE* **2013**, *8*, e82095.

(37) Schell, J. C.; Olson, K. A.; Jiang, L.; Hawkins, A. J.; Van Vranken, J. G.; Xie, J.; egnatchik, R. A.; earl, E. G.; deberardinis, R. J.; Rutter, J. A Role for the Mitochondrial Pyruvate Carrier as a Repressor of the Warburg Effect and Colon Cancer Cell Growth. *Mol. Cell* **2014**, *56*, 400–413.

(38) Vigueira, P. A.; McCommis, K. S.; Schweitzer, G. G.; Remedi, M. S.; Chambers, K. T.; Fu, X.; McDonald, W. G.; Cole, S. L.; Colca, J. R.; Kletzien, R. F.; et al. Mitochondrial Pyruvate Carrier 2 Hypomorphism in Mice Leads to Defects in Glucose-Stimulated Insulin Secretion. *Cell Rep.* **2014**, *7*, 2042–2053.

(39) Le, Y.; Miller, J. L.; Sauer, B. GFPcre Fusion Vectors with Enhanced Expression. *Anal. Biochem.* **1999**, *270*, 334–336.

(40) Gray, L. R.; Sultana, M. R.; Rauckhorst, A. J.; Oonthonpan, L.; Tompkins, S. C.; Sharma, A.; Fu, X.; Miao, R.; Pewa, A. D.; Brown, K. S.; et al. Hepatic Mitochondrial Pyruvate Carrier 1 Is Required for Efficient Regulation of Gluconeogenesis and Whole-Body Glucose Homeostasis. *Cell Metab.* **2015**, *22*, 669–681.

(41) Vacanti, N. M.; Divakaruni, A. S.; Green, C. R.; Parker, S. J.; Henry, R. R.; Ciaraldi, T. P.; Murphy, A. N.; Metallo, C. M. Regulation of Substrate Utilization by the Mitochondrial Pyruvate Carrier. *Mol. Cell* **2014**, *56*, 425–435.

(42) Yang, C.; Ko, B.; Hensley, C. T.; Jiang, L.; Wasti, A. T.; Kim, J.; Sudderth, J.; Calvaruso, M. A.; Lumata, L.; Mitsche, M.; et al. Glutamine Oxidation Maintains the TCA Cycle and Cell Survival During Impaired Mitochondrial Pyruvate Transport. *Mol. Cell* 2014, *56*, 414–424.

(43) Barker, N.; Van Es, J. H.; Kuipers, J.; Kujala, P. Identification of Stem Cells in Small Intestine and Colon by Marker Gene Lgr5.

Nature **2007**, *449*, 1003-1007.

(44) van der Flier, L. G.; Clevers, H. Stem Cells, Self-Renewal, and Differentiation in the Intestinal Epithelium. *Annu. Rev. Physiol.* **2009**, *71*, 241–260.

(45) Powell, A. E.; Wang, Y.; Li, Y.; Poulin, E. J.; Means, A. L.; Washington, M. K.; Higginbotham, J. N.; Juchheim, A.; Prasad, N.; Levy, S. E.; et al. The Pan-ErbB Negative Regulator Lrig1 Is an Intestinal Stem Cell Markerthat Functions as a Tumor Suppressor. *Cell* **2012**, *149*, 146–158.

(46) Powell, A. E.; Vlacich, G.; Zhao, Z. Y. Inducible Loss of One Apc Allele in Lrig1-Expressing Progenitor Cells Results in Multiple Distal Colonic Tumors with Features of Familial Adenomatous Polyposis. *Am. J. Physiol. Gastrointest. Liver Physiol.* **2014**, *307*, G16-G23.

(47) Pate, K. T.; Stringari, C.; Sprowl-Tanio, S.; Wang, K.; TeSlaa, T.; Hoverter, N. P.; McQuade, M. M.; Garner, C.; Digman, M. A.; Teitell, M. A.; et al. Wnt Signaling Directs a Metabolic Program of Glycolysis and Angiogenesis in Colon Cancer. *EMBO J.* **2014**, *33*, 1454–1473.

(48) Abdul Khalek, F. J.; Gallicano, G. I.; Mishra, L. Colon Cancer Stem Cells. *Gastrointest. Cancer Res.* **2010**, Suppl. 1, S16–S23.

(49) Cheung, A. F.; Carter, A. M.; Kostova, K. K.; Woodruff, J. F.; Crowley, D.; Bronson, R. T.; Haigis, K. M.; Jacks, T. Complete Deletion of Apc Results in Severe Polyposis in Mice. *Oncogene* **2010**, *29*, 1857–1864.

(50) Fodde, R. The APC Gene in Colorectal Cancer. *Eur. J. Cancer* **2002**, *38*, 867–871.

(51) Kim, H.; Jang, H.; Kim, T. W.; Kang, B.-H.; Lee, S.-E.; Kyung Jeon, Y.; Hyun Chung, D.; Choi, J.; Shin, J.; Cho, E.-J.; et al. Core Pluripotency Factors Directly Regulate Metabolism in Embryonic Stem Cell to Maintain Pluripotency. *Stem Cells* **2015**, *33*, 2699-2711.

(52) Varlakhanova, N. V.; Cotterman, R. F.; deVries, W. N.; Morgan, J.; Donahue, L. R.; Murray, S.; Knowles, B. B.; Knoepfler, P. S. Myc Maintains Embryonic Stem Cell Pluripotency and Self-Renewal. *Differentiation* **2010**, *80*, 9–19.

(53) Dang, C. V. MYC, Metabolism, Cell Growth, and Tumorigenesis. *Cold Spring Harb. Perspect. Med.* **2013**, *3*, 1–15.

(54) Bricker, D. K.; Taylor, E. B.; Schell, J. C.; Orsak, T.; Boutron, A.; Chen, Y. C.; Cox, J. E.; Cardon, C. M.; Van Vranken, J. G.; Dephoure, N.; et al. A Mitochondrial Pyruvate Carrier Required for Pyruvate Uptake in Yeast, Drosophila, and Humans. *Science* **2012**, *337*, 96–100.

(55) Herzig, S.; Raemy, E.; Montessuit, S.; Veuthey, J. L.; Zamboni, N.; Westermann, B.; Kunji, E. R. S.; Martinou, J. C. Identification and Functional Expression of the Mitochondrial Pyruvate Carrier. *Science* **2012**, *337*, 93–96.

(56) Cai, H.; Kumar, N.; Ai, N.; Gupta, S.; Rath, P.; Baudis, M. Progenetix: 12 Years of Oncogenomic Data Curation. *Nucleic Acids Res.* **2014**, *42* (Database issue), D1055–D1062.

(57) Chen, R.; Bronner, M. P.; Crispin, D. A.; Rabinovitch, P. S.; Brentnall, T. A. Characterization of Genomic Instability in Ulcerative Colitis Neoplasia Leads to Discovery of Putative Tumor Suppressor Regions. *Cancer Genet. Cytogenet.* **2005**, *162*, 99–106.

(58) Tibiletti, M. G.; Trubia, M.; Ponti, E.; Sessa, L.; Acquati, F.; Furlan, D.; Bernasconi, B.; Fichera, M.; Mihalich, A.; Ziegler, A.; et al. Physical Map of the D6S149-D6S193 Region on Chromosome 6Q27 and Its Involvement in Benign Surface Epithelial Ovarian Tumours. *Oncogene* **1998**, *16*, 1639–1642.

(59) Knudson, A. G. Mutation and Cancer: Statistical Study of Retinoblastoma. *Proc. Natl. Acad. Sci. U.S.A.* **1971**, *68*, 820–823.

(60) Clapper, M. L.; Cooper, H. S.; Chang, W.-C. L. Dextran Sulfate Sodium-Induced Colitis-Associated Neoplasia: a Promising Model for the Development of Chemopreventive Interventions. *Acta Pharmacol. Sin.* **2007**, *28*, 1450–1459.

(61) Moolenbeek, C.; Ruitenberg, E. J. The“ Swiss Roll”: a Simple Technique for Histological Studies of the Rodent Intestine. *Lab. Anim.* **1981**,*15*, 57–59.

CHAPTER 5

CONCLUSION

The discovery of the genes encoding the MPC has provided a new lens for us to view cancer metabolism. The work presented in this thesis provides answers to just a small portion of the questions that remain regarding the MPC and its role in normal and pathologic cellular metabolism.

The regulation of the MPC, both transcriptionally and post-translationally have yet to be determined and will play an important role in understanding how mitochondrial pyruvate metabolism is modulated in normal physiology. Many biochemical questions remain unanswered, such as the molecular structure of the MPC complex, substrate cooperativity, and binding partners of the MPC, and the mechanism of MPC complex removal from the mitochondria when either MPC1 or MPC2 are absent. As pointed out in Chapter 2, the fate of pyruvate is highly regulated by enzymes and proteins other than the MPC, and determining which contexts the MPC becomes the rate limiting step in pyruvate metabolism (vs. a redundant blockade in its absence), will be essential to effective therapeutic exploitation of this discovery.

Beyond the scope of the MPC, the field of cancer metabolism continues to rapidly grow. One of the most interesting, and challenging facets to the field will be understanding and modelling metabolic tumor heterogeneity. Currently no models exist to study tumor heterogeneity, nor does robust technology exist to assess metabolism at the single-cell level. As discussed in Chapter 2, this hurdle is essential to overcome if metabolic cancer therapies are to expand in their use beyond adjuvant chemotherapy.

The study of stem cell metabolism is still a nascent field, and many of the mechanisms described in cancer metabolism may also play a role in stem cells. Our initial study on the effects of *Mpc1* knockout in colon stem cells suggests that the MPC may play an important role in the maintenance of stemness, and/or the determination of cell fate. The question of whether forcing the Warburg Effect via *Mpc1* knockout metabolically primes cells for transformation is an exciting prospect, and such a discovery would redefine our understanding of oncogenesis.